TABLE OF CONTENTS

Page

INTRODUCTION 2

CHAPTER 1 FUNDAMENTALS OF pH MEASUREMENT 3
1.1 pH Definition 3
1.2 Importance of pH measurement 3
1.2.1 Importance of pH in environmental monitoring 3
1.2.2 Importance of pH in food processing 5
1.2.3 Importance of pH in medical diagnostic and prognostic 5
1.3 Existing commercial solution for pH measurement 6
1.3.1 pH Paper strips 6
1.3.2 Glass electrode 7
1.3.3 pH Electrodes based on Ion Sensitive Field Effect Transistor 8
1.4 Conclusion 9

CHAPTER 2 IRIDIUM OXIDE 11
2.1 Introduction 11
2.2 pH Sensing Mechanism of Iridium Oxide 11
2.3 Different deposition techniques of Iridium oxide 13
2.3.1 Sol-gel Deposition of Iridium oxide 13
2.3.2 Electrodeposition of Iridium oxide 20
2.4 Conclusion 24

CHAPTER 3 pH SENSOR FABRICATION TECHNIQUES 25
3.1 Introduction 25
3.2 MEMS pH sensor 25
3.2.1 Photolithography 26
3.2.2 Sputtering 27
3.2.3 Liftoff 28
3.2.4 IrO_x deposition 28
3.3 Laser micromachined pH sensor 32
3.4 LTCC based pH sensor 34
3.5 Conclusions 39

CHAPTER 4 NOVEL MINIATURIZED WIRELESS pH SENSING SYSTEMS 41
4.1 Introduction 41
4.2 Miniaturized wireless LTCC based pH sensing device 41
4.2.1 Circuit and layout design 41
4.2.2 Integration 43
4.2.3 Wireless user interface 46
4.3 Other prototypes 48
4.3.1 Flexible pH sensing device 48
4.3.2 Glass based microfluidic pH sensing device 50

4.4 Conclusion 53

CHAPTER 5 WIRELESS POWER TRANSFER FOR BATTERY-LESS APPLICATIONS 55
5.1 Introduction 55
5.2 The concept of wireless power transfer 56
5.3 Transmitter antenna design 59
5.3.1 Antenna parameters 60
5.3.2 Transmitter tuning and performances 63
5.4 Receiver antenna design 67
5.4.1 Air core antenna 68
5.4.2 Flexible spiral antenna 73
5.4.3 LTCC antenna 75
5.5 Results and conclusion 80

CONCLUSION 83

LIST OF BIBLIOGRAPHICAL REFERENCES 87

LIST OF TABLES

Page

Table 1.1 Comparison of different commercial pH sensing devices 10

Table 2.1 Sensitivity vs size 19

Table 2.2 Comparisons between sol-gel and electrodeposition of IrO_x 24

Table 3.1 Comparison of different fabrication techniques 39

Table 5.1 Common unlicensed ISM frequency 59

Table 6.1 Comparison of different pH sensing devices 106

LISTE DES FIGURES

Page

Figure 1.1 pH paper strip 7

Figure 1.2 Glass electrode 8

Figure 1.3 pH Electrode based on Ion Sensitive Field Effect Transistor 9

Figure 2.1 Rutile structure 12

Figure 2.2 Sol-gel process 14

Figure 2.3 SEM and EDS after sol-gel deposition of Iridium oxide 15

Figure 2.4 Different sized working electrodes 16

Figure 2.5 Energy dispersive spectroscopy of different sized electrodes (Iridium vs Oxygenin mass percent) 17

Figure 2.6 Nernst response of different sized working electrode vs. a commercial Ag/Ag-Cl electrode at 19°C 18

Figure 2.7 Sensitivity of a WE based on sol-gel vs temperature 20

Figure 2.8 Electrodeposition of Iridium oxide 21

Figure 2.9 pH sensor calibration at room temperature 22

Figure 2.10 a) SEM image, b) EDS analyses, c) Map distribution 23

Figure 3.1 Photolithography 26

Figure 3.2 Sputtering 27

Figure 3.3 Liftoff 28

Figure 3.4 Electrode thickness measurement 29

Figure 3.5 Electrodeposition result with sputtered thin conductor 29

Figure 3.6 Cracks formation due to thermal stress 30

Figure 3.7 Microfabrication steps 31

Figure 3.8 Uniform surface of IrO_x after laser cutting and sol-gel deposition 32

Figure 3.9 Laser etching fabrication chain 33

Figure 3.10 Laser micro-machined pH sensor response at 19°C 34

Figure 3.11 LTCC pH sensor fabrication chain 35

Figure 3.12 Silver thickness measured before electrodeposition of IrO_x 36

Figure 3.13 a) SEM image, b) EDS analyses, c) Map distribution 37

Figure 3.14 LTCC pH sensor calibration at room temperature 38

Figure 4.1 a) Sensing device schematic; b) Sensing device layout 42

Figure 4.2 LTCC fabrication chain 44

Figure 4.3 Validation of the integrated design 45

Figure 4.4 Block diagram 46

Figure 4.5 Graphical user interface 46

Figure 4.6 Real-time pH testing of our system 47

Figure 4.7 Flexible pH sensing device fabrication chain 49

Figure 4.8 Microfluidic glass based miniaturized pH sensing device 51

Figure 4.9 System block diagram of blood pH monitoring system 52

Figure 5.1 Different zones of an EM field generated by an antenna 56

Figure 5.2 WPT system block diagram 58

Figure 5.3 Examples of different antennas orientation 58

Figure 5.4 Equivalent antenna circuit 61

Figure 5.5 Extraction of antenna equivalent electric circuit from Smith's chart 62

Figure 5.6 Transmitter antenna performances before matching 63

Figure 5.7 Transmitter antenna impedance matching 65

Figure 5.8 Transmitter antenna performances after matching 66

Figure 5.9 Air core antenna equivalent circuit 68

Figure 5.10 Air core antenna performances before tuning 69
Figure 5.11 Air core antenna performances after tuning 71
Figure 5.12 Bandwidth tuning 72
Figure 5.13 Flexible spiral antenna equivalent circuit....73
Figure 5.14 Flexible spiral antenna performances before tuning 73
Figure 5.15 Flexible spiral antenna performances after tuning 74
Figure 5.16 One layer LTCC spiral antenna equivalent circuit....75
Figure 5.17 One layer LTCC spiral antenna performances before tuning....76
Figure 5.18 One layer LTCC spiral antenna performances after tuning....77
Figure 5.19 Four layers LTCC spiral antenna equivalent circuit....78
Figure 5.20 Four layers LTCC spiral antenna performances....79
Figure 5.21 Wireless power transfer efficiency....80
Figure 5.22 Electric and magnetic field distribution 81

LIST OF ABBREVIATIONS

IrOx	Iridium oxide
FDA	Food and Drug Administration
CFR	Code of Federal Regulations
ISFET	Ion Sensitive Field Effect Transistor
SEM	Scanning Electron Microscopy
EDS	Energy Dispersive Spectroscopy
WE	Working Electrode
RE	Reference Electrode
CV	Cyclic Voltammetry
MEMS	Micro-Electro-Mechanical System
LTCC	Low-Temperature Co-fired Ceramic
PCB	Printed Circuit Boards
RF	Radio-Frequency
ADC	Analog-Digital Converters
BLE	Bluetooth Low Energy
SMD	Surface-Mount Device
LOD	Limit Of Detection
IMDs	Implantable Medical Devices
WPT	Wireless Power Transfer
RL	Return losses
EMF	Electro Magnetic Field
WPE	wireless power efficiency

ISM	Industrial, Scientific, and Medical
FCC	Federal Communications Commission
LF	Low Frequency
HF	High Frequency
UHF	Ultra-High Frequency
AWG	American Wire Gauge
VSWR	Voltage Standing Wave Ratio
BW	Band Width

LIST OF SYMBOLS

$[H^+]$	hydrogen ion concentration
Ag	silver
Au	gold
S	sensitivity expressed in mV/pH
CO_2	carbon dioxide
HCO_3-	bicarbonate
$C_2H_6O_6$	oxalic acid dehydrates
K_2CO_3	potassium carbonate
E0	standard potential produced by the reference electrode (expressed in mV)
R	gas constant (with a value of 8.314, expressed in J/mol·K)
T	temperature
F	Faraday's constant with a value of 96,485 expressed in C/mol.
E	electric field
H	magnetic field
λ	wavelength
Γ	reflection coefficient
dB	decibel
S12	transmitted power from port 2 to port 1
S11	reflected power in port 1

INTRODUCTION

pH sensors are useful in numerous applications, such as environmental monitoring, food quality control, clinical testing, etc. Nowadays there is a multitude of available commercial solutions to perform the pH measurement. Those devices have some advantages making them useful for general applications. But they also have some disadvantages limiting their use in some specific applications such as medical diagnostic and prognostic. The objective of the research work is to design pH sensing systems targeting some specific applications which require: better integration, low power, short response time, high precision, etc. Chapter 1 will cover that aspect.

In chapter 2, we will use IrO_x as a pH sensing material and we will compare two different deposition techniques (Sol-gel and electro-deposition). In chapter 3, we will compare various fabrication techniques (MEMS, laser etching, LTCC. Selection criteria (feasibility, sensitivity, cost, complexity, etc.) may change according to the application.

Chapter 4 will present our prototype of a wireless pH monitoring system; we used a modular approach to prove the concept. Due to biocompatibility, infections, and size concerns, the need for a wireless and battery-less system is evident, especially for medical devices. For those reasons, we will design an optimized inductive link (transmitter antenna, receiver antenna) to transmit power wirelessly. This last part is covered in chapter 5.

To give credibility to our research, we published a paper in IEEE Sensors using some of our results illustrated in this thesis.

CHAPTER 1

FUNDAMENTALS OF pH MEASUREMENT

1.1 pH Definition

The pH scale was introduced in 1909 by the biochemist, Soren Peter Lauritz Sorensen as the negative common base 10 logarithmic measurement of the hydrogen ion concentration, $[H^+]$ (number of moles of hydrogen ions H^+ per liter). The "p" prefix in pH stands for potential, while the upper-case letter "H" stands for the element hydrogen and it is expressed mathematically as (Jensen, 2004):

$$pH = - \log([H^+]) \tag{1.1}$$

Every aqueous solution contains a certain amount of hydrogen ions; then it is possible to measure its pH value. This chemical quantity range from 0 to 14 pH, pH of 7 is the center of the scale. A pH of 7 reveals neutral property; the solution is neither acidic nor basic. Values below pH of 7 indicate acidic properties. Values above pH of 7 show alkaline properties.

1.2 Importance of pH measurement

The measure and the control of the pH are fundamental in numerous applications, such as food processing, chemicals, petrochemicals, pharmaceutical manufacturing, industrial processing, environmental and clinical monitoring. There is a tremendous number of potential applications. We will just introduce some of them.

1.2.1 Importance of pH in environmental monitoring

Water is the most common and vital substance on Earth. Pure water is a clear, colorless, and odorless liquid made up of one oxygen and two hydrogen atoms. At 25^0 C in pure water, the amount of hydrogen and hydroxide ions is equal. That is why pure water is described as a

neutral solution. The pH of the water has been identified as one of the most important parameters affecting the quality of the water. In fact, chemical, biological, and physical factors can affect the pH of water (Maciel et al., 2013).

Rainwater is naturally acidic, around pH of 5.6. But nowadays, due to the excessive release of CO_2 and some pollutants, the rain is becoming excessively acidic (Sumari et al., 2010). CO_2 dissolves in water to form carbonic acid as follows:

$$CO_2 + H_2O \rightarrow H_2CO_3 \quad (1.2)$$

In some places, the acidity increases to harmful levels between 4.0 and 5.0 pH. Plants will grow better if the soil is maintained at an optimal pH (Warudkar et Dorle, 2016). This variation of the pH of the rainwater is destroying many plantations. For this reason, various environmental agencies are trying to minimize the pollutants that cause acid rain, and pH measurement is a good indicator for environmental monitoring.

Ocean acidification is another alarming environmental issue, essentially caused by the atmospheric carbon dioxide. In fact, like water and air mix at the surface CO_2 dissolves in water to form carbonic acid (Irish et al., 2010). Oceans, lakes, and rivers absorb roughly one third of carbon dioxide emissions which represent 22 million tons each day and this gas will increase the acidity of the water. Before the industrialization, the usual pH of the ocean was about 8.2. Current ocean pH is roughly 8.09. This change of 0.11 pH in logarithmic scale may be seen to be harmless but it is equivalent to a 30% increase in acidity, and it is already affecting and stressing the marine life which leads to dying and severely disturbing ecosystems. According to the Australian government, if the emission of CO_2 keeps the same tendency, by 2100 it could make the oceans up to 320% more acidic. Then the marine life may not survive in that extreme environment((ASOC), 2010). Many governments are extremely concerned by this problem, Australia is the first concerned because it does not only have an impact on ecology, it also has an economic impact (fisheries, aquaculture, tourism). They are massively investing in remote data monitoring and try to reduce the effect of this phenomenon ((AIMS),

2016). There is a lack of data, which result in a bad model prediction especially data collected in depth water and open ocean ((IMOS), 2016).

1.2.2 Importance of pH in food processing

In food production, pH levels control is an essential step in the manufacture of a multitude of high-quality products. For instance, during food processing, managing and maintaining an optimal pH range is critical in many chemical and physical reactions (Huang et al., 2012). For example, controlled pH during the production of Yogurt will lead to undesired taste, discoloration and so forth. The Proper pH level is not only necessary to get the desired taste, look, and quality; but also maintaining a healthy pH is a food safety requirement. In the USA, Food and Drug Administration (FDA) regulates acidified food processing, Title 21 Section 114.90 of the Code of Federal Regulations (CFR).

Monitoring pH level can also help to check the freshness and detect deadly bacteria such as Botulism in preserved foods. In fact, there is a correlation between food freshness and pH level (Shah et Chauhan, 2015).

1.2.3 Importance of pH in medical diagnostic and prognostic

All living things (human beings, animals, vegetables, and so forth) depend on a balanced pH level to sustain life. They rely on internal mechanisms to maintain an appropriate pH level of their organism: For us human beings, the blood circulating through our body should have a pH balanced between 7.35 and 7.45 (Fu, Lin et Xu, 2011). Exceeding this interval by as little as 0.1 of a pH could be deadly (Mand et al., 2015). The kidneys and lungs are the primary organs involved in blood pH balance. For instance, raising and lowering the respiratory rate affects the concentration of CO_2, and this influence blood pH. The kidneys regulate the concentration of bicarbonate (HCO3-) in blood. Blood pH changes due to increases or decreases in HCO3- concentration. The effect is slower compared to the carbon dioxide concentration in blood, in fact, it may take hours or days. Many diseases (especially diseases affecting lungs and kidneys)

can interfere with pH balance in the body and cause blood pH to fall outside of healthy limits, monitoring the blood pH balance allows a better diagnostic and prognostic (Chemistry, 2014) and (Mand et al., 2015).

According to literature, pH is also an important factor in tissue regeneration, a typical range of the pH during healing can be between 5.7 and 7.8, many studies reported a correlation of healing process with pH values (Puchberger-Enengl, Krutzler et Vellekoop, 2011). It is possible to monitor a burn and detect the presence of bacteria by incorporating pH sensor into bandages; known as smart bandages (Shorrock et al., 2000) (Farooqui et Shamim, 2016). There is a correlation between the value of pH and many other medical conditions and diseases; we will not talk about all of them because there is a tremendous number of medical applications. It is evident that pH is an important parameter for medical monitoring, very useful for a correct diagnostic and appropriate prognostic.

1.3 Existing commercial solution for pH measurement

Nowadays, there is a multitude of available commercial solutions to perform the pH measurement. For instance, in the market, we can find pH paper strips, glass electrodes, and Ion Sensitive Field Effect Transistor (ISFET). Each device has some advantages and disadvantages; we will briefly present each solution.

1.3.1 pH Paper strips

pH papers (Figure 1.1) contain reactive compounds which will change to a specific color at a particular pH value. The pH paper can be used to obtain quick pH measurements. The paper strip is dipped in the sample to measure the pH (Ke Dehong, 2014). The obtained color is compared to the given reference chart. This method is very cheap and does not require any calibration. However, the comparison of the color to the reference chart is based on visual inspection and is subjective; then this method is not very accurate. A maximum accuracy which could be obtained is between 0.3 and 1 pH units.

Figure 1.1 pH paper strip

1.3.2 Glass electrode

German chemist Fritz Haber and his student Zygmunt Klemensiewicz developed the glass electrode idea in 1909. Thanks to their invention they won a Nobel-Prize. Today the most widely used pH sensing device is the sensitive glass electrode. This kind of electrode which is illustrated in figure 1.2, uses a thin glass membrane that is responsive to changes in H^+ activity and it is manufactured primarily from SiO_2. Also, varying amounts of other metal oxides, like Na_2O and CaO are incorporated inside the sensitive glass. When this membrane is placed in an aqueous solution containing H^+, the external surface is hydrated as water enters a short distance into the crystal, and the interior part remains dry. Ions (such as Na^+) can diffuse slowly from one site to another. The response time is long because the membrane resistance is very high (approximately 45 MΩ), and some H^+ ions can charge pair with oxygen near the glass surface. A difference in the H^+ activities on each side of the membrane leads to an imbalance in the surface charge between the internal and the external layer (A, 1948). This results in a membrane potential that is pH dependent described according to the Nernst equation:

$$E\ membrane = E\ inner - E\ outer \quad (1.3)$$

Figure 1.2 Glass electrode

A second Ag/AgCl electrode is used as a reference to measure that potential correctly. Usually, glass pH sensors are a combined design, in which the sensitive electrode and needed reference electrodes are mounted on the same body. The modern, pH sensors are still using the conventional glass electrodes (invented more than a century ago), which provide high precision and reliability over an extended period. However, they are relatively expensive, the bulkiness, the lack of integration, long response time, and their high impedance have limited their use in many applications especially in medical monitoring.

1.3.3 pH Electrodes based on Ion Sensitive Field Effect Transistor

Piet Bergveld invented Ion Sensitive Field Effect Transistor (ISFET) in 1970. This new generation of sensors (Figure 1.3) was developed by the combination of semiconductor technology and pH sensitive materials. For instance, source and drain are constructed as for a MOSFET; the difference resides on the metal gate of a transistor which is normally used as input. In ISFET the metal gate is modified and replaced by an ion-sensitive membrane. The current through the transistor will change proportionally to the amount of H^+ proton (which means therefore to pH level) (Jimenez-Jorquera, Orozco et Baldi, 2010). This new generation of sensors could be miniaturized, have a rapid response time, and they are robust. For those reasons, it is a good alternative to conventional glass-based sensing electrode.

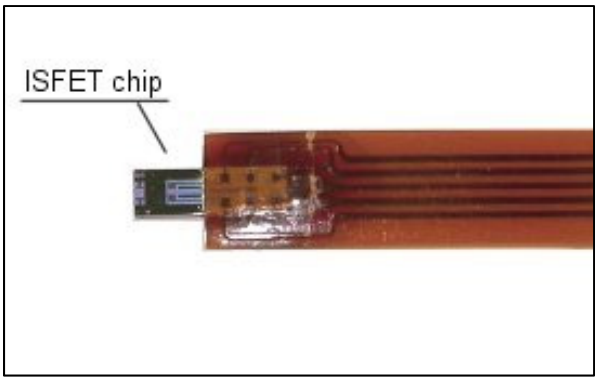

Figure 1.3 pH sensor based on Ion Sensitive Field Effect Transistor

However, ISFET is more expensive than glass sensing electrode and still requires a standard reference electrode to perform measurements. A classical type reference electrode used in contact with the solution can also be bulky and fragile. Then, ISFET sensor will suffer the same limitations as conventional glass-based pH sensing electrodes (Jimenez-Jorquera, Orozco et Baldi, 2010).

1.4 Conclusion

An accurate pH value detection in real time is of keen interest in a significant number of applications (such as environmental monitoring, food quality control, and medical diagnostics). Some devices or methods are available to perform the pH measurement; they have many advantages. However, they also have some disadvantages (the bulkiness the lack of integration, excessive prices, etc.) limiting their use (Table 1.1).

A small change of the pH has a tremendous impact on ecosystems. Then the pH measurement is crucial for environmental monitoring. Existing pH sensors are bulky, fragile and especially very expensive. Not only but pH is a critical factor in the production of many food products and accuracy is the most important criteria for measuring pH level in the food industry. pH is also paramount for clinical monitoring. Due to biocompatibility, infections and size concerns, the need for wireless and battery-less is evident. Also, the large size of these pH-measuring devices makes them unsuitable for invasive diagnostics and use in medicine, for example:

more specific applications where existing commercial pH sensors are not well adapted and have some disadvantages, limiting their use.

Table 1.1 Comparison of different commercial pH sensing devices

pH sensing technology	**Advantages**	**Disadvantages**
Paper strips	• disposable, • very cheap, • no need for calibration, • no need for a reference electrode.	• very low precision, • subjective visual reading, • non-connectable with electronic devices.
Glass pH electrodes	• high precision, • high reliability.	• fragile (risk of broken glass), • bulky, • expensive, • need to be correctly stored, • long response time, • needs calibration before each measure, • need a reference electrode.
ISFET pH Electrodes	• resistant (no risk of broken glass), • can be stored dry, • short response time.	• more expensive than glass pH electrodes, • hasn't the same stability and accuracy offered by glass electrodes, • known drifting problem, • need calibration before each measure, • need a reference electrode.

CHAPTER 2

IRIDIUM OXIDE

2.1 Introduction

As mentioned in the previous chapter, to perform the pH measurement, it is important to have two electrodes: a working electrode (sometimes called sensing electrode) and a reference electrode. In this section, we will try to make materials investigation to find the best material for pH sensing and the best deposition technique.

Various metal oxides have been proposed for pH sensing including Iridium oxide, RuO_2, TiO_2, PtO_2, OsO_2, Ta_2O_5, SnO_2 and RhO_2 (Muaz et al., 2015). As literature suggests (Huang, 2010), IrO_x is the best-adapted material for pH sensing. In fact, PtO_2 and Ta_2O_5 can only be used for pH range from 5 to 10; redox cation interference is reported on OsO_2, TiO_2, RhO_2, PtO_2 and RuO_2; SnO_2 presented calibration issues due to drift problems and unstable responses. However, IrO_x offered high thermal and chemical stability over wide pH ranges, rapid responses, and high durability. For those reasons, Iridium oxide has been proposed to be one of the best pH sensing materials (Huang, 2010). Concerning the reference electrode, we will use the well-known Ag/AgCl, it produces a standard electrical potential that remains the same in different pH range. In this section, we will briefly introduce the mechanism involved in pH sensing, and make a preliminary material investigation.

2.2 pH Sensing Mechanism of Iridium Oxide

Since the 1970s, iridium oxide became a topic of interest in material science for its remarkable chemical, electrochemical and physical properties. In fact, the iridium (Ir) is a noble metal; iridium oxide has a rutile structure shown in figure 2.1; for this reason, it has shown very high resistance to aggressive chemical reagents such as strong acids; it is stable at all pH levels, etc. IrO_x has become the best material for pH measurements in different fields such as biomedical, food industry, environmental and so forth (Huang, 2010).

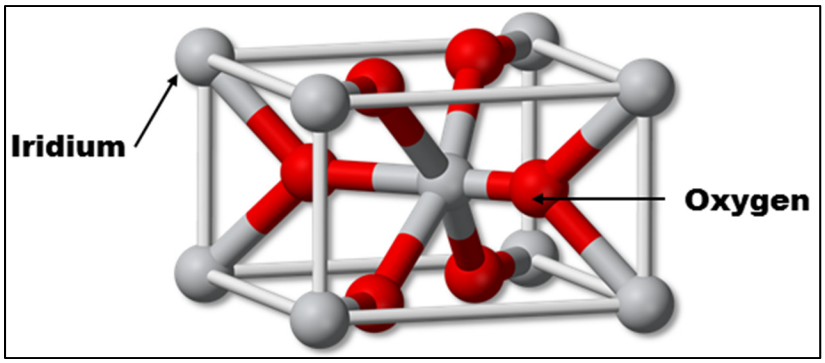

Figure 2.1 Rutile structure

According to literature, at atmospheric pressure and 25ºC, iridium can absorb over 800 times its own volume of hydrogen. IrO_x has a low-temperature coefficient and is one of the few naturally highly conductive oxides; for those reasons it provides a stable and rapid response. The pH response of the iridium oxide electrode is attributed to Ir(IV)/Ir(III) redox transitions which can be illustrated as follows (Huang, 2010):

$$\text{Ir(IV) oxide} + \text{n } e^- + \text{q } H^+ \leftrightarrow \text{Ir(III) oxide} + \text{p } H_2O \tag{2.1}$$

$$2Ir + 3H_2O \leftrightarrow Ir_2O_3 + 6H^+ + 6e^- \tag{2.2}$$

$$Ir + 2H_2O \leftrightarrow IrO_2 + 4H^+ + 4e^- \tag{2.3}$$

$$2\ IrO_2 + 2H^+ + 2e^- \leftrightarrow Ir_2O_3 + H_2O \tag{2.4}$$

The transition effect between two oxidation states Ir_2O_3 and IrO_2 leads to a pH dependent potentiometric response (Huang, 2010):

$$\text{V (Sensing electrode)} = 2{,}303 \times \frac{R \times T}{F} \times pH \tag{2.5}$$

To be able to measure the sensing electrode response, we need a reference electrode which has a potential independent of pH or temperature; it is called standard potential. In this case, the

pH sensor response is the differential potential between the reference electrode and the working electrode; this response is called Nernst equation (Huang, 2010):

$$Vout = V(refrence\ electrode) - V(working\ electrode) \quad (2.6)$$
$$= E^0 - 2{,}303 \times \frac{R \times T}{F} \times pH$$

Where:

- E is the differential potential measured between the working electrode and the reference electrode (expressed in mV);
- E0 is the standard potential of the reference electrode (expressed in mV);
- 2.303 is a constant obtained from Ln-to-Log conversion;
- R is the gas constant (with a value of 8.314, expressed in J/mol·K);
- T is the temperature expressed in K;
- F is the Faraday's constant with a value of 96,485 expressed in C/mol.

2.3 Different deposition techniques of Iridium oxide

According to literature, there are three known deposition techniques for Iridium oxide: Sol-gel (Huang et al., 2011), electrodeposition (Hu et al., 2009), and sputtering (Franklin et al., 2009). In this part, we will briefly describe and consider only the first two deposition techniques (Sol-gel and electrodeposition), because sputtering requires pure Iridium target (very rare material) which is expensive and we do not have it.

2.3.1 Sol-gel Deposition of Iridium oxide

Sol-gel deposition is a technique developed in the 1960s; the aim is to dissolve the desired compound in a solution to bring it back to a solid, in a controlled process. The sol-gel coating of Iridium oxide process usually consists of the following steps (Figure 2.2) (Huang, 2010) (Huang et al., 2011):

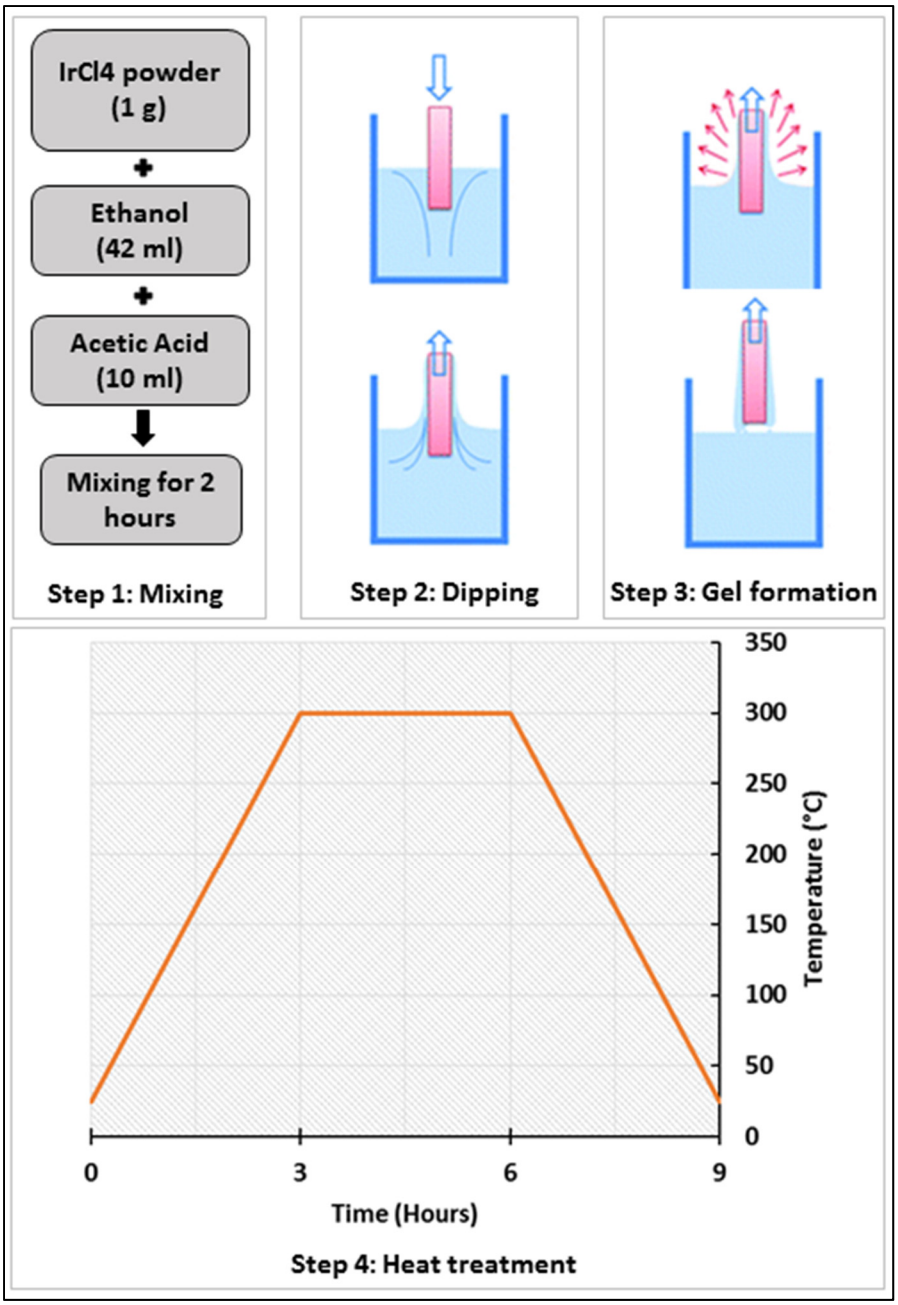

Figure 2.2 Sol-gel process

Step 1: The Iridium particles are dispersed in a solution, to prepare the solution we dissolved 1 gram of $IrCl_4$ into 42 ml of Ethanol and 10 ml of Acetic acid, the solution was mixed for 2 hours at room temperature using magnetic rod stirring. The resulting solution (a stable dispersion of Iridium particles) has a dark-brown color;

Step 2: The substrate is dipped in the solution and is progressively covered by a coating containing the desired material (Iridium);

Step 3: The particles in the solution are polymerized through the removal of the stabilizing components (by evaporation) and provide a gel coat;

Step 4: Heat treatment removes the remaining organic components and oxidize the Iridium to become IrO_x. By using a programmable oven, we progressively increase the temperature with a rate of 1.5 °C/min, when it reaches 300 °C the temperature is kept stable at that value for 3 hours, and finally, it decreases progressively with a rate of 1.5 °C/min, until it cools down. Figure 2.3 shows the results of a Scanning Electron Microscopy (SEM) and Energy Dispersive Spectroscopy (EDS). The results confirm that we get a uniform Iridium oxide formation.

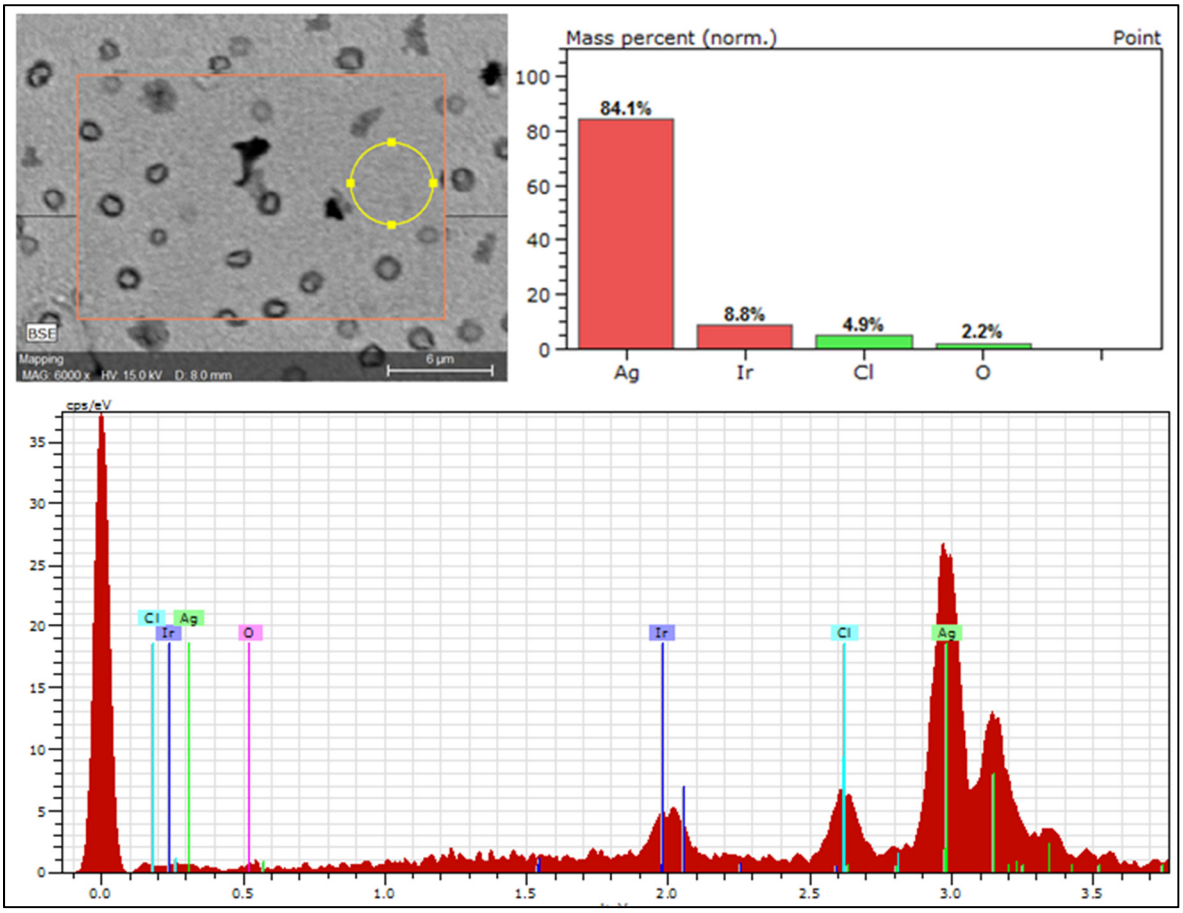

Figure 2.3 SEM and EDS after sol-gel deposition of Iridium oxide

The most important parameter for the working electrode is its sensitivity (S) expressed in (mV/pH) as follows (Huang, 2010):

$$S = \frac{2.303 \times R \times T}{F} \tag{2.7}$$

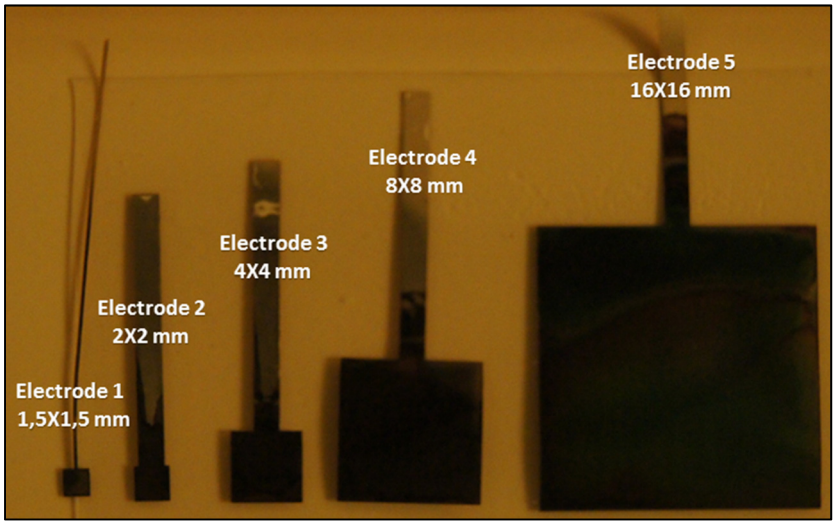

Figure 2.4 Different sized working electrodes

Our aim is to develop a miniaturized pH sensor. For this reason, it is important to study the effect of the miniaturization on the sensitivity. To do that, we prepared five different sized electrodes (figure 2.4) using the sol-gel process described previously. To study the effect of size, we have to be sure that all electrodes have the same properties: the same chemical composition, structure, etc. To be able to do that, all those electrodes were prepared at the same time in the same batch and exposed to the same parameters. In fact, they were made simultaneously using the same sol-gel solution and heated in the same oven at the same time. Then, we are sure that only the size of each electrode was different. To confirm that, we performed an Energy Dispersive Spectroscopy (EDS). According to the EDS analyses shown in figure 2.5, all electrodes have approximately the same chemical composition, only the size changes. Since only IrOx is involved in pH sensing (Huang, 2010); then, in this EDS analyze we setup the software to show only the ratio in mass percent of Iridium vs. Oxygen, and ignore other chemical elements such as Chlorine, Carbon, etc.

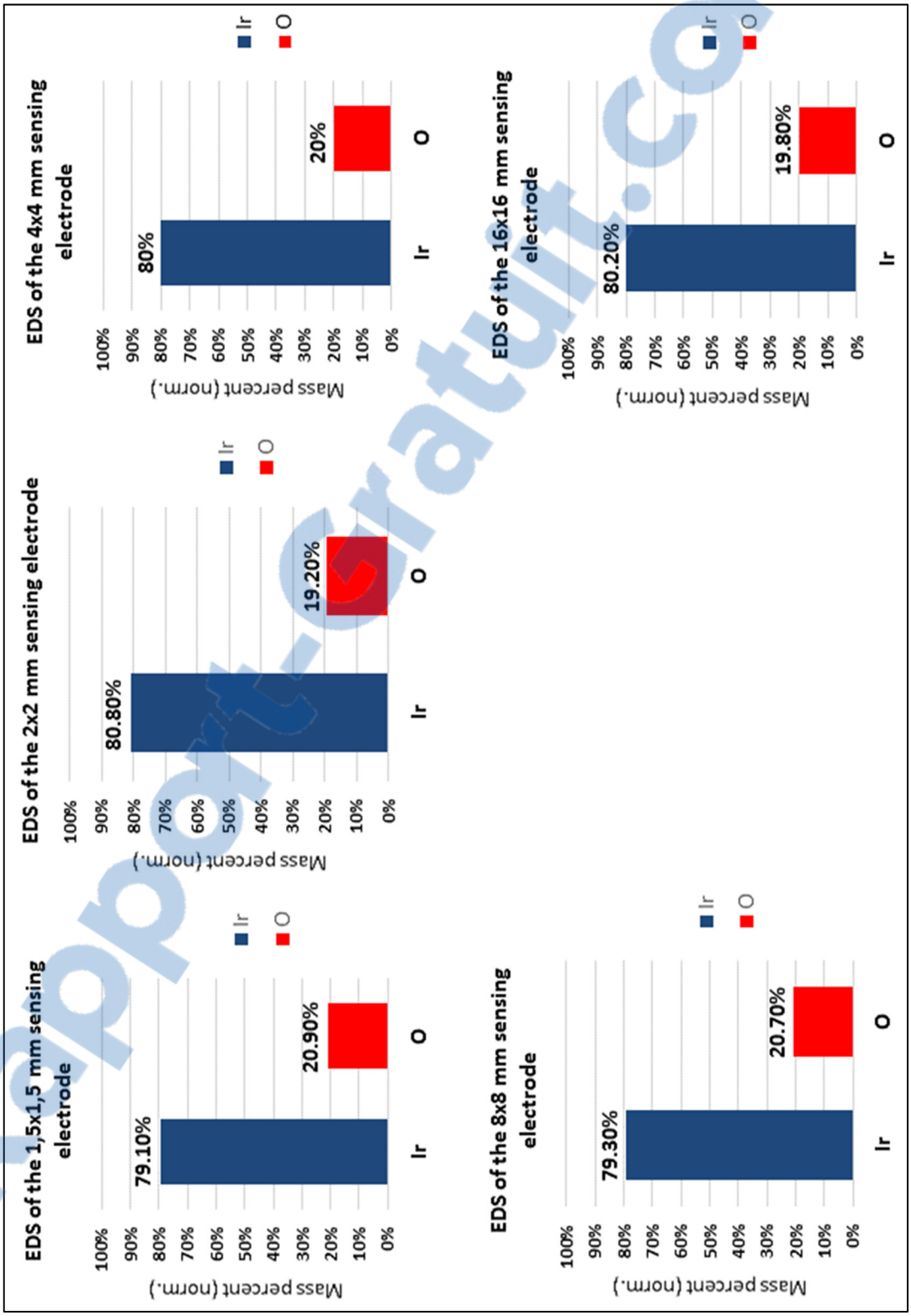

Figure 2.5 Energy dispersive spectroscopy of different sized electrodes (Iridium vs Oxygen in mass percent)

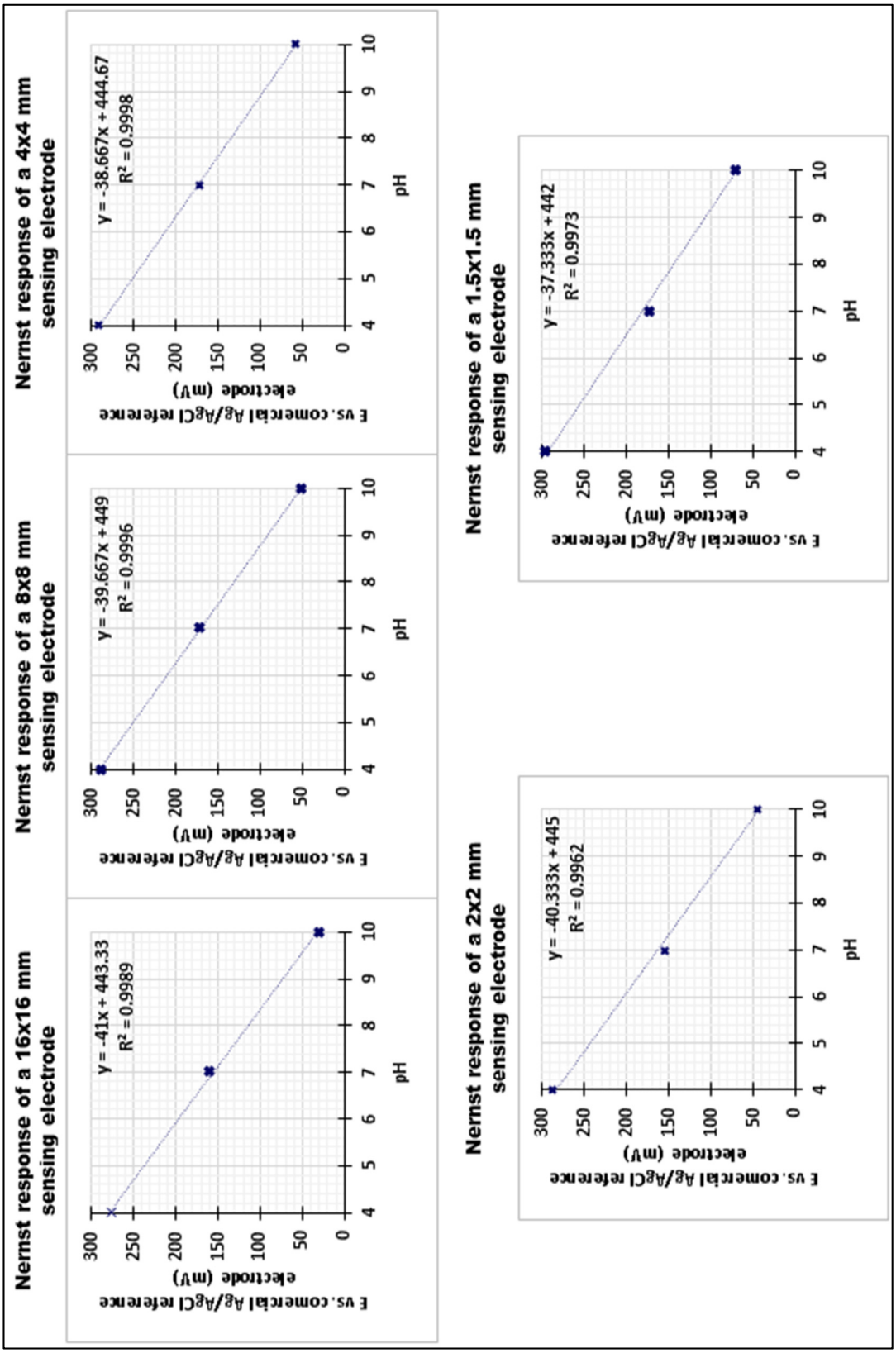

Figure 2.6 Nernst response of different sized working electrode vs. a commercial Ag/Ag-Cl electrode at 19°C

To calculate the sensitivity of each electrode we used three buffer solutions with a known pH; pH of 4.01(Acid), pH of 7 (Neutral) and pH of 10 (Alkaline). According to results illustrated in figure 2.6, the miniaturization does not have a significant impact on the sensitivity and all electrodes (Based on sol-gel) showed a Nernstian response. For this reason, iridium oxide is a good candidate for pH sensing. Using the Nernst response, we can extract the standard potential of the commercial reference electrode and the sensitivity of each sensing electrode (Table below).

Table 2.1 Sensitivity vs size

Sensing electrode size	**Sensitivity at 19°C**	**standard potential of the commercial electrode**
16x16 mm	41 mV/pH	443 mV
8x8 mm	39.66 mV/pH	449 mV
4x4 mm	38,6 mV/pH	444 mV
2x2 mm	40,33 mV/pH	445 mV
1.5x1.5 mm	37,33 mV/pH	442 mV

To characterize each sensing electrode, we used the same commercial Ag/Ag-Cl reference electrode. In literature, many people claimed that they get a sensitivity equal to 50-60 mV/pH using sol-gel deposition (Huang, 2010) (Huang et al., 2011). Initially we thought that we had achieved worse results; we get only 41 mV/pH but in reality, we have good results. In fact, according to the Nernst equation, the sensitivity is correlated with temperature as follows (Bhadra et al., 2013):

$$S = 2{,}303 \times \frac{R \times T}{F} = cte \times T \tag{2.8}$$

R and F are constant and known, so the sensitivity of the sensor is associated with the temperature: if the temperature increases the sensitivity increases too and vice versa (the reactivity of IrO_x increases at a higher temperature and absorbs more H^+ protons). We

measured the sensitivity at room temperature (On that day, it was 19°C. We did not control the temperature, we just used an external thermometer to measure it.) while others measured it at different room temperature 25°C. It had a significant impact. For instance, at 19°C, it was 41 mV/pH and at 25°C, it became 53 mV/pH.

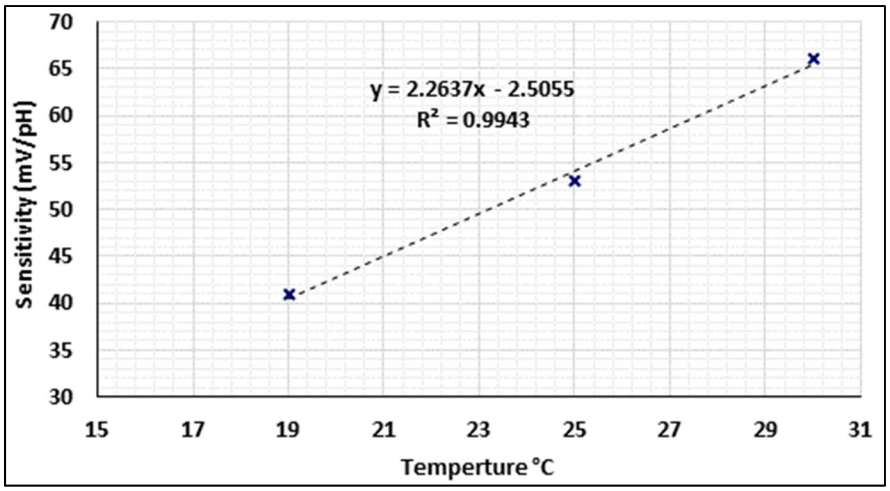

Figure 2.7 Sensitivity of a WE based on sol-gel vs temperature

Figure 2.7 illustrates the sensitivity of a working electrode (WE) based on sol-gel deposition of IrO_x at different temperatures. For this reason, a temperature sensor is generally used with commercial pH sensors to allow adequate compensation (Bhadra et al., 2013).

2.3.2 Electrodeposition of Iridium oxide

Electrodeposition is the application of a conductive coating to another conducting surface by an electrochemical process. The item to be plated is made the cathode of an electrolysis cell through which an electric current is applied. The article is immersed in an aqueous solution (the bath) containing the desired metal in a soluble form (as cations or as ions).

The anode is usually made from noble metal, such as Platinum. IrO_x films can be formed by electrodeposition using a potentiostat (We used model 700E, CH Instruments, Austin, TX). Electrodeposition steps are illustrated in Figure 2.8 as follows (Hu et al., 2009):

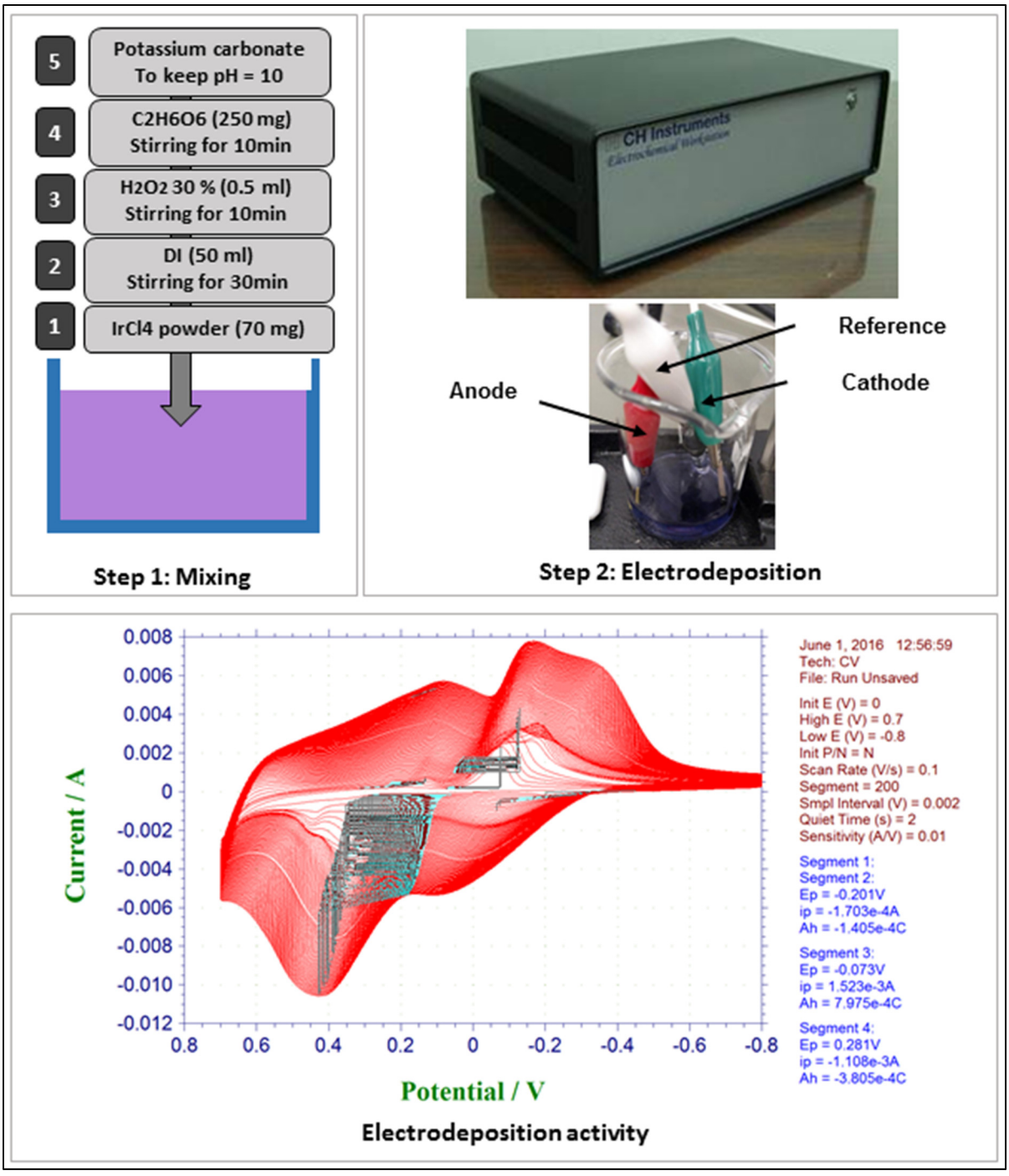

Figure 2.8 Electrodeposition of Iridium oxide

Step 1: We prepared the Yamanaka solution at room temperature as follows. First, 70 mg of $IrCl_4$ (purchased from Artcraft Chemicals, NJ) was dissolved in 50 ml of DI water by stirring

for 30 minutes, followed by adding 0.5 ml of H_2O_2 (30%). After 10 minutes, 250 mg of oxalic acid dehydrates ($C_2H_6O_6$ from Sigma-Aldrich) was added and the solution was stirred for another 10 minutes. The pH was then adjusted to 10.5 by slowly adding potassium carbonate (K_2CO_3 from Sigma-Aldrich). The resulting solution was left for four days to stabilize;

Step 2: To form the IrO_x sensing film, the working electrode was electrodeposited using cyclic voltammetry (CV) feature of the potentiostat with a potential range of -0.8 V to +0.7 V and a scan rate of 0.1 V/s for 50 minutes. Electrodeposition activity which is illustrated in figure 2.8 shows that the current is increasing after each cycle this means that the thickness of electroplated IrO_x is increasing too (IrO_x has higher electrical resistance than Silver).

According to results illustrated in Figure 2.9, we get a linear response, better than the Nernstian response (Called super-Nernstian) with higher sensitivity. In fact, the sensitivity at room temperature (22°C at that time) was equal to 70.66 mV/pH. This non-Nernstian response slopes presented here is explained by the complexation processes in IrO_x membrane (Miyake et al., 2012) We also performed a SEM and an EDS to confirm the formation of Iridium oxide; figures 2.10 (a) and (b) show a uniform deposition of IrO_x. Figure 2.10 (c) shows a map distribution of each element. As we can see, we have a uniform distribution of Iridium and oxygen.

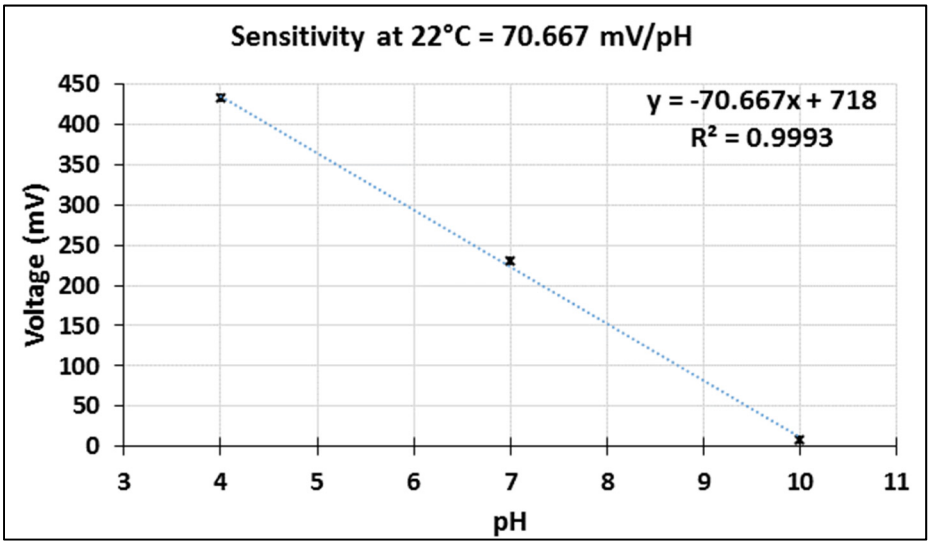

Figure 2.9 pH sensor calibration at room temperature

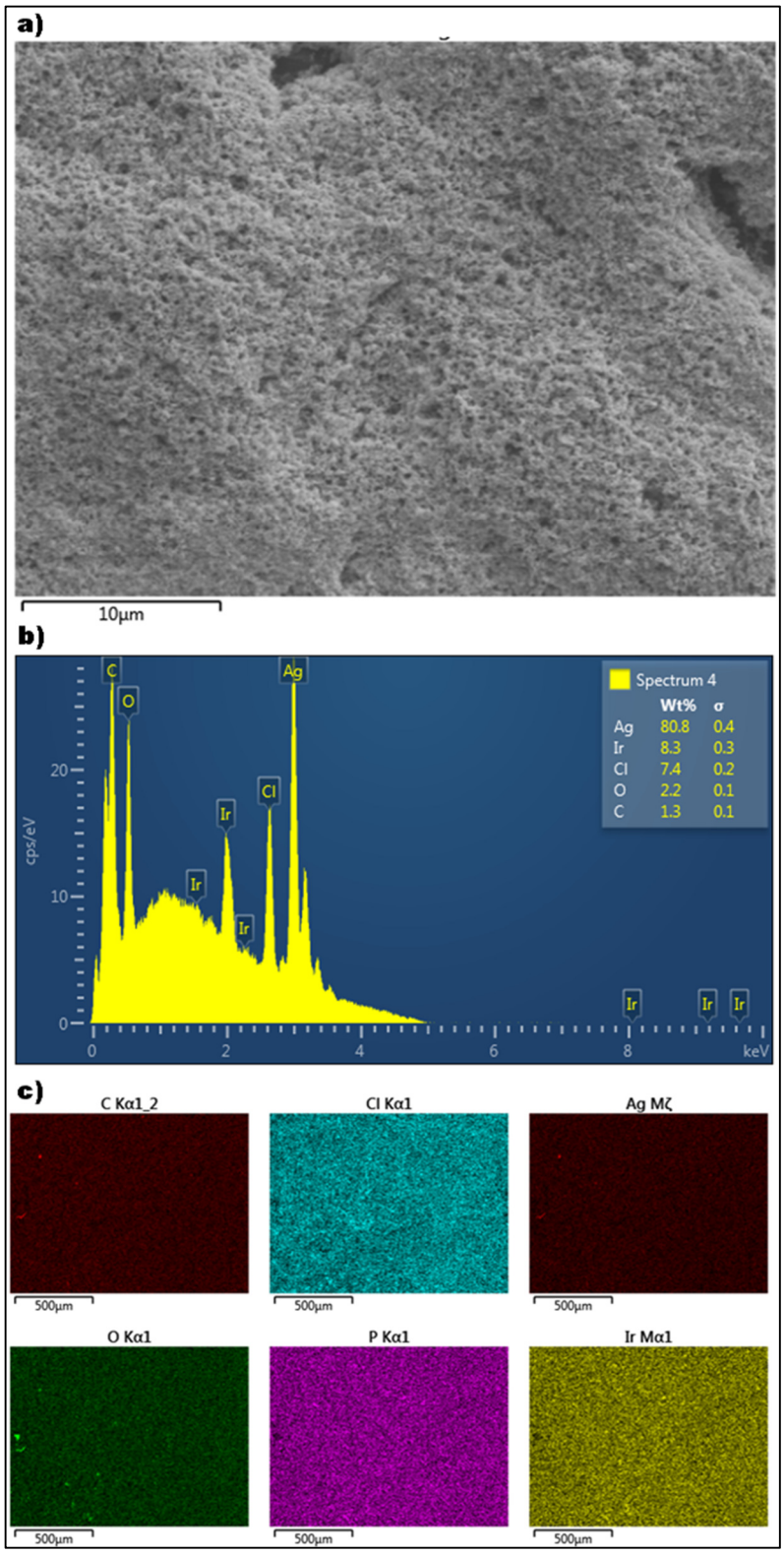

Figure 2.10 a) SEM image, b) EDS analyses, c) Map distribution

2.4 Conclusion

Thanks to its high thermal and chemical stability, Iridium oxide is one of the best materials for pH sensing. We have different deposition techniques; the following table (table 2.2) illustrates a comparison between the two methods: Sol-gel and electroplating. According to our characterization, the working electrode made by the first technique had a Nernstian response with a sensitivity equal to 45 mV/pH at 22°C, when the working electrode made by electrodeposition had a linear but non-Nernstian response with a higher sensitivity equal to 70.66 mV/pH at 22°C (Super-Nernstian response). Unlike sol-gel process which needs thermal treatment; electroplating is done at room temperature which eliminates heat stresses. Then, electroplating is a better deposition technique for IrO_x.

Table 2.2 Comparisons between sol-gel and electrodeposition of IrO_x

Deposition technique	**Advantages**	**Disadvantages**
Sol-gel	• Maybe an alternative to electrodeposition if the last method is Incompatible.	• Nernstian response (Low sensitivity equal to 45 mV/pH at 22°C), • Chemical process (use of solvents), • Require heat treatment (generates heat stress), • Time consuming.
Electrodeposition	• Super Nernstian response with high sensitivity (71 mV/pH at 22°C), • Done at room temperature, • Only two steps.	• Incompatible with thin electrodes (peel off during electrodeposition activity).

CHAPTER 3

pH SENSOR FABRICATION TECHNIQUES

3.1 Introduction

In the previous chapter, we found that IrO_x is one of the best materials for pH sensing. Also, that electrodeposition is better than sol-gel. According to literature, we have many options to make a sensor, the most popular one for sensors are MEMS (Micro-Electro-Mechanical System), and LTCC (Low-Temperature Co-fired Ceramic) (Pietrikova, 2001). In this chapter, we will evaluate different fabrication processes, and try to select the best-adapted technique for the manufacturing of a miniaturized pH sensor targeting specific applications (Medical, food, enviremental monitoring). Selection criteria (feasibility, sensitivity, cost, simplicity, etc.) depends on the target application.

3.2 MEMS pH sensor

MEMS (Micro-Electro-Mechanical System), has been identified as one of the most promising technologies for the 21st century. It is a microfabrication technology similar to integrated circuits. The goal is to manufacture miniaturized components (can range in size from a few micrometers to millimeters). It offers many benefits that's why it is commonly used to design sensors (such as pressure sensors, gyroscopes, etc.). For instance, microfabrication process enables the production of batch devices which reduces the cost and production time, also MEMS devices are more accurate, have lower power consumption and their small size facilitate their integration (Klaus, Paris et Sommer, 2016). To make the pH sensor there are three main steps:

Part 1: Design of electrodes (to design the electrodes, we used three different processes: photolithography, sputtering, and lift-off.);

Part 2: IrO_x deposition (Sensing electrode);

Part 3: Ag/AgCl deposition (reference electrode).

3.2.1 Photolithography

The photolithography is a photographic approach to transfer a pattern from a mask onto the surface of a substrate. A thin layer of a polymer, which is sensitive to ultraviolet (photoresist), is then deposited on the substrate by centrifugal force; The coated substrate is exposed to the ultraviolet transferring the pattern from the mask to the photoresist which is then developed in a way similar to the process used for developing photographic films. The radiated ultraviolet causes a chemical reaction in the exposed areas of the photoresist. There are two types of photoresist positive and negative. Positive photoresist is polymerized and strengthened by UV whereas negative photoresists are weakened. A developer is used to remove the weakened part and reveal the desired patterns (figure 3.1).

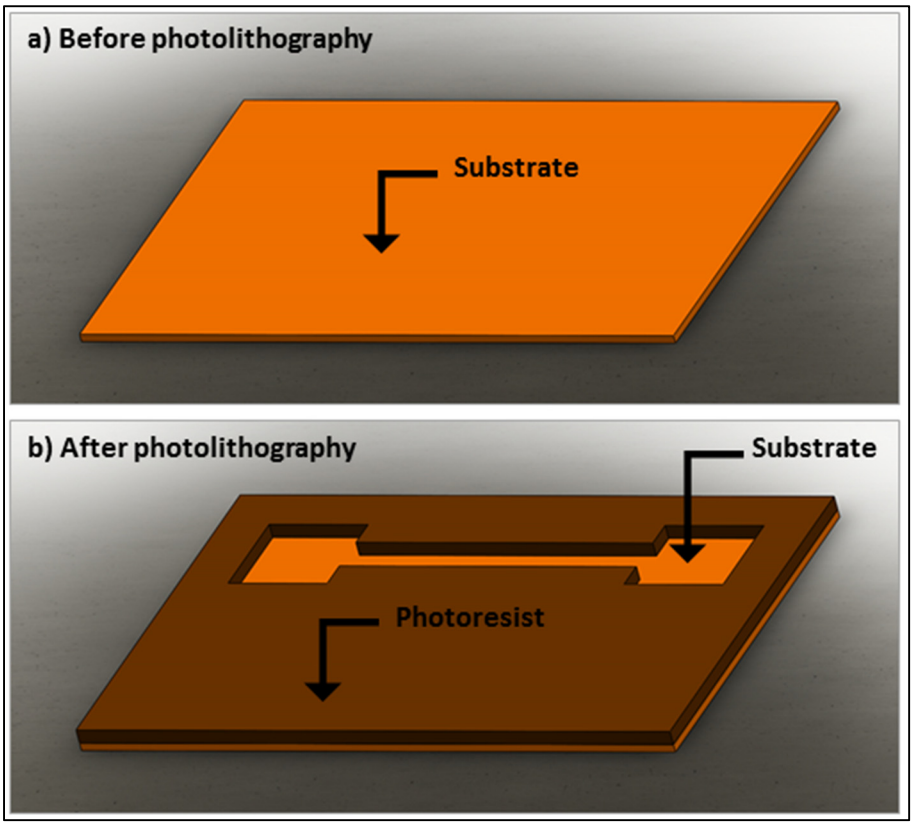

Figure 3.1 Photolithography

3.2.2 Sputtering

Sputtering is a process used to deposit very thin films of material onto a surface of a substrate. It is a physical deposition technique: it starts by the generation of a plasma and then the acceleration of ions from this plasma into the source material which is commonly called target. If the material is a metal; then, we use a direct current (DC) to generate the plasma if it is not; then, RF current is preferred. The arriving ions attack the target and eject neutral particles via energy transfer in the form of which will travel in a straight line unless they come into contact with the substrate which will be coated with a thin film of the source material. For our case, we deposited a thin layer of chromium 100 nm to allow a better adhesion of the second layer of silver 700 nm (known to be one of the best conductive material). Finally, we deposit 200 nm of gold known to be chemically inert (Figure 3.2).

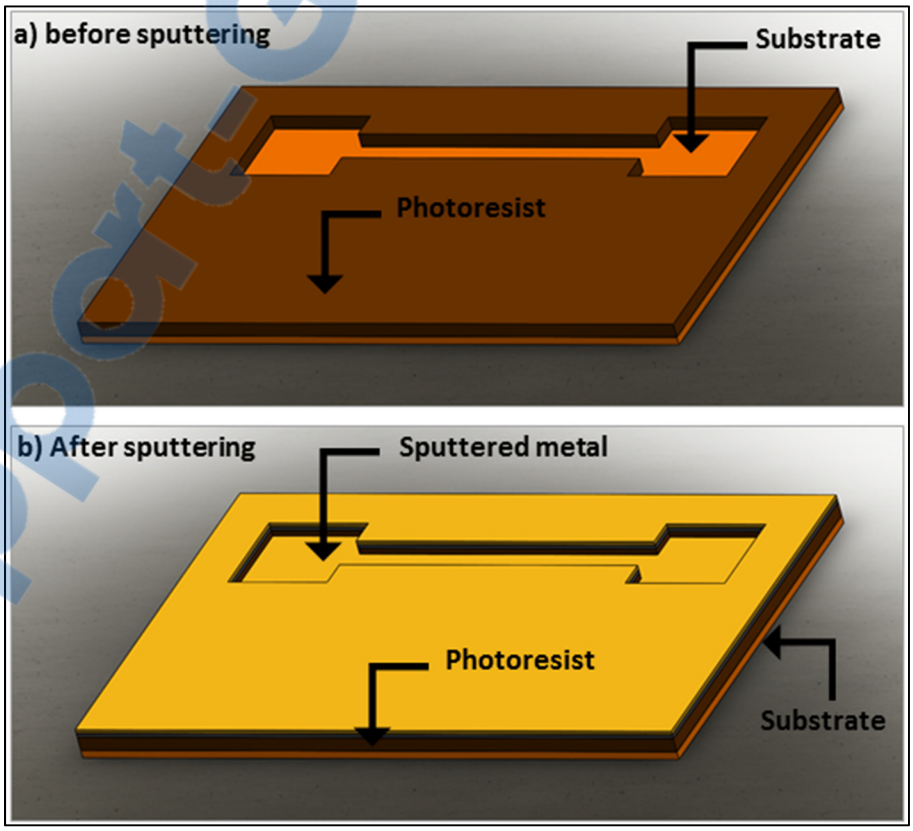

Figure 3.2 Sputtering

3.2.3 Liftoff

We used Acetone to remove the photoresist; the material directly deposited on top of the substrate will remain, and the material sputtered in the upper part of the photoresist will be removed exposing the desired electrodes. (Figure 3.3).

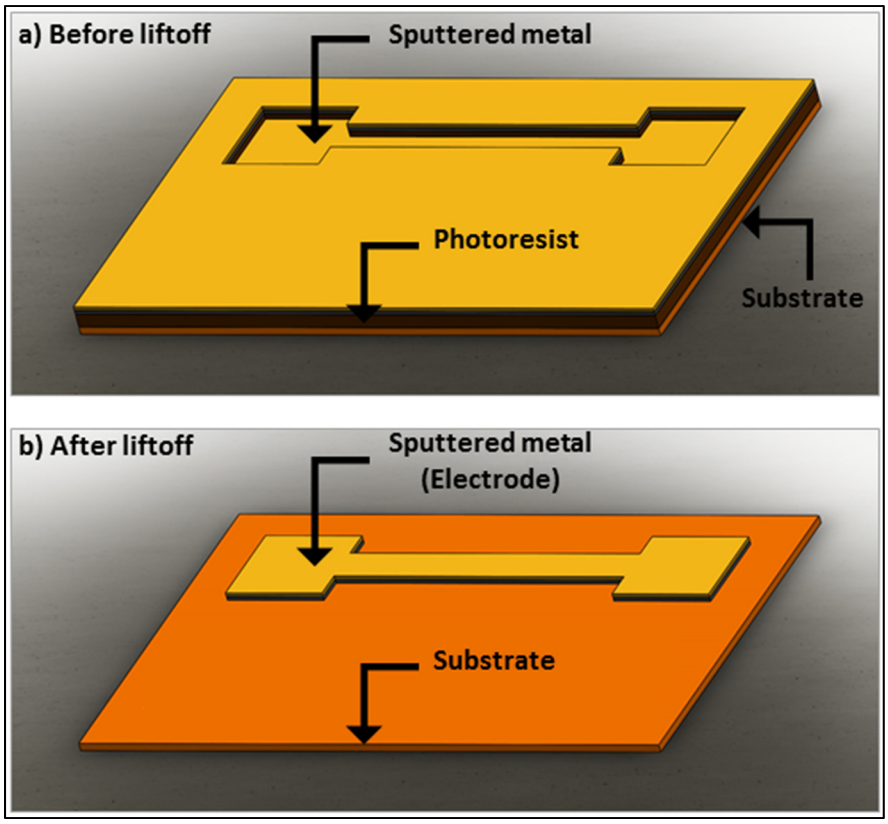

Figure 3.3 Liftoff

3.2.4 IrO_x deposition

Sputtering allows the deposition of very thin layers; Figure 3.4 shows that the thickness of our electrodes is 0.9 um. According to our investigation in chapter 2, electrodeposition offers a better sensitivity compared to sol-gel deposition. For instance, at room temperature (22°C) sol-gel deposited IrO_x has a sensitivity equal to 45 mV/pH; electrodeposited IrO_x sensitivity is equal to 71 mV/pH.

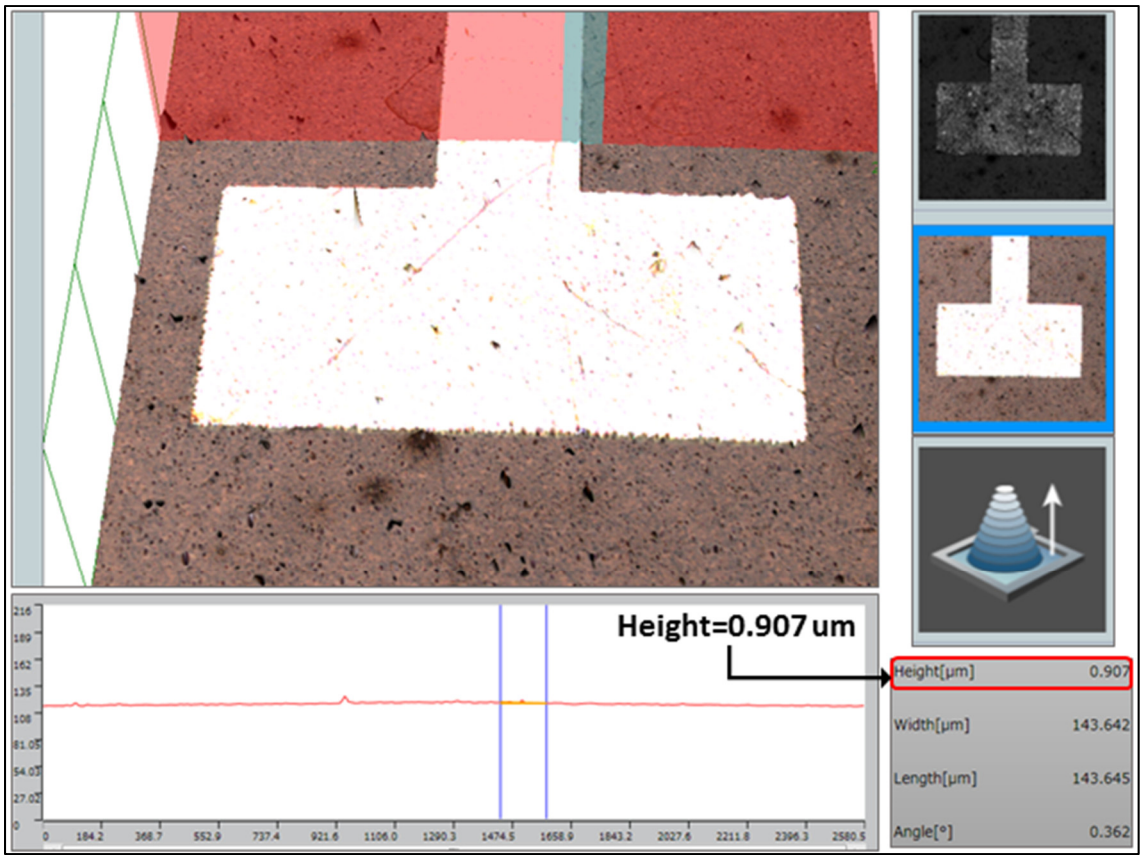

Figure 3.4 Electrode thickness measurement

For that reason, first, we tried to deposit IrO_x via electrodeposition. Unfortunately, the thickness of the sputtered electrode is not enough to support the electrodeposition activity, for instance, the sputtered metal peel off during this process (figure 3.5).

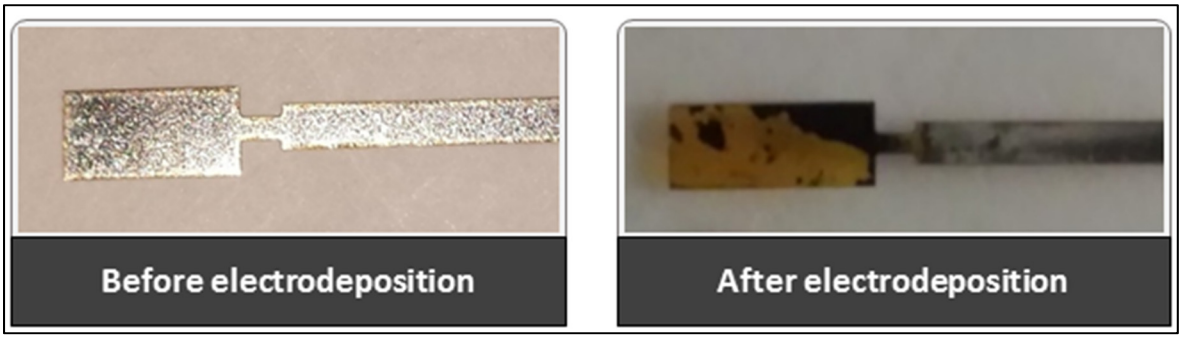

Figure 3.5 Electrodeposition result with sputtered thin conductor

To overcome the problem encountered in electrodeposition; we tried sol-gel deposition as an alternative (explained in chapter 2); here too, we faced many difficulties:

- We first tried to use Lithography and Lift-off process to protect some area and deposit IrO_x only in the desired areas; the problem is that we used solvents (Developer and Acetone) to remove the photoresist, but solvents will also remove the deposited gel containing Iridium;
- To solve the problem, we used a laser-cutting machine to create a protective mask made from an electrostatic film; we aligned it manually then we deposited the gel containing Iridium. (manual alignment, reduce the precision);
- When the gel containing Iridium became dry, we removed the mask, and the batch of sensors was co-fired. The heat stress generated by the dilatation of different superposed materials (Kapton, Chromium, Silver, Gold, IrO_x), created many cracks (illustrated in Figure 3.6).

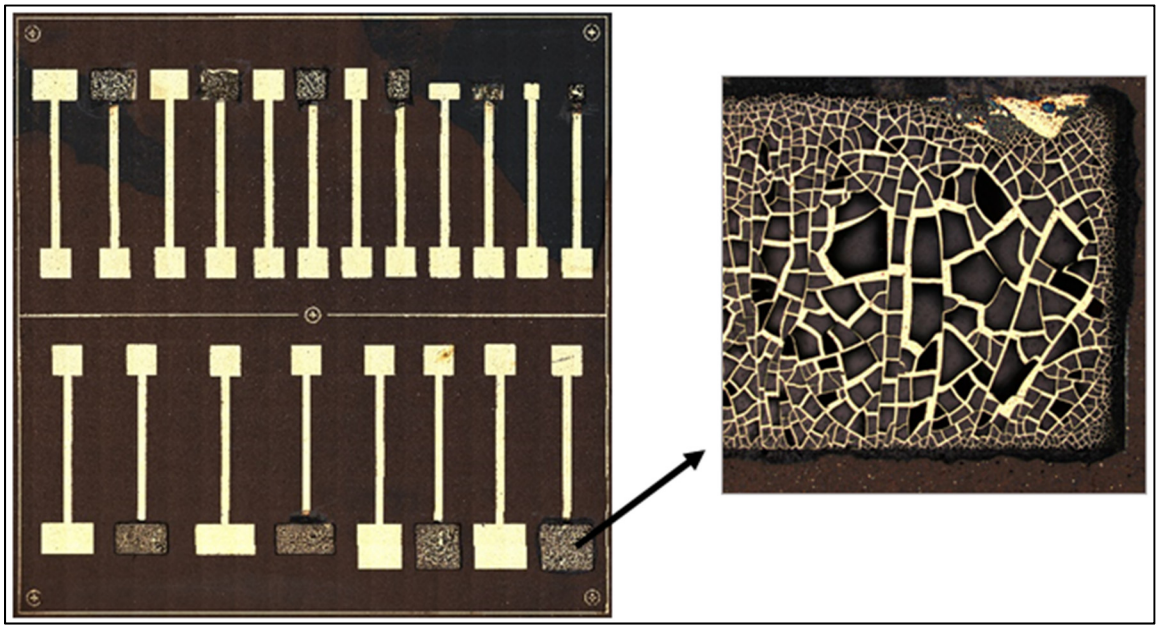

Figure 3.6 Cracks formation due to thermal stress

Then, we have to admit that microfabrication technique (steps are shown in figure 3.7) is simply not well adapted to the two deposition techniques of IrO_x (electrodeposition and sol-gel) then it is not the fabrication process for our pH sensor.

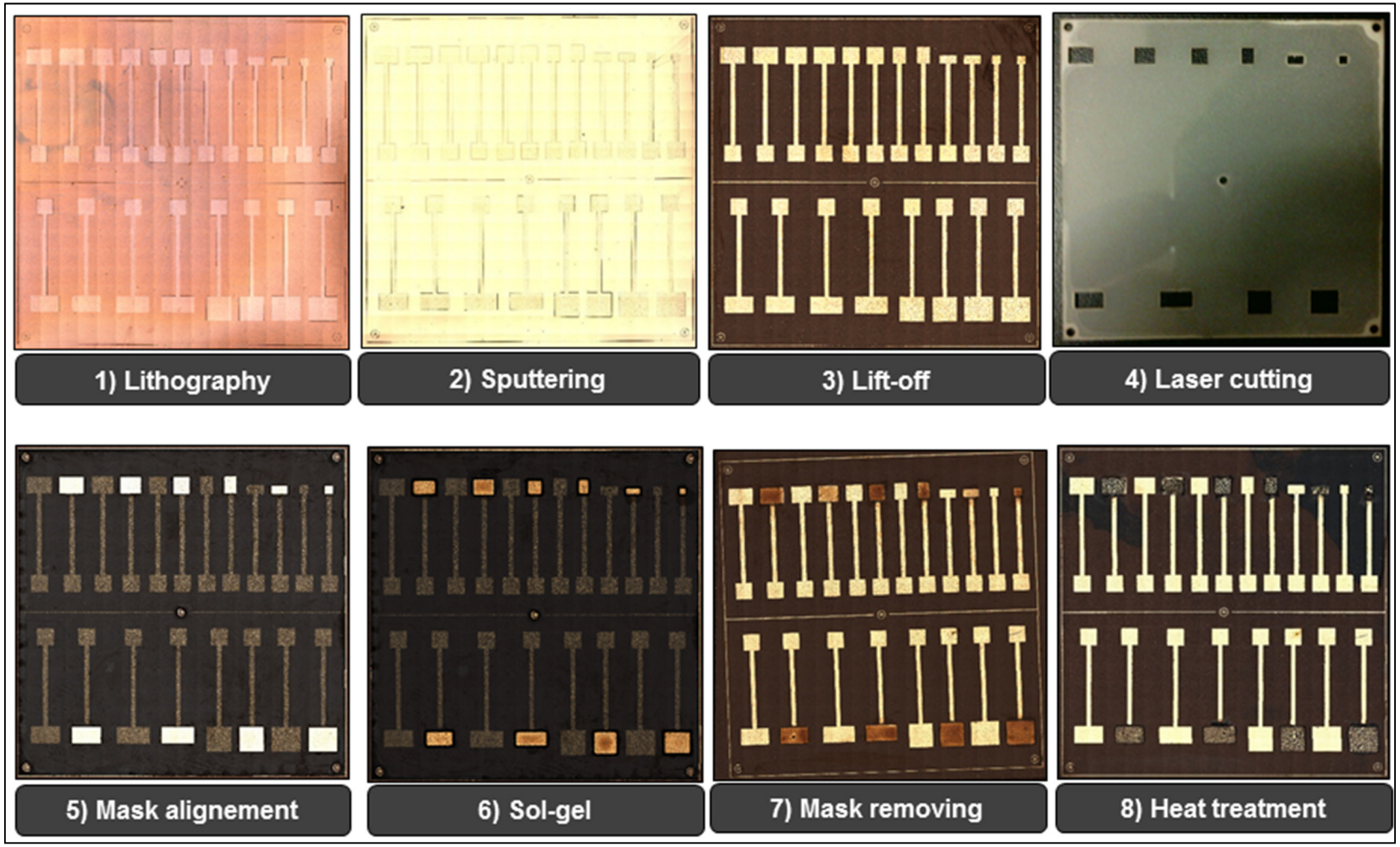

Figure 3.7 Microfabrication steps

3.3 Laser micromachined pH sensor

To avoid the use of solvents, we developed a process (Figure 3.9) using infrared laser etching instead of chemicals:

Step 1: we cleaned and prepared the substrate;

Step 2: we sputtering a thin layer of silver;

Step 3: we designed the layout;

Step 4: we used a laser to etch and cut the electrodes;

Step 5: Sol-gel deposited iridium was then heat treated to transform it into IrO_x (working electrode);

Step 6: Finally, we applied Ag/AgCl paste as a reference electrode.

With this technique we cut the electrodes before co-firing; then, we reduced the surface, doing so, we reduced heat stresses. As a result, (Figure 3.8) we get a uniform deposition of IrO_x.

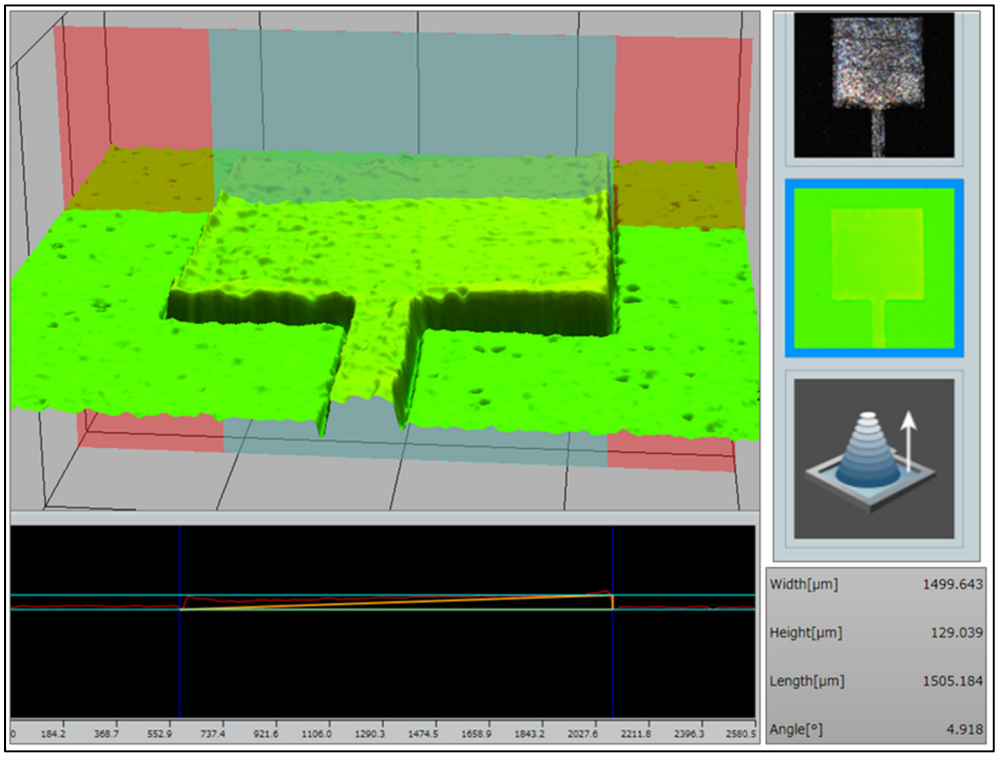

Figure 3.8 Uniform surface of IrO_x after laser cutting and sol-gel deposition

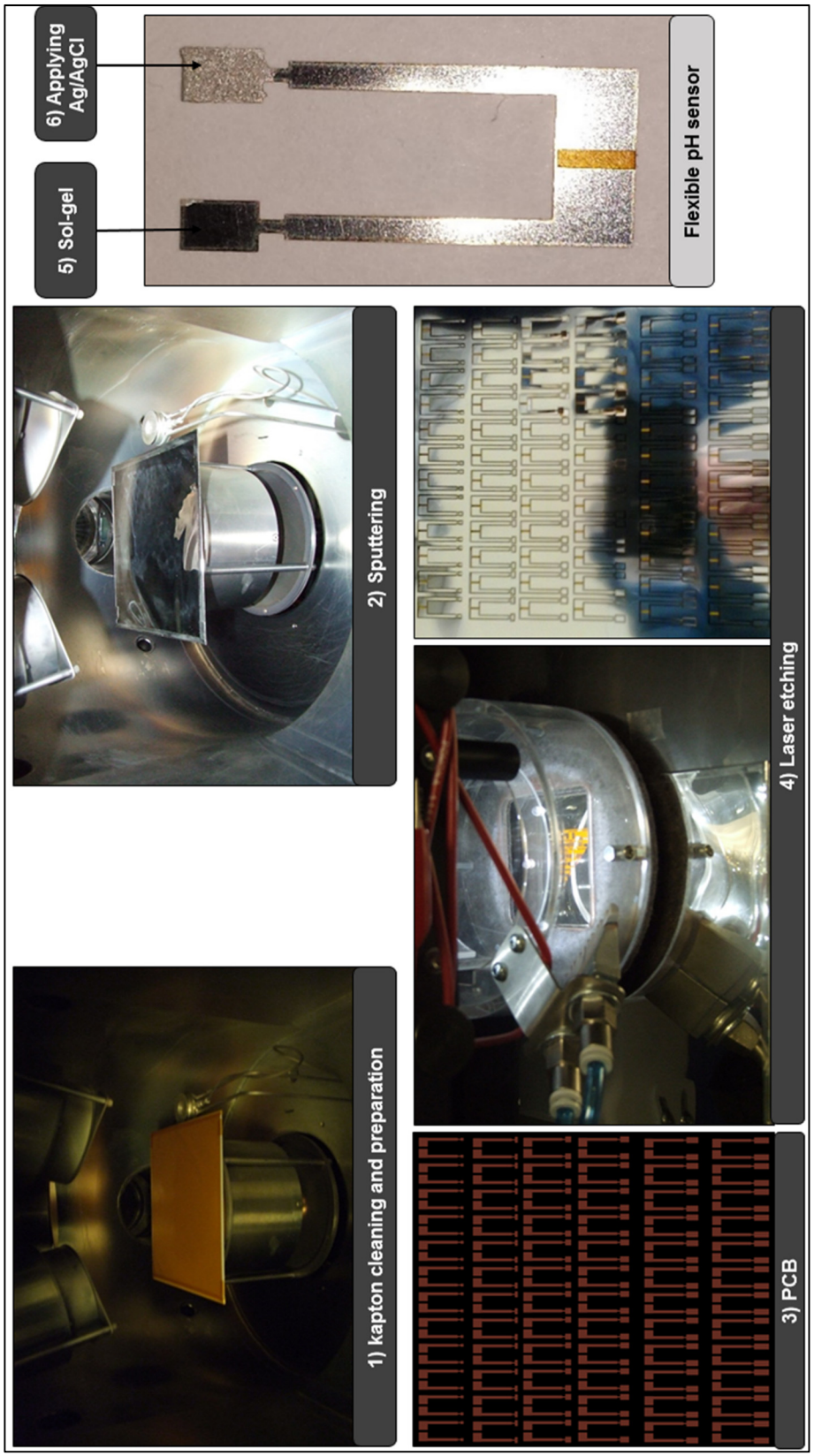

Figure 3.9 Laser etching fabrication chain

To calculate the sensitivity of this sensor we used three buffer solutions with a known pH; pH of 4.01(Acid), pH of 7 (Neutral) and pH of 10 (Alkaline). According to results illustrated in figure 3.10, we get a linear Nernstian response, in fact, the sensitivity at 19°C is equal to 40 mV/pH.

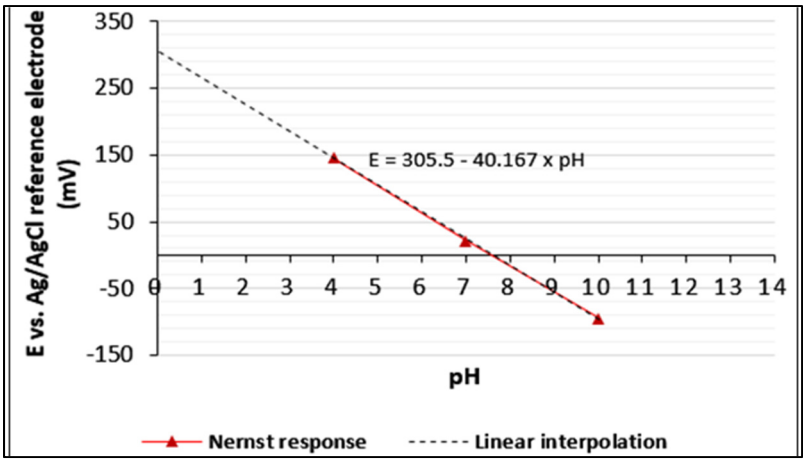

Figure 3.10 Laser micro-machined pH sensor response at 19°C

Compared to MEMS, this technique is simpler, faster, doesn't need chemicals and is compatible with the sol-gel deposition but it is still not compatible with electrodeposition because of the thickness of the conductive layer (very thin). Then, this technique is suitable for flexible devices because sputtered conductive thin layer is flexible in opposition to thick traces.

3.4 LTCC based pH sensor

Low temperature co-fired ceramic (LTCC) technology has been used since the 1950s, especially for radio-frequency (RF) and high-frequency applications. Further, it also offers an excellent integration capability (up to 10 layers, feature size can be 15 µm) to reduce the entire device size compared with systems based on printed circuit boards (PCB). For instance, it allows for the production of three-dimensional structures while providing integration with sensors and electronic components in the same ceramic substrate (Pietrikova, 2001). As Au and Ag's metal traces are used, providing enhancements in conductor thickness compared to sputtering.

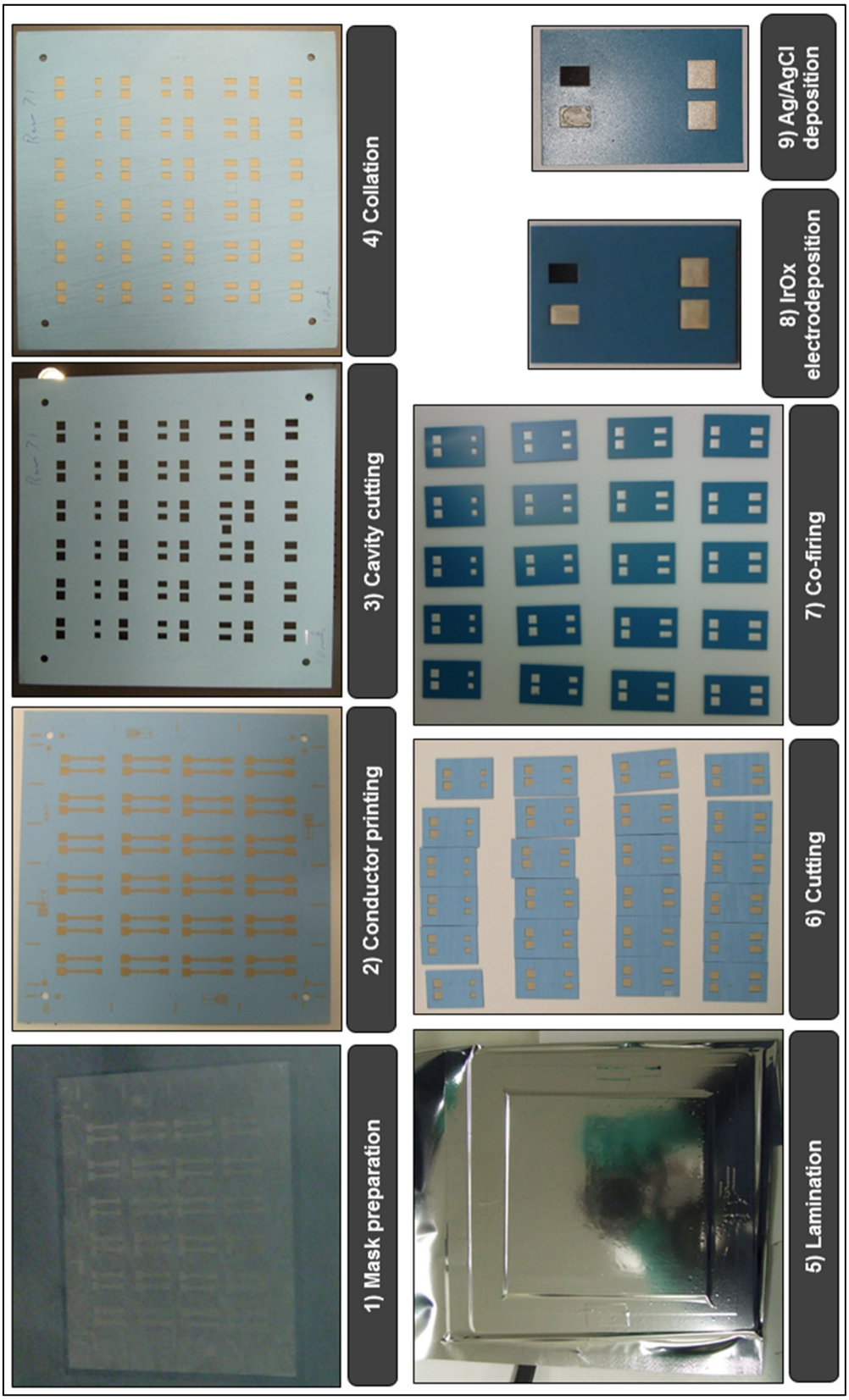

Figure 3.11 LTCC pH sensor fabrication chain

We used two DuPont's 951AT layers as a substrate, and all steps followed an industry-standard LTCC fabrication chain (figure 3.11). The first step was to prepare the mask. Next, the traces were printed using a mask and DuPont's silver paste. A laser-cutting machine was used to create a testing chamber. The two layers were aligned using a high-precision aligner and pressed together using hydraulic pressure. Finally, the batch of sensors was separated using a guillotine and the resulting laminated circuit was co-fired.

Further, since the thickness of the printed conductor (shown in figure 3.12, is equal to 9.955 um) is significantly greater than those formed by other methods, such as sputtering (0.9 um); then, LTCC is convenient with both sol-gel and electrodeposition of IrO_x. Knowing that electrodeposition allows a better sensitivity; then, we chose this last method.

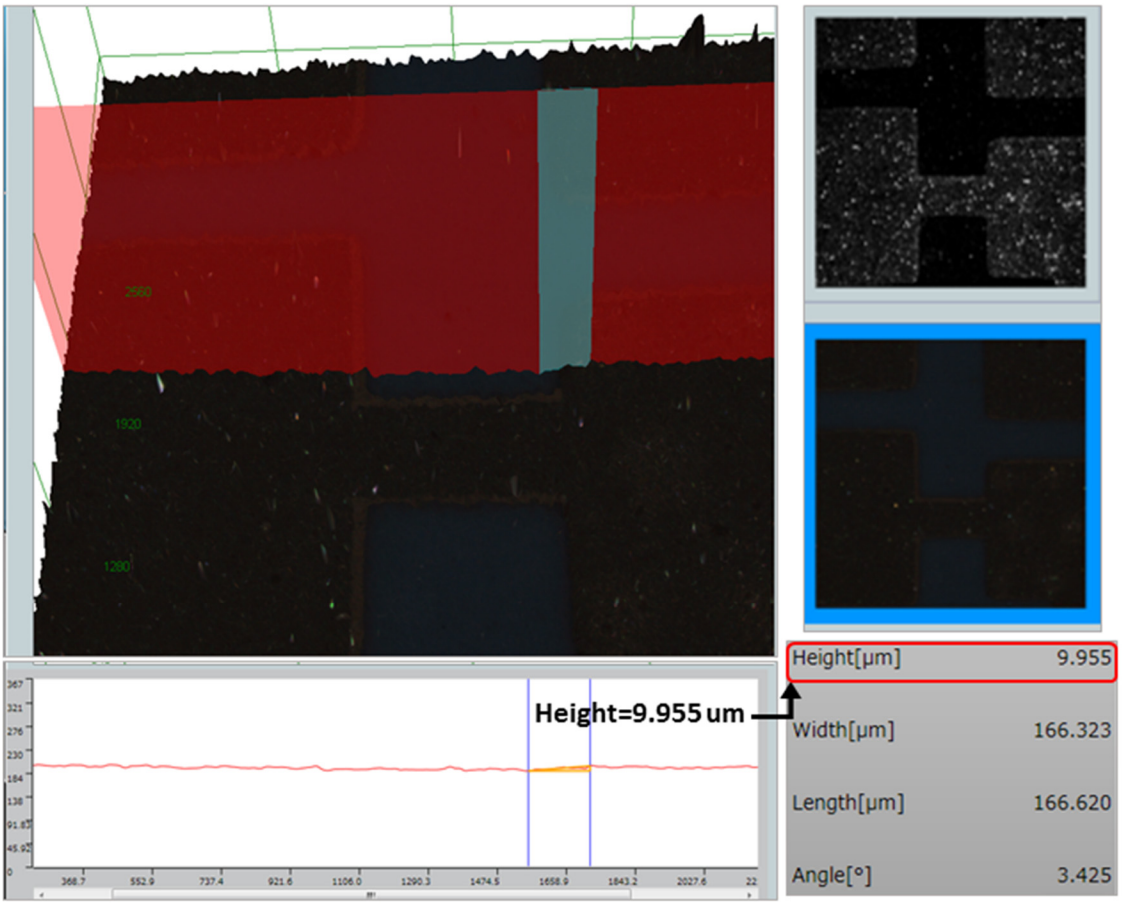

Figure 3.12 Silver thickness measured before electrodeposition of IrO_x

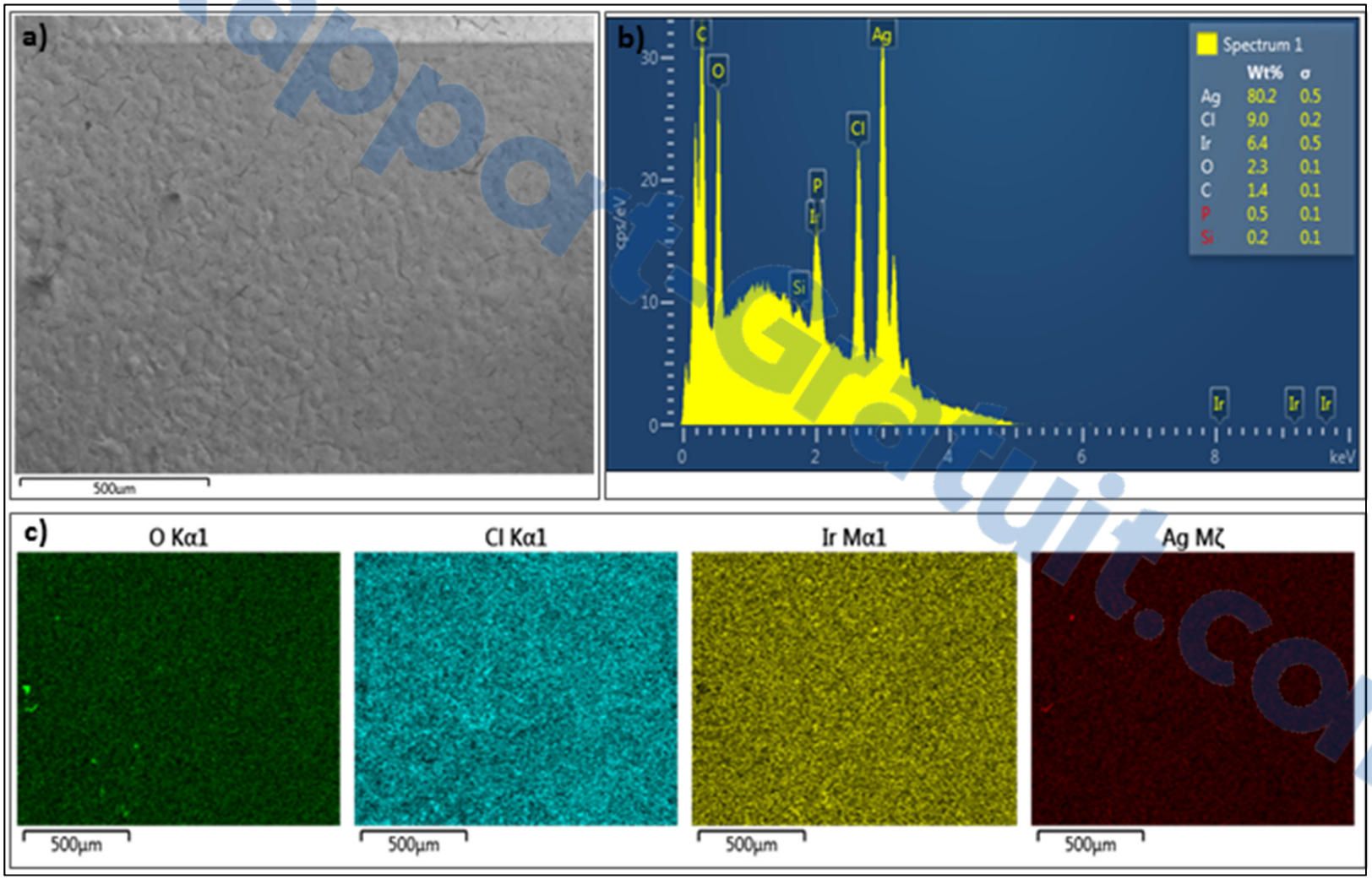

Figure 3.13 a) SEM image, b) EDS analyses, c) Map distribution

To form the IrO_x sensing film, the WE was electrodeposited using cyclic voltammetry (CV) feature of the potentiostat with a potential range of -0.8 V to +0.7 V and a scan rate of 0.1 V/s for 50 minutes. Figure 3.13 shows the results of a Scanning Electron Microscopy (SEM) and Energy Dispersive Spectroscopy (EDS). The results confirm that we get a uniform Iridium oxide formation. To reduce costs and time, as well as to obtain a compact size of the system compared with those using the glass RE electrode, our RE was simply printed using the Ag/AgCl paste.

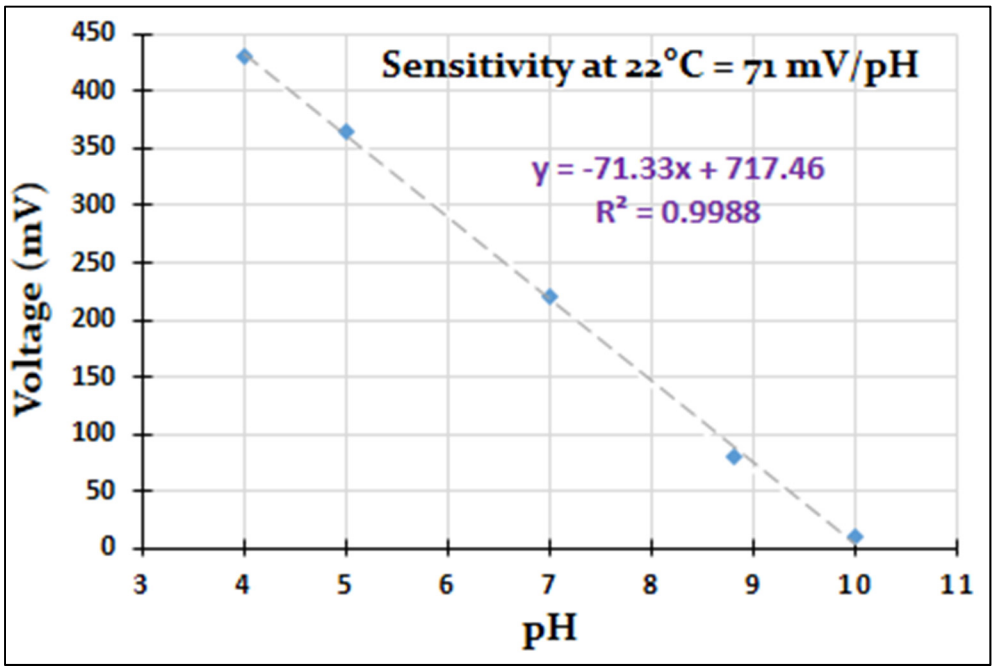

Figure 3.14 LTCC pH sensor calibration at room temperature

We used five different solutions with pH values of 4, 5, 7, 8.8 and 10 to calibrate our pH sensor, at room temperature. Buffer solutions with pH of 10, 7 and 4 were purchased from Fisher Scientific, while the ones with pH of 5 and 8.8 were made in house using DI water and buffer solutions. The pH values were determined using a commercial pH meter (SPER Scientific). The calibration results were plotted in figure 3.14, showing a super-Nernstian response with the sensitivity slope of 71 mV/pH. The response was also highly linear ($R^2 = 0.9988$).

3.5 Conclusions

Microfabrication technique (MEMS) is simply not adapted for the two deposition techniques of IrO_x (electrodeposition and sol-gel). In fact, heat treatment generates heat stresses, resulting in the formation of cracks. Also, the use of solvent dissolves the coating during sol-gel. Then, this technique is not a convenient fabrication process for our pH sensor. In terms of simplicity and cost, laser micro-machined pH sensor is a good option; except the fact that, sputtered thin conductor cannot support electrodeposition activity. Then, it is only compatible with sol-gel deposition (Electrodeposited IrO_x have a better sensitivity than sol-gel deposited IrO_x). LTCC proved to be the most suitable fabrication technique, in fact, it allows a better integration and miniaturization; it is compatible with both electrodeposition and sol-gel deposition of IrO_x, and it allows batch production which reduces costs. (Table 3.1 resumes the main advantages and disadvantages of each fabrication technique).

Table 3.1 Comparison of different fabrication techniques

Fabrication technique	**Advantages**	**Disadvantages**
MEMS pH sensor	• High integration (Precision 10 um).	• Incompatibility with sol-gel deposition due to the use of solvents, • Heat stresses are generated during heat treatment (cracks formation), • Sputtered electrodes are very thin and did not resist to electrodeposition activity (they peel off).

Laser micromachined pH sensor	• Precision 15 um, • Very simple and fast, • Allow batch fabrication (Low cost), • No chemicals, • Uniform sol-gel deposition, • Sputtered electrodes are very thin (sensor may be flexible if the substrate is also flexible).	• Sputtered electrodes are very thin and did not resist to electrodeposition activity, they peel off (not compatible with electrodeposition), • Only one-layer schematic design.
LTCC pH sensor	• High integration, • Multilayer 3D design, • Allow batch fabrication (Low cost), • Printed traces are thick, so it is compatible with both sol-gel and electrodeposition of IrO_x.	• Not flexible, • Ceramic contain some traces of plumb (incompatible with in vivo medical applications).

CHAPTER 4

NOVEL MINIATURIZED WIRELESS pH SENSING SYSTEMS

4.1 Introduction

In the previous chapter, LTCC proved to be the best fabrication technique. In fact, it offers an excellent integration capability to overcome the size constraint. For instance, it allows the production of three-dimensional structures while providing integration with sensors and electronic components in the same ceramic substrate. The technology also helps improve the performance and reliability as well as reduce the cost. We proposed and developed a novel miniaturized LTCC based wireless pH sensing system which could be used for several applications aiming for environmental or food-safety monitoring purposes.

4.2 Miniaturized wireless LTCC based pH sensing device

4.2.1 Circuit and layout design

The pH sensor act as a small battery (producing a potential proportional to pH level). The output signal is included between -0.5V and +0.5V. Many analog-digital converters (ADC), which are embedded in low-cost microcontrollers, are monopolar and read a potential range from 0V to 3V. To use the ADC in full scale and get the best resolution, we amplified the signal using the LMP7721 amplifier which is typically designed to be the conditioning circuit for pH sensors. To get a monopolar signal from the LMP7721; the input needs to be offset. To transform the bipolar signal (produced by the pH sensor) to a monopolar signal, we used the REF3312 as a voltage reference to offset the reference voltage from 0V to +0.5 V. Then the output of the pH sensor (after the conditioning circuit) will be between 0V and 3V. The sensor part consists of two electrodes with the size of 1×1 mm^2 each. Figure 4.1 shows the circuit schematic and the designed layout of the pH sensing device.

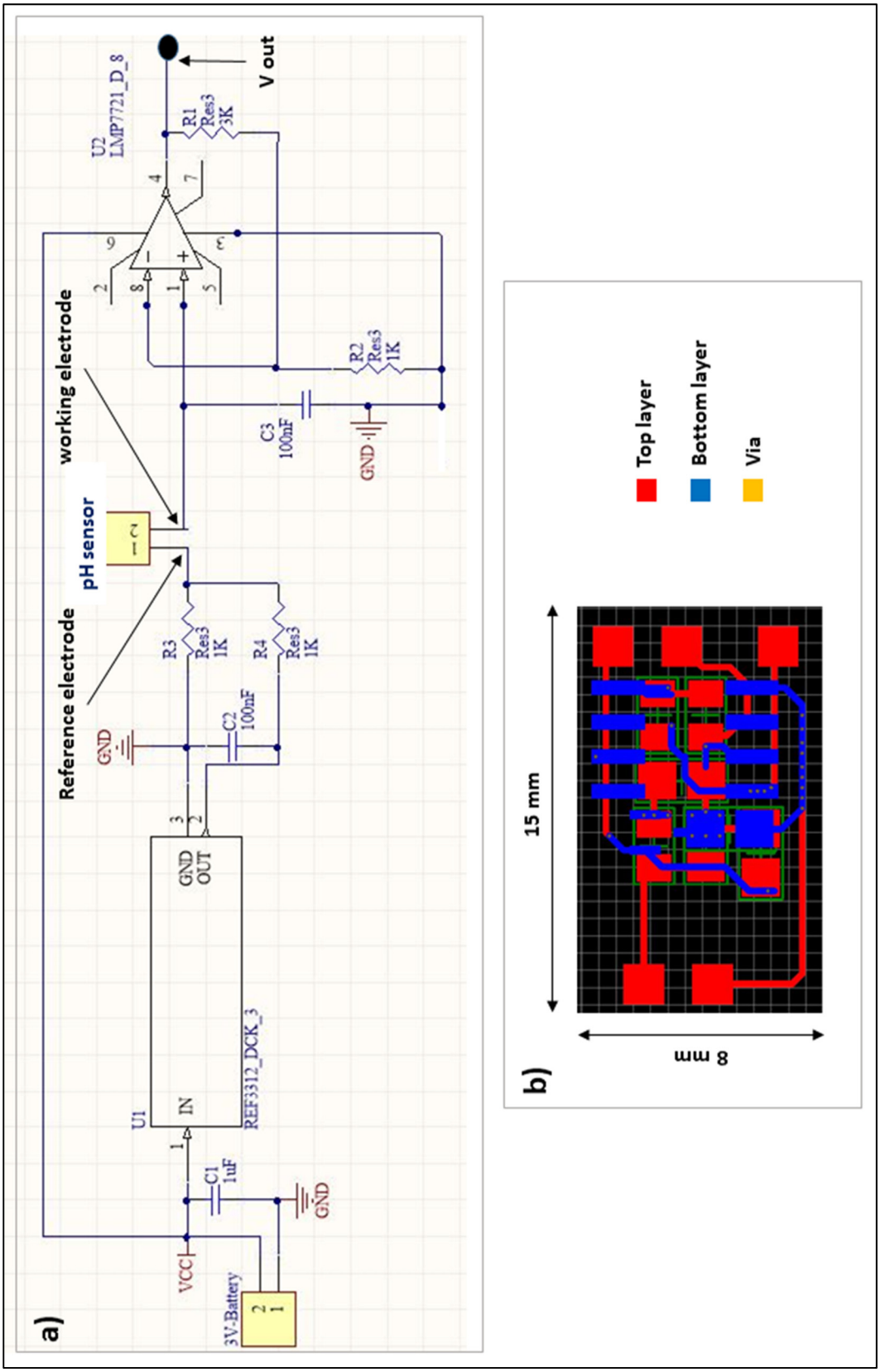

Figure 4.1 a) Sensing device schematic; b) Sensing device layout

4.2.2 Integration

We used four DuPont's 951AT layers as a substrate, and all steps followed an industry-standard LTCC fabrication chain (Figure 4.2). The first step was to form via holes using a punching machine, which was then filled with conductive paste. Next, the traces were printed using a mask and DuPont's silver paste. A laser-cutting machine was used to create a testing chamber and access to contact pads for soldering surface-mount device (SMD) components. All layers were aligned using a high-precision aligner and pressed together using hydraulic pressure. Finally, the batch of sensors was separated using a guillotine or laser cutting for better precision, and the resulting laminated circuit was co-fired. To form the IrO_x sensing film, the WE was electrodeposited using cyclic voltammetry (CV) feature of the potentiostat with a potential range of -0.8 V to +0.7 V and a scan rate of 0.1 V/s for 50 minutes.

In the previous chapter, we showed that electroplating is not compatible with a thin layer of the conductor, in fact, the sputtered conductor (MEMS, laser etching) peeled off during the process, and only thicker printed silver (LTCC) was able to support electroplating.
To reduce costs and time, as well as to obtain a compact size of the system compared with those using the glass RE electrode, our RE was simply printed using the Ag/AgCl paste during the serigraphy process of the LTCC chain. Further, since the thickness obtained by this method is significantly greater than those formed by other methods, such as electroplating, our sensor is more durable and reliable. And finally, all SMD components were soldered.

LTCC fabrication is a great option for industrial mass production, in fact, it allows the production of 50 sensors in the same batch. For LTCC the most time-consuming step is the co-firing (8 hours), but it is possible to get around it using an industrial oven (able to fire more than 20 batches at the same time). To validate the design and demonstrate the repeatability, we designed two similar pH sensors, and we measured their response simultaneously (Blue plot is the response of sensor 1, and the yellow plot is the response of sensor 2). The results shown in figure 4.3 indicate that our integrated device provides fast responses (3 seconds) with excellent repeatability.

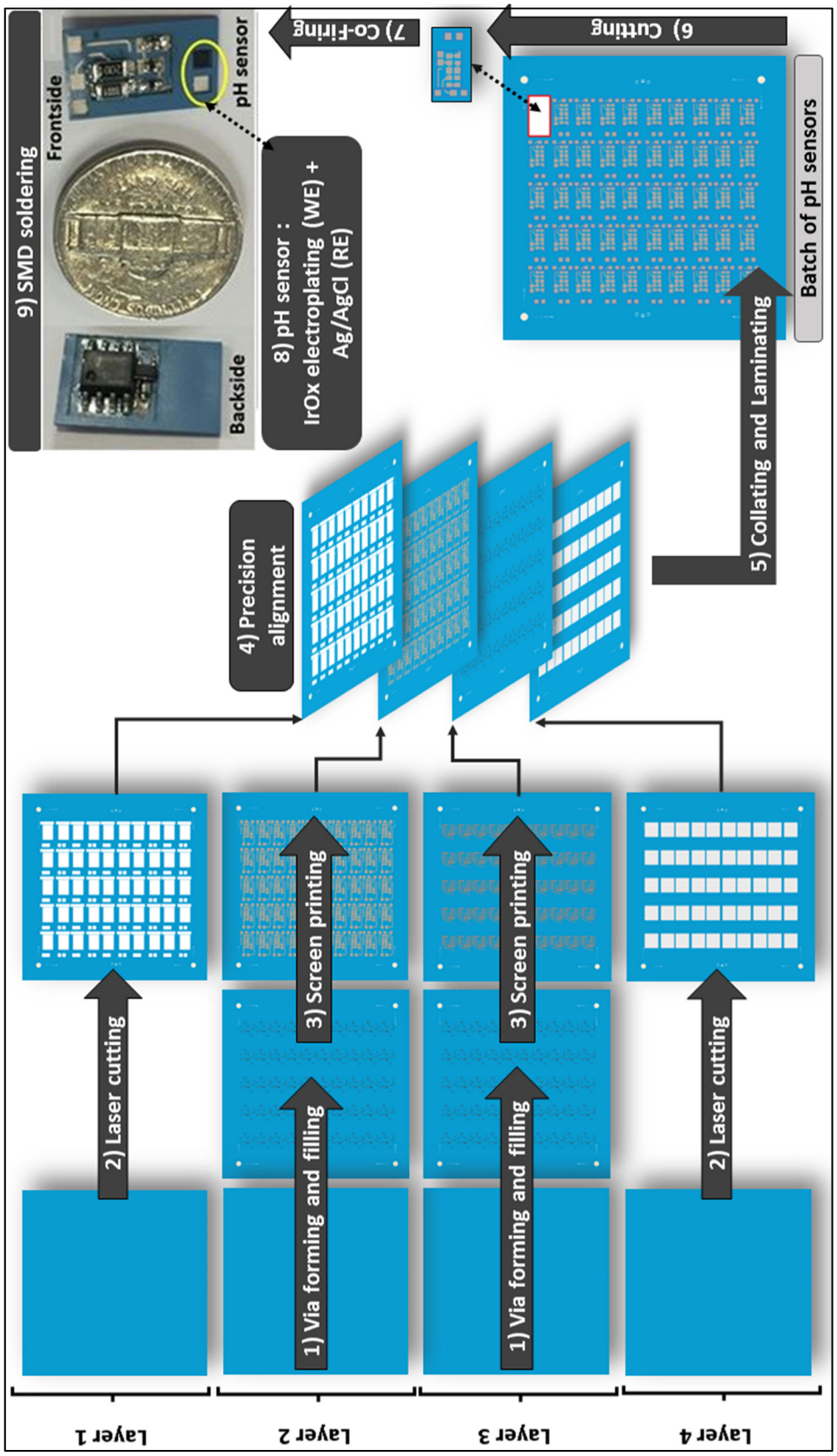

Figure 4.2 LTCC fabrication chain

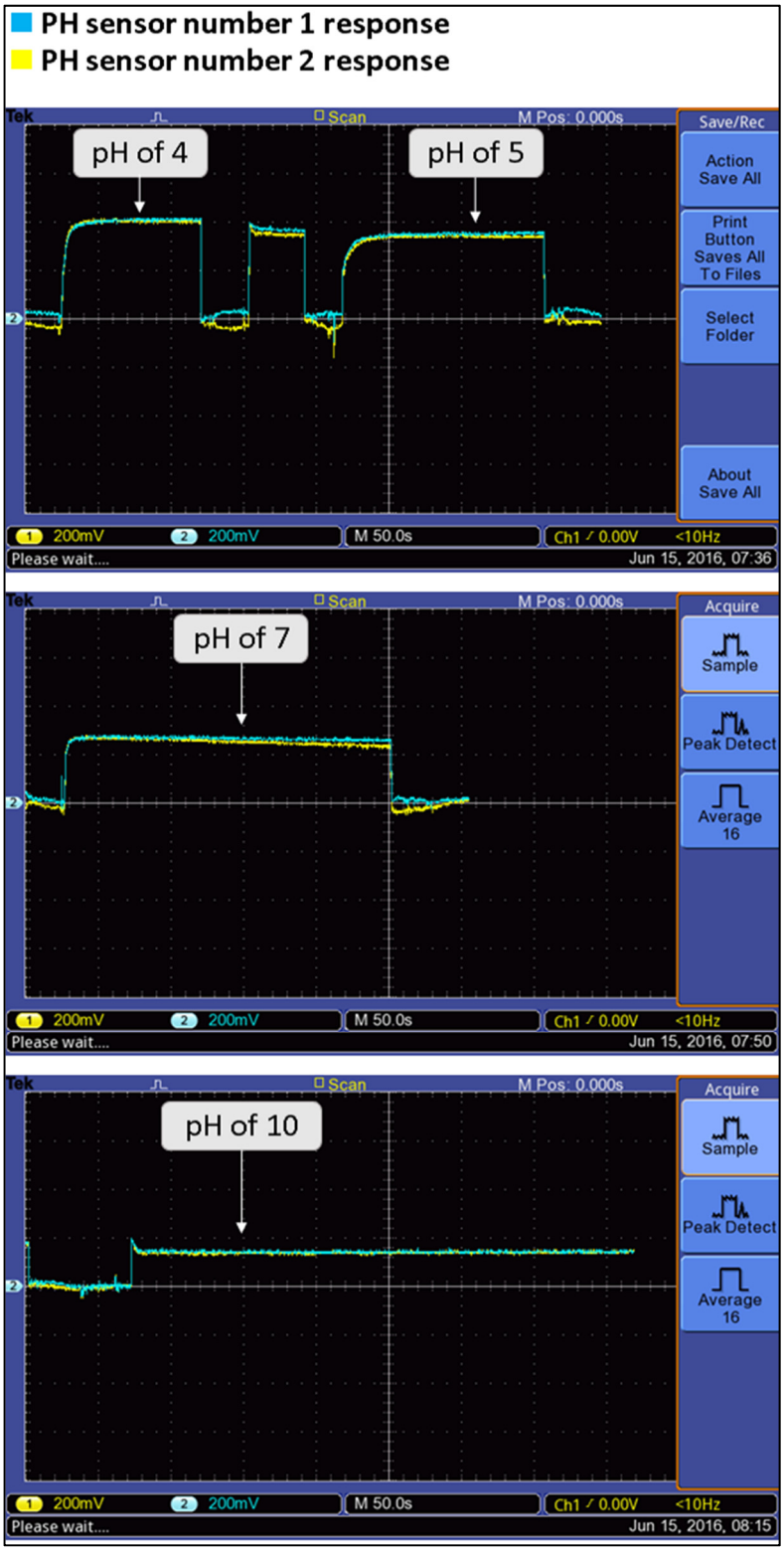

Figure 4.3 Validation of the integrated design

4.2.3 Wireless user interface

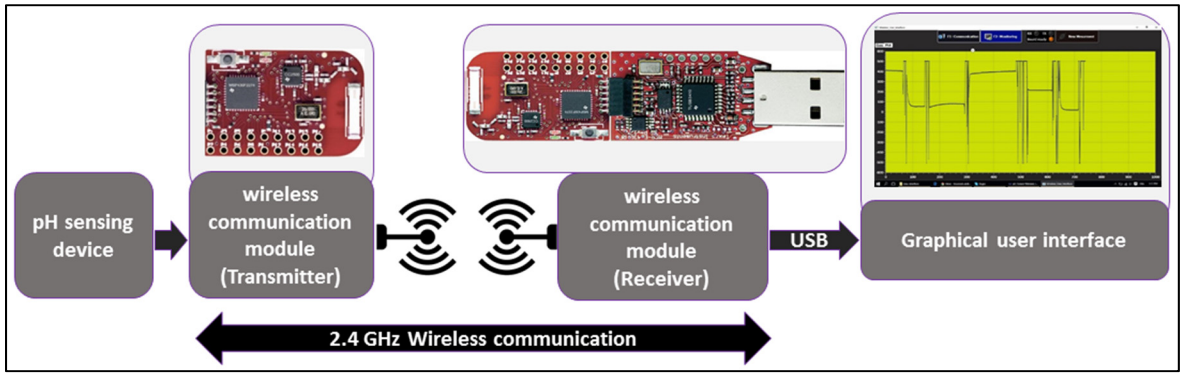

Figure 4.4 Block diagram

For a proof of concept, we used modular approach (Sensing device and communication part are separated). Future work may integrate them in the same substrate. For the communication part, we used the wireless module EZ430-RF2500 (Texas instrument). It is a complete development tool for the ultra-low power with embedded MSP430 microcontroller and CC2500 2.4 GHz wireless transceiver.

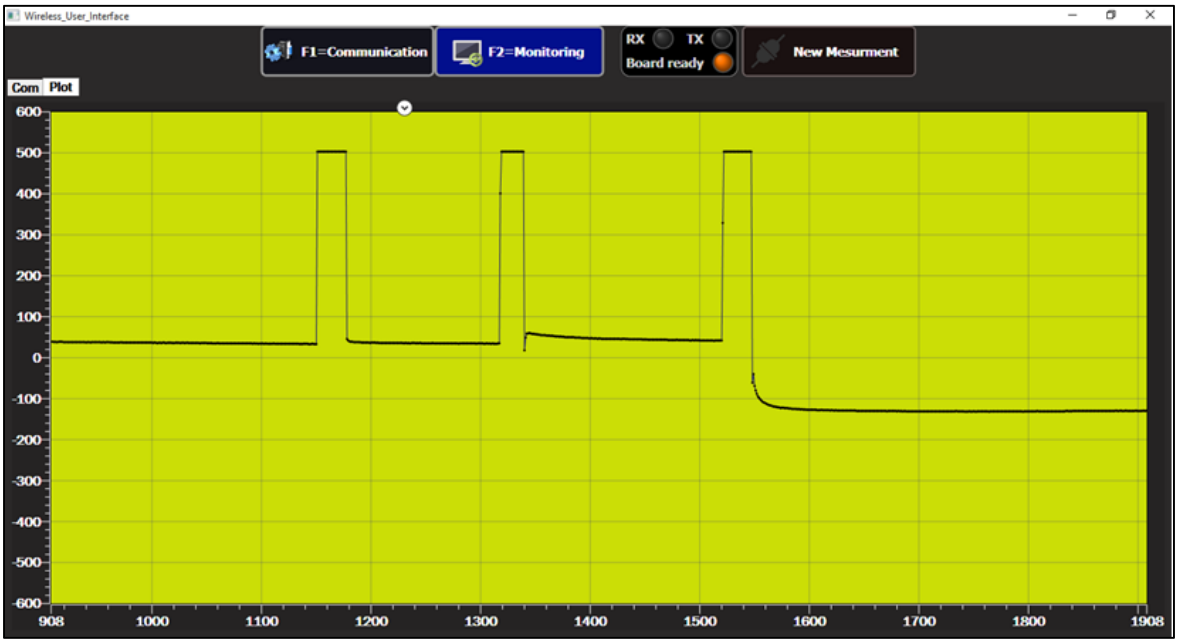

Figure 4.5 Graphical user interface

This module offers a good communication range, up to 35 m in normal conditions. Any other wireless communication module can be used (Bluetooth Low Energy, ZigBee, etc.). Figure 4.4 illustrates the block diagram of the entire wireless pH sensing system. A graphical user interface (figure 4.5) was developed using Visual Studio to display and store data in an Excel file. We used five different solutions with pH values of 4, 5, 7, 8.8 and 10 to calibrate our pH sensor, at room temperature. Buffer solutions with pH of 10, 7 and 4 were purchased from Fisher Scientific, while the ones with pH of 5 and 8.8 were made in house using DI water and buffer solutions. The pH values were determined using a commercial pH meter (SPER Scientific).

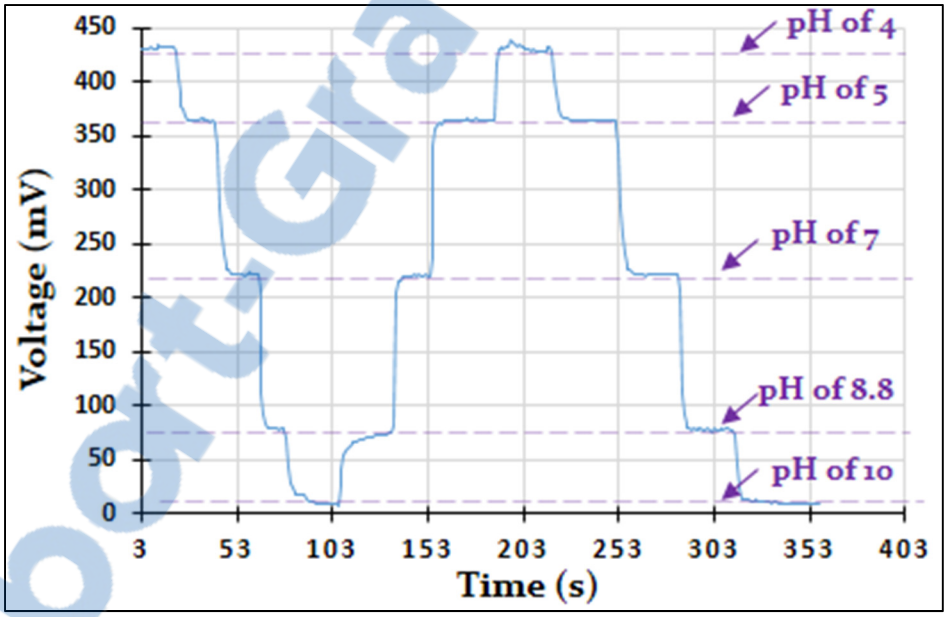

Figure 4.6 Real-time pH testing of our system

We introduced the pH solutions into the testing chamber, and we recorded the voltage values. The results show that our IrO_x film formed by CV is among the best for sensing pH (71 mV/pH) compared to those obtained by conventional methods with a sensitivity of 50-60 mV/pH. Assuming interferences are Gaussian, the limit of detection (LOD) can be evaluated as 3 times of the standard deviation of the baseline. Through the data we obtained, a LOD of ~0.054 was determined. Figure 4.6 demonstrates the device capability in wireless sensing pH in real time.

4.3 Other prototypes

LTCC proved to be the most suitable fabrication technique, in fact, it allows a better integration and miniaturization; it is compatible with electrodeposition of IrO_x, and it allows batch production which reduces costs. Then it is suitable for environmental and food quality monitoring applications. However, LTCC has few limitations (As shown in the previous chapter), for instance, it is not flexible, ceramic is breakable, and it is not biocompatible (it contains traces of plumb). For those reasons, LTCC is not suitable for few applications where flexibility, biocompatibility, and robustness are required. So we developed other prototypes:

- Flexible pH sensing device (flexibility);
- Glass based microfluidic pH sensing device (biocompatibility).

Unlike LTCC devices, we did not make the pH measurement for these (lack of time and we made only one prototype of each), we just proved the fabrication feasibility.

4.3.1 Flexible pH sensing device

We already explained in chapter 1 that pH is an important factor in tissue regeneration. Then, it is possible to monitor a burn or wound healing and detect the presence of bacteria by incorporating pH sensor into smart bandages (Shorrock et al., 2000). Here comes one potential use of our flexible pH sensor (described and characterized in chapter 3). To prove the feasibility, we designed a flexible pH sensing device including a miniaturized pH sensor ($1x1mm^2$) and required electronics (amplifier, offset, etc.). The prototype was designed using a similar technique described in chapter 3. The process is shown in figure 4.7. Step 1: we prepared the layout; step 2: we sputtered silver; step 3: we laser etched and cut the desired patterns; step 4 we deposited IrOx via sol-gel; step 5: we deposited Ag/AgCl paste as a reference electrode, and finally we soldered SMD components. We used Kapton as a substrate which is a flexible and biocompatible polyimide film, which remains stable across a wide range of temperatures, from −269 to +400C. It is used in, among other things, space instruments, flexible printed circuits (flexible electronics), etc.

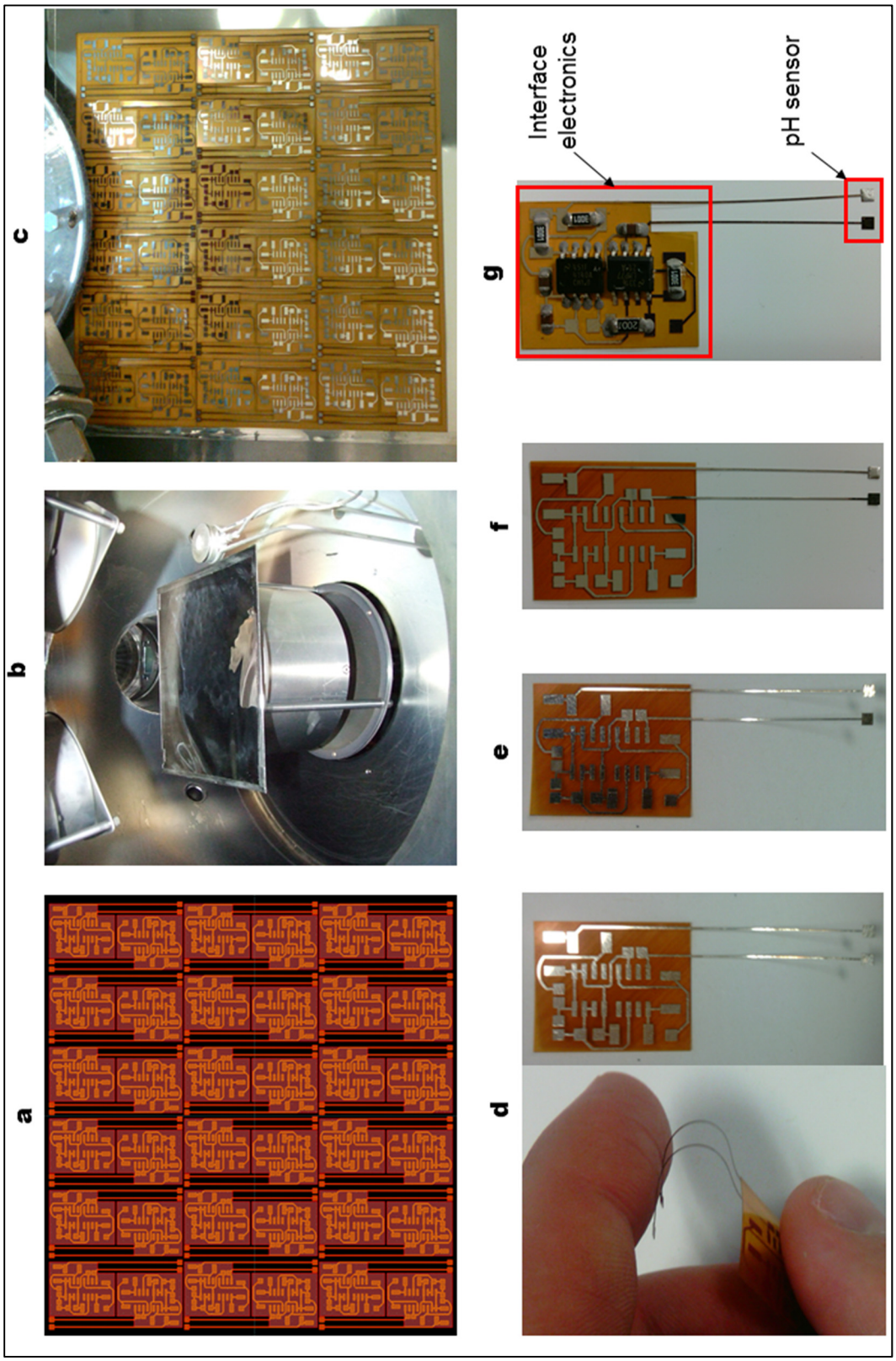

Figure 4.7 Flexible pH sensing device fabrication chain

4.3.2 Glass based microfluidic pH sensing device

As discussed in chapter 1, an accurate pH value detection in real time is of keen interest in a significant number of medical applications. For instance, the blood circulating through our body should have a pH balanced between 7.35 and 7.45. Exceeding this interval by as little as 0.1 of a pH could be deadly. Some patients with kidney problems are forced to use a dialysis machine to clean their blood: a micropump is forcing the blood thru filters to clean it and then reinject it back to the body, actually, the pH of the blood (very important parameter) is not monitored in real time during dialysis.

The only advantage of glass compared to LTCC is biocompatibility: due to the presence of plumb (according to DuPont's 951AT datasheet), LTCC is not biocompatible. So, we developed a glass-based microfluidic pH sensing device to prove the feasibility of a miniaturized glass based pH sensing device targeting potential microfluidic applications (The pH of a fluid can be measured in a closed loop thru the microfluidic channel). We saw an opportunity to improve existing dialysis machines, we thought about adding this pH sensing device which is potentially capable of measuring the pH level of blood in real time and in a closed loop. According to literature, we know that there is a correlation between the pH level of blood and kidney dysfunctionality. Due to lack of time and also because we have only one prototype, then we only made a proof of concept, to prove the feasibility; but, without making a test with blood. The fabrication chain is illustrated in Figure 4.8 as follows: Step 1: we etched 1x1mm^2 cavity for each electrode using a controlled laser beam; then, we sputtered a thin layer of silver. Step 2: we laser etched the desired layout. Step 3: we deposited IrO_x via sol-gel to form the sensing electrode, and Ag/AgCl to form the reference electrode. Step 4: SMD components were soldered. Step 5: using a controlled laser beam we etched a microfluidic channel and we also etched cavity to fit with SMD components. And finally, step 6: the two pieces obtained in steps 4 and 5 were stuck together (a biocompatible glue could be used). Doing so, SMD components are hermetically sealed, and a liquid solution can circulate thru the microfluidic channel; in contact with the pH sensor.

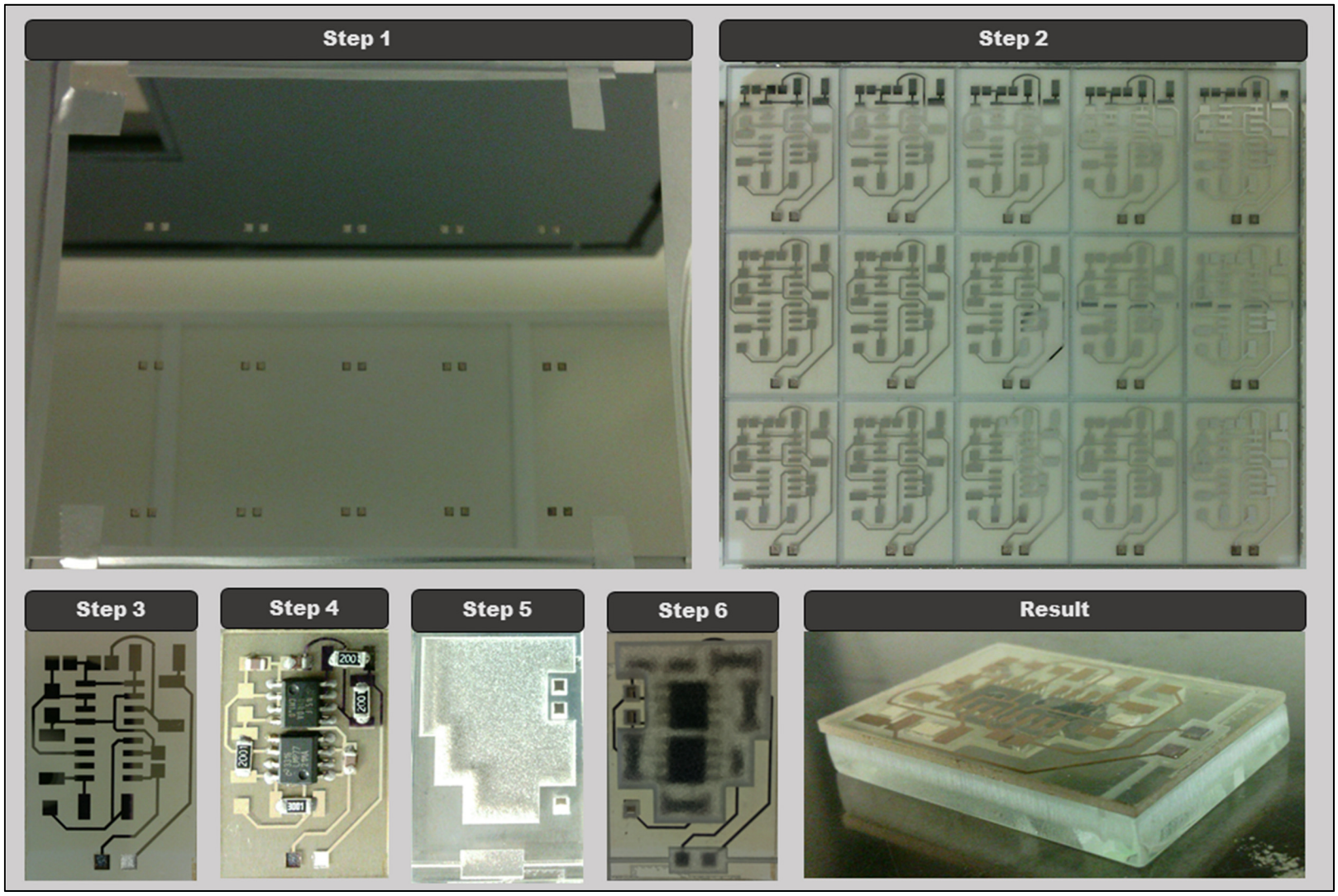

Figure 4.8 Microfluidic glass based miniaturized pH sensing device

Figure 4.9 illustrate the system block diagram of a blood pH monitoring system. Many other sensors could potentially be added such as arterial pressure, salinity, etc. Our device is designed to monitor pH level in real time wirelessly. The fluid (blood) could circulate in a closed loop which eliminates coagulation and infectious risks.

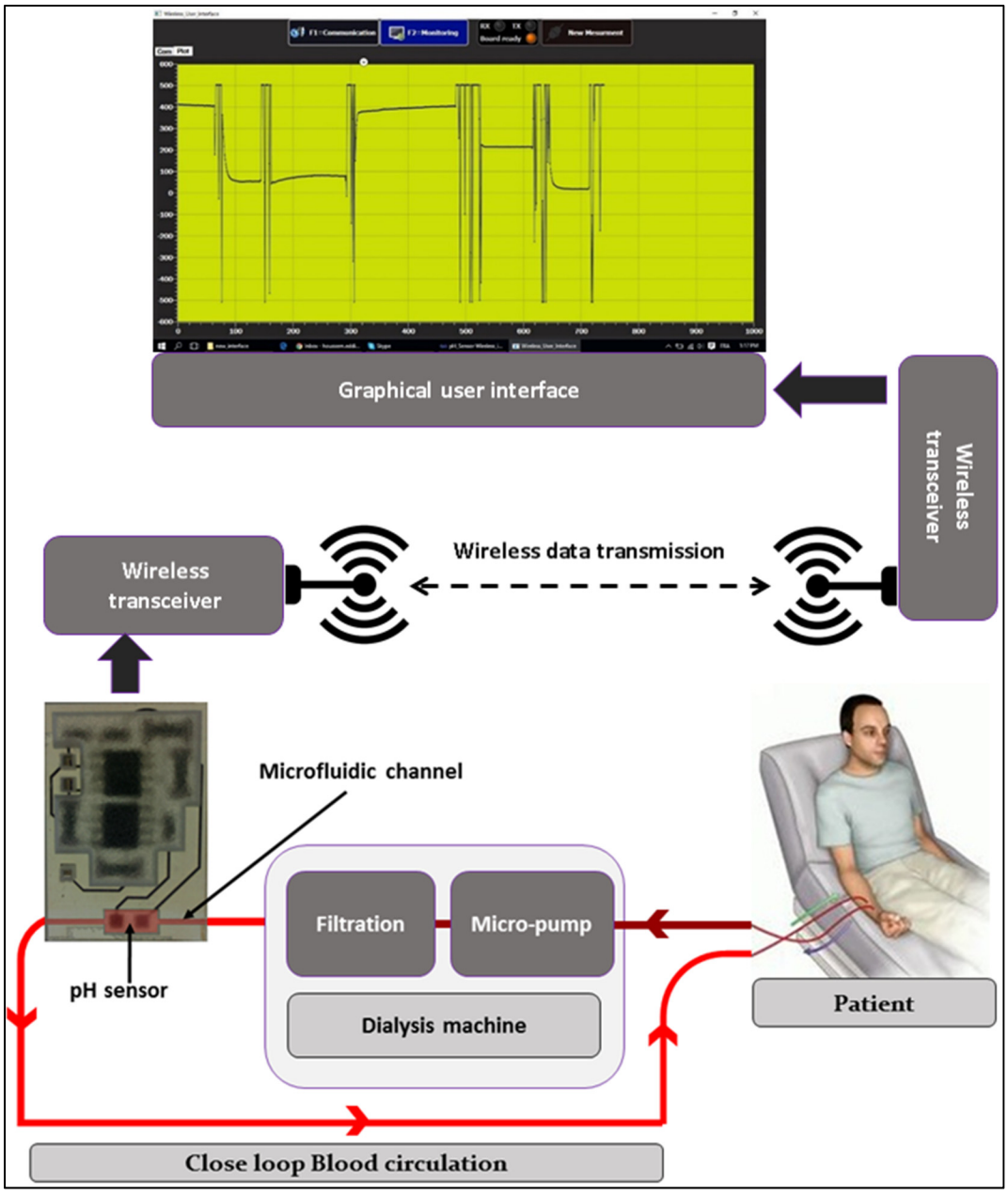

Figure 4.9 System block diagram of blood pH monitoring system

4.4 Conclusion

LTCC proved to be the most suitable fabrication technique, in fact, it allows a better integration and miniaturization; it is compatible with the electro-deposition of IrO_x, and it allows batch production which reduces costs. Then it is suitable for environmental and food quality monitoring applications. However, LTCC has few limitations. For instance, it is not flexible, it is breakable, and it is not biocompatible. For those reasons, LTCC is not suitable for few applications where flexibility and biocompatibility are required. Then, other substrates (we showed some examples such as Kapton, Glass, etc.) could be used as an alternative. We used modular approach (Sensing device and communication part are separated), future work may integrate them in the same substrate. It is a battery-based solution; battery-less may be a great option for better miniaturization, and sanitization. Due to biocompatibility, infections and size concerns, the need for wireless and battery-less is evident, especially for medical devices. A new expectation raises for those devices, in fact, power becomes an essential issue.

CHAPTER 5

WIRELESS POWER TRANSFER FOR BATTERY-LESS APPLICATIONS

5.1 Introduction

In chapter one we mentioned that pH measurement is knee interest for many medical applications (For example: analyzing the pH of blood, wound, and gastric fluid). Due to biocompatibility and size concerns, there is an urgent need for wireless and battery-less, especially for medical devices which have been utilized for years to improve healthcare, helping or replacing functions of certain organs. They can be employed for diagnosis, prognosis, and/or treatment. Nowadays, numerous chronic diseases have been targeted with the uses of IMDs throughout the body, from the brain, cochlea, retina to heart, lungs, knee joints and even vessels, esophagus, and bladder.

With the development of technologies in the last decade, healthcare has been changed in several aspects. Nano, micro and wireless technologies have transformed medical diagnosis, monitoring, and intervention to individualized care. Self-care, e-care, and mobile-health have been emerged changing traditional roles of doctors and patients. A new expectation raises for medical devices; for instance, they need to be battery-less and wirelessly communicate with external units for real-time tracking and sensing, diagnosis and treatment.

Nikola Tesla is the first person who had a vision of wirelessly distributing power over long distances through the air (Tesla, 1914). Today, after over a century, many devices are already using wireless charging, for instance: electric teeth brush, Mp3 players, smartphones, etc. Power became an essential issue, not only for biomedical devices but also for other applications. Therefore, we take a more general approach to wireless power transfer. In this chapter, we will try to prove the feasibility of wireless power transmission and focus on the design and optimization of an efficient Wireless Power Transfer (WPT) setup (Transmitter antenna and different receiver antennas).

5.2 The concept of wireless power transfer

The idea of wireless power involves the transmission of energy without the constraint of a power cord from a transmitter to a receiver via the Electro-Magnetic Field (EMF). A signal from a transmitter applied to an antenna creates an EM fields.

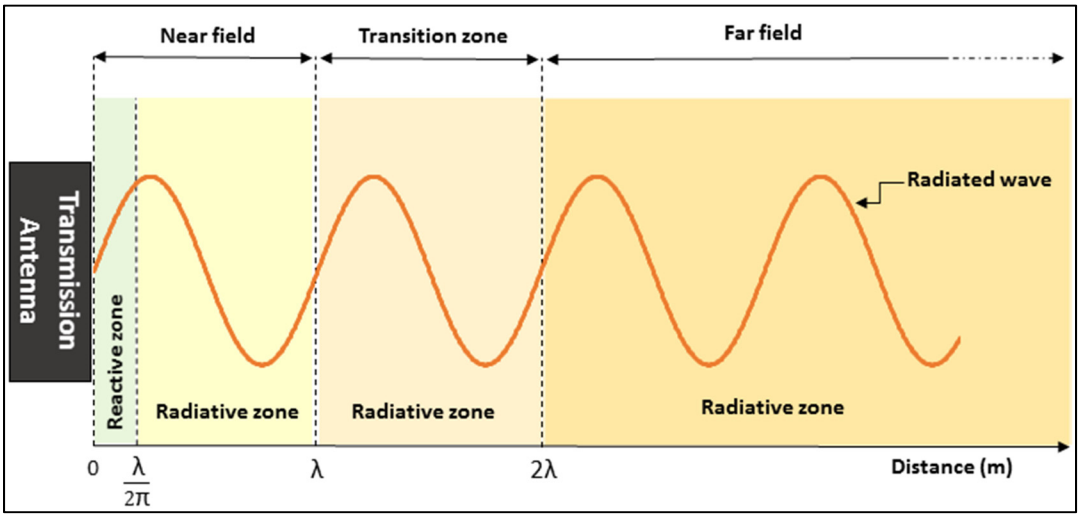

Figure 5.1 Different zones of an EM field generated by an antenna

The characteristics of those fields' change depending on the distance from the transmitter antenna (Figure 5.1), and they are separated into two segments: the near field and the far field. Between those two segments, there is a transition area called transition zone. The near field is split into two regions, the radiative and the reactive. In the reactive area, the electric fields E and the magnetic field H have the maximum values. Depending on antenna type one field will dominate the other. In the case of the loop antenna, for example, the magnetic field (H) will dominate. This antenna will act as the primary of a transformer. The near field is the zone less than one wavelength (λ) from the antenna. Wavelength λ in meters is given as follows:

$$\lambda = \frac{v}{f} \tag{5.1}$$

With v the speed of light 3×10^8 m/s and f frequency in Hz.

In the near field, the strength of the fields varies inversely with the cube of the distance from the antenna ($1/r^3$). This field is divided into two zones: the reactive area where distance $0 \leq d$ (m) $\leq \frac{\lambda}{2\pi}$ and the radiative area ($\frac{\lambda}{2\pi} \leq d$ (m) $\leq \lambda$). The transition zone refers to the undefined area between the near and far fields. It is the beginning of the far field.

The far field (at a distance of 2λ and beyond) is the real radio wave. It propagates through space at a speed of light. The E and H fields support and regenerate one another as their strength decreases inversely as the square of the distance ($1/r^2$).

It is possible to efficiently transmit power over large distances using the radiated EM field from appropriate antennas. However, it increases system complexity and raises safety concerns. It is also possible to transmit power over short distances using non-radiative near fields. The concept is similar to the operation of a transformer which can be considered a form of wireless power transfer since it uses the principle of magnetic coupling to transfer energy from a primary coil to a secondary coil without a direct electrical connection (Keskin et Liu, 2015). To date, the resonance-based inductive coupling has been proved as the most reliable method for short-range power charging. It was usually done with two antennas at a low-MHz frequency to minimize the power absorbed by the body. The amount of energy transferred between the two coils depends on mutual inductance which can be defined as the amount of magnetic field linkage between them. The factors affecting the wireless power efficiency (WPE) include the coil geometry, the distance between them, the misalignment, and the optimization of matching parameters. Inductive coupling is a short-range coupling of RF energy: the receive antenna is small (at low frequency the range is decreased, but the size of the antenna is reduced); the receiver needs to be placed on a charging surface (Liu, Hu et Georgakopoulos, 2016).

The class-E amplifier configuration has been widely utilized owing to the high efficiency in power amplification before transmission (Keskin et Liu, 2015). No battery is then required. With the external inductive antenna, the interface electronics and the RF communication

module draws all of their operating power from the transmitter's electromagnetic field (Figure 5.2).

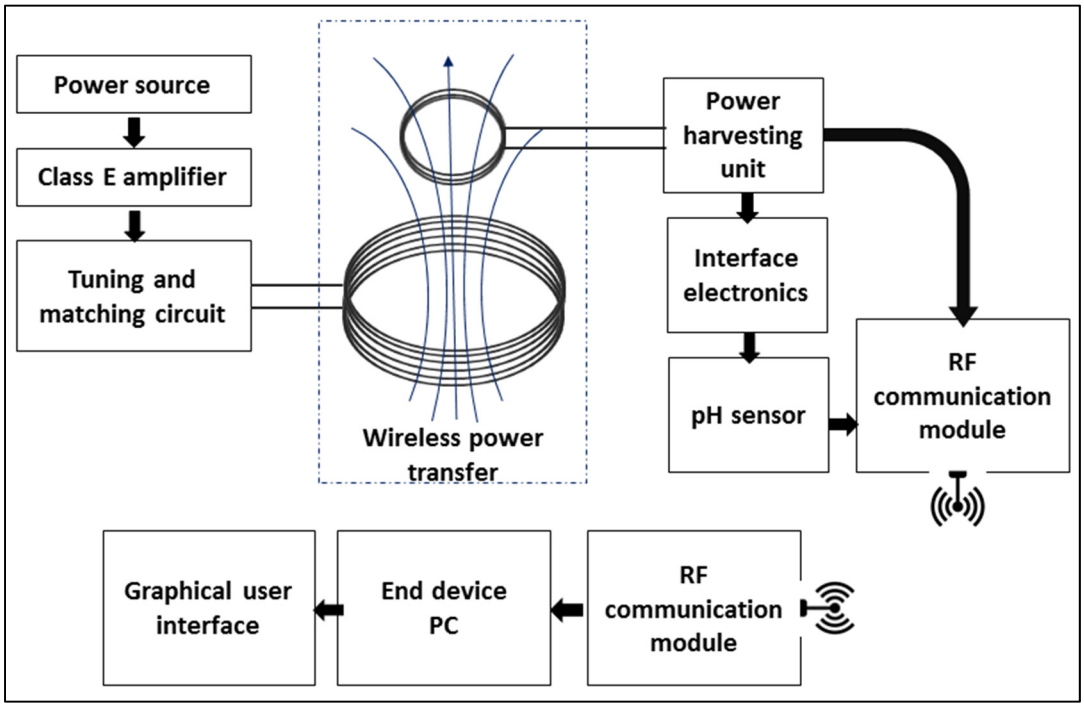

Figure 5.2 WPT system block diagram

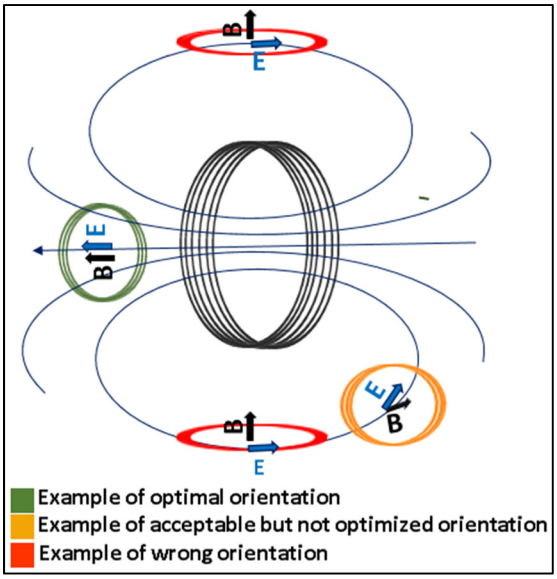

Figure 5.3 Examples of different antennas orientation

Both coils are tuned with capacitors to resonate at the desired frequency to increase the magnetic field generated by the transmitter and the voltage received by the receiver. Effective tuning helps to improve the efficiency; the use of loop antennas poses another problem. In fact, since the antennas sense a magnetic field, the orientation between the transmitter and the receiver has an impact. For instance, electromagnetic theory stipulates that if the two coils show a 90-degree phase shift in space (Figure 5.3), there will be no induced voltage on the secondary coil (Liu, Hu et Georgakopoulos, 2016).

5.3 Transmitter antenna design

Choosing the size and type of antenna circuit depends on the system design. As a designer we are not allowed to choose an arbitrary frequency, in fact, each country has its signal emission limits, there are only few radio frequency bands where no license is required, which are known as ISM (Industrial, Scientific, and Medical). These are frequencies set for industrial, medical, and scientific applications and have fewer emissions limitations because they do not interfere with safety, military, and emergency communications (America, 2003).

Table 5.1 Common unlicensed ISM frequency

Frequency band	Standard frequency	Coupling	Range	Cost
LF	125 to 135 KHz	Inductive	20 cm	Low
HF	13.56 MHz	Inductive	10 cm	Medium
UHF	868 to 928 MHz	Backscatter	≥ 3m	High
Microwave	2.4 GHz	Backscatter	≥ 3m	High

Table 5.1 lists the frequency categories of most standard unlicensed frequency bands; each frequency band has some advantages and few limitations which must be considered when designing a wireless system. Today many smart devices are already equipped with near-field communication antenna which operates at 13.56 MHz; then the smart device can potentially be used to power our device wirelessly. For this reason, we chose 13.56 MHz as operating frequency.

The frequency tolerance of the carrier frequency and output power level from the transmission antenna is regulated by government regulations, in the USA. FCC (Federal Communications Commission) limits for 13.56 MHz frequency band are as follows(America, 2003):

- Tolerance of the carrier frequency should be 13.56 MHz ±0.01% (± 1.356 kHz);
- Frequency bandwidth: ±7 kHz;
- The power level of the fundamental frequency should be less than 10 mv/m at 30 meters from the transmitter;
- The power level for harmonics: at least -50.5 dB down from the fundamental signal;
- Operating at 13.56 MHz generates few complications;
- Class E amplifiers operating at this frequency are very expensive, low power, very delicate. It can only dissipate 1W and gate voltage cannot exceed 6V. Otherwise, transistors could be destroyed;
- Parasitic capacitance between the drain and source of transistors is not negligible;
- Rising and falling time has to be small enough to achieve appropriate switching.

The efficiency of the wireless power transfer setup depends on the effectiveness of the amplifier and the efficiency of the coupling between the two antennas. The manufacturer gives the efficiency of the amplifier and it may change from a model to another in some cases it can achieve 93% of effectiveness. We cannot modify the efficiency of the amplifier, but we can design the electromagnetic coupling, match it and improve the coupling efficiency.

5.3.1 Antenna parameters

To design the transmitter antenna, we used an air core coil (5 turns, radius=3.25cm, 28awg).
In practical applications, the antenna is not a pure inductor, in fact, distributed parasitic capacitance is present between turns. The parasitic capacitance in a typical tag antenna coil is a few (pF). This parasitic capacitance increases with operating frequency (Li et Liang, 2015), at a particular frequency called self-resonance frequency the antenna, stops acting as an inductor and start acting as a capacitor. For a realistic modeling, the antenna represented by an equivalent electrical circuit instead of pure inductance (figure 5.4).

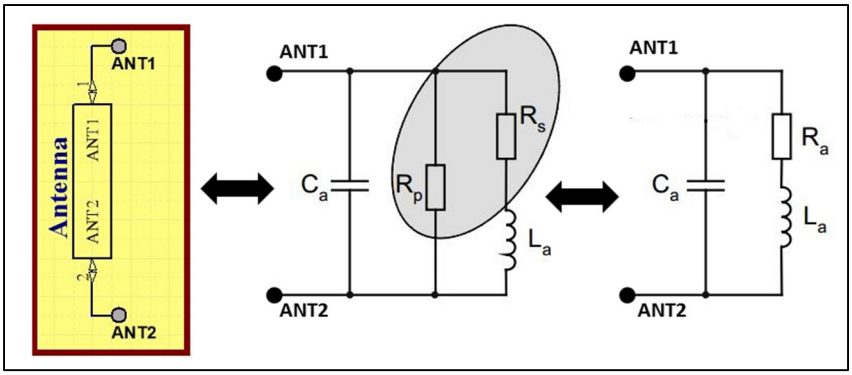

Figure 5.4 Equivalent antenna circuit

Where:

- Rs: Equivalent resistance at f = 1 MHz;
- Fsr: self-resonance frequency;
- Rp: Equivalent parallel resistance at the self-resonance frequency;
- Ra: The series equivalent resistance of the antenna at the operating frequency (calculated from Rs and Ra);
- Ca: the parasitic capacitance.

At operating frequency (Fop) we have:

$$\text{Rp (at Fop)} = \frac{Rp\ (at\ Fsr)}{\sqrt{\frac{Fop}{Fsr}}} \tag{5.2}$$

$$\text{Ra} = \text{Rs} + \frac{(2 \times \pi \times Fop \times La)^2}{\text{Rp (at Fop)}} \tag{5.3}$$

$$Ca = \frac{1}{(2 \times \pi \times Fsr)^2 \times La} \tag{5.4}$$

There is a correlation between all those parameters and the geometry of the antenna (Mohan et al., 1999). In fact, Ca is mainly affected by the distance between turns. Rs is mostly affected

by the thickness of the conductor. Rp is influenced by the skin effect and can be changed by thickness and spacing between the turns. The equivalent inductance La of the antenna is a geometrical value that can be estimated by calculation. A network analyzer can be used in combination with some calculation to determine the antenna equivalent electrical circuit. We should connect the antenna to the network analyzer by using an appropriate test fixture that minimizes the influence on the antenna. The network analyzer should be calibrated using a suitable calibration kit before each measurement.

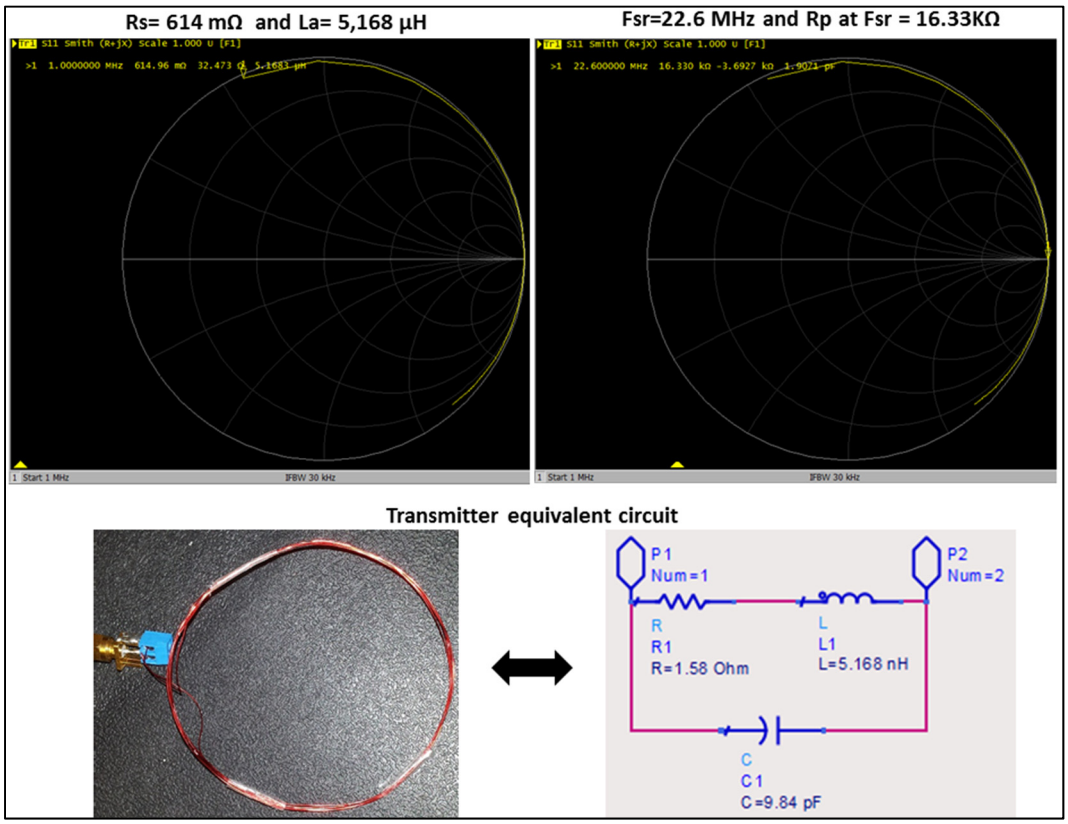

Figure 5.5 Extraction of antenna equivalent electric circuit from Smith's chart

According to the results illustrated in figure 5.5 we have: Rs= 614 mΩ, La= 5,168 µH, Fsr=22,6 MHz, Rp at self-resonance frequency (Fsr)= 16,33 KΩ. Then at 13.56MHz we have:

- La= 5,168 µH;
- Based on equation 5.3, Ca= 9.84 pF;
- Based on equations 5.1 and 5.2, Ra= 1.58Ω.

5.3.2 Transmitter tuning and performances

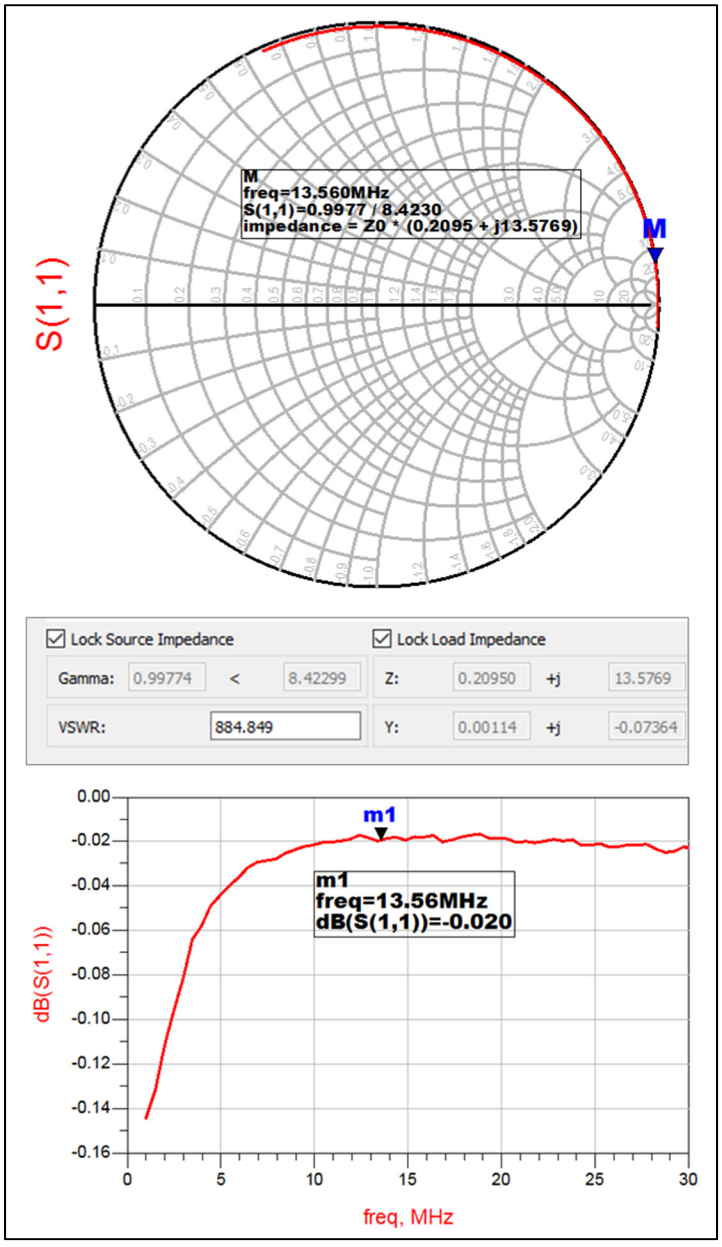

Figure 5.6 Transmitter antenna performances before matching

In RF, impedance matching is crucial; the goal is to design an RF system so that all the source and load, match, to ensure maximum power transfer and minimum reflected power (Pozar, 2012). Figure 5.6 shows that in the transmission line, the antenna is mismatched and is

reflecting a lot of power between the source and load. In fact, return loss is one measure of the reflected power, usually expressed as a negative number in dB which is a logarithmic ratio of the power of the signal reflected back and the power input. Return loss ranges from zero for open or short circuits to infinity, for a perfectly matched system. Some devices and tools are sensitive to reflected power and require lower return loss to minimize impedance discontinuities and signal reflection. Return loss can be calculated as follows (Pozar, 2012):

$$RL(dB) = -20\,Log10(\,|\,\Gamma\,|\,) \tag{5.5}$$

Where Γ is the reflection coefficient can be calculated using the following formula (Pozar, 2012):

$$\Gamma = \frac{(Zload - Z0)}{(Zload + Z0)} \tag{5.6}$$

Values of Γ range from zero for a perfect impedance match to one for an open or short circuit. According to figure 5.6, at 13.56 MHz our antenna has a reflection coefficient = 0.997 and a return loss = -0.02dB, it is clear that the antenna is not performing well. VSWR (Voltage Standing Wave Ratio) ; as its name implies, is the ratio of the largest to the smallest amplitude values of the standing wave created by the interaction of the incident and reflected waveforms. It is another useful measure of reflected power and impedance matching in an RF system.. Values of VSWR can range from one for a perfect impedance match to infinity for an open or short circuit. In our case, we have at 13.56 MHz, VSWR= 884. Then, some of the power transported in the line goes thru the other side (P_out), some is lost in the resistance of the cable itself, and the main part is reflected back to the source. Depending on the phase. Both waves (forward and reflected) can add or subtract. Because of that on the line, we can get places where the voltage equals zero (maximum current); or places where the voltage is the sum of both voltages. If the standing wave is configured in such a way on the transmission line; so, the maximum voltage or current is applied to the class E amplifier which can overheat and be destroyed.

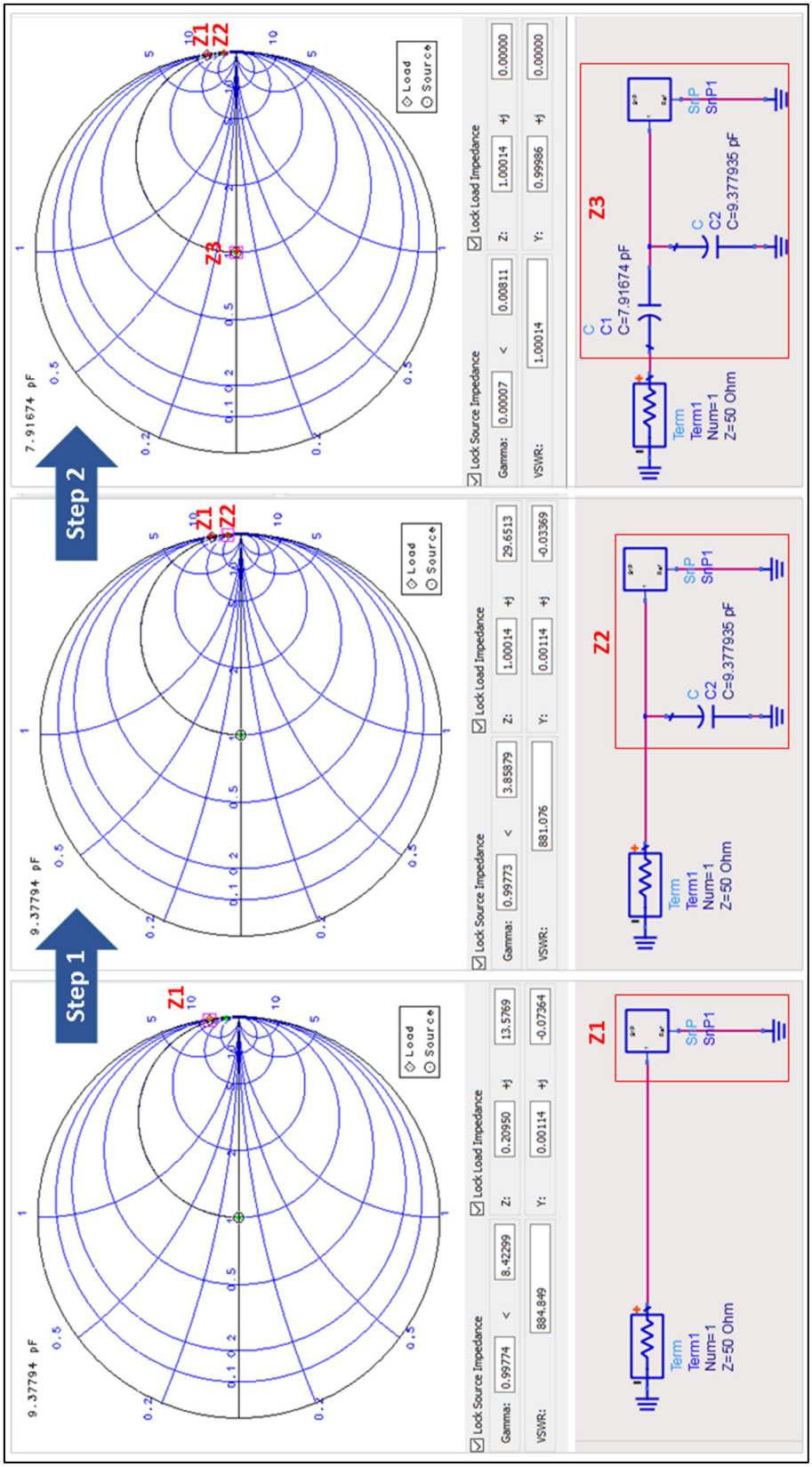

Figure 5.7 Transmitter antenna impedance matching

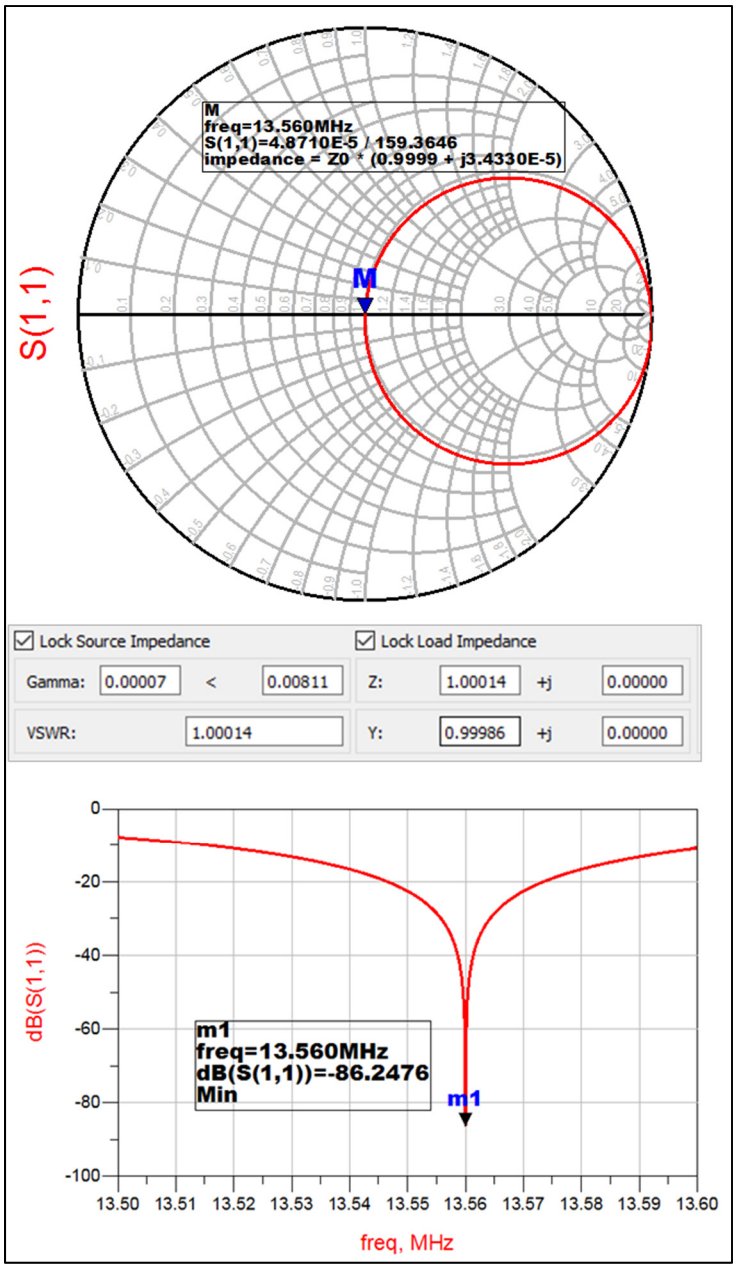

Figure 5.8 Transmitter antenna performances after matching

Impedance matching is needed to provide maximum power transfer between the source and its load (Pozar, 2012). The condition for impedance matching in RF is that real part of the load should be equal to the real part of the impedance and reactance's should be opposite. The generator typical output impedance is 50 Ω. Then the matching network has to make R load =50Ω and jX = 0. There are three basic methods of matching (Pozar, 2012):

- Transformer matching where an RF transformer can be used to produce a very wide band impedance matching, the main limitation is the frequency limitation;
- Transmission line matching: by using a transmission line of an appropriate length and characteristic impedance, the crucial composite match can be obtained. It is hard to tune the length and characteristic impedance once constructed;
- LC matching where inductors and capacitors are used to affect the impedance transformation. LC matching is very practical at a frequency from 3 MHz to 300 MHz, and it allows a very easy tuning, that is why we used this method.

Figure 5.7 shows how we transformed the unmatched impedance of the antenna (Z1=10.475+j 678.845) to a matched impedance Z3=50 Ω by adding a parallel capacitor (9.37 pF) and another series capacitor (7.91 pF). According to the results in figure 5.8 the antenna is well matched and has excellent performances in fact Γ=0.0007 and return loss= -86.24 dB at 13.56 MHz.

5.4 Receiver antenna design

Choosing the type and characteristics of the antenna depends on the system design constraints and standards. The series resonant circuit has a minimum impedance at the resonance frequency. Then, it draws a maximum current at that frequency. On the other hand, a parallel resonant circuit has a maximum impedance at the resonance frequency. Then, at the resonance frequency, the maximum voltage is available. For that reason; this type of antenna is suitable for the design of the receiver. An entirely real impedance characterizes resonance point. When this condition exists, the input voltage and current are in phase.

The inductance of the receiver antenna coil for 13.56 MHz is typically in the range of a few micro-Henries (μH). The antenna can be made by air core or ferrite core inductors. The antenna can also be formed by a metallic or conductive trace on PCB board, LTCC or a flexible substrate. The coil circuit must be tuned to the operating frequency to maximize power efficiency. The tuned LC resonant circuit is the same as the band-pass filter that passes only a

selected frequency. The Q of the tuned circuit is related to both transmission power range and bandwidth of the circuit.

The frequency tolerance of the carrier frequency and output power level from the read antenna is regulated by government regulations (FCC in the USA). The transmission circuit including the antenna coil must be designed to meet the FCC limits; the antenna should fulfill the requirements of standards as follows:

- 1uH ≤ La ≤ 3uH, the optimal value is 1.8uH;
- 3pF ≤ Ca ≤ 30pF;
- Self-resonance frequency ≥ 25 MHz;
- A suggested value for quality factor Q is 30. If it is too high, then an external resistor has to be added in series to the antenna to reduce the Q-factor to the desired value.

5.4.1 Air core antenna

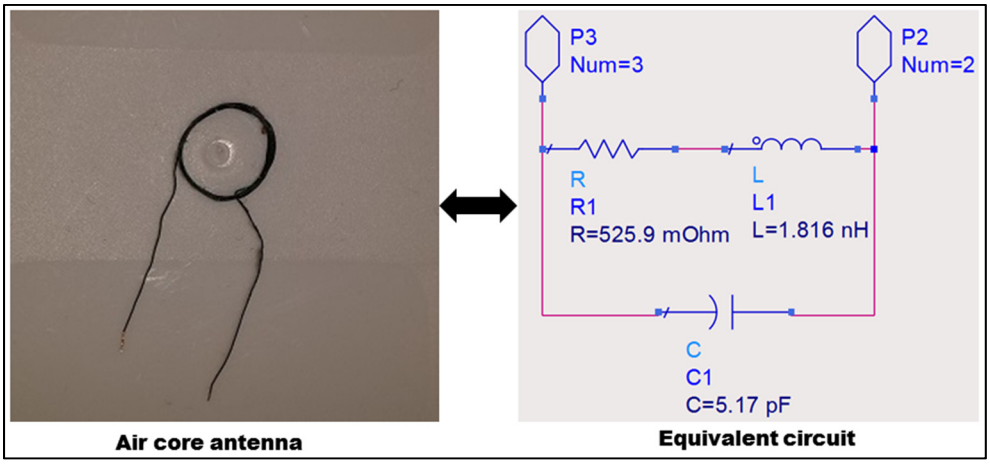

Figure 5.9 Air core antenna equivalent circuit

Air core antenna has many advantages, in fact, it is very easy to make and doesn't request complicated fabrication process, it can be tiny and offers excellent performances. To make the receiver antenna we used an isolated copper wire 32 AWG, 12 turns, and a radius = 4 mm. The transfer function of the equivalent circuit shown in Figure 5.9 is expressed as follows:

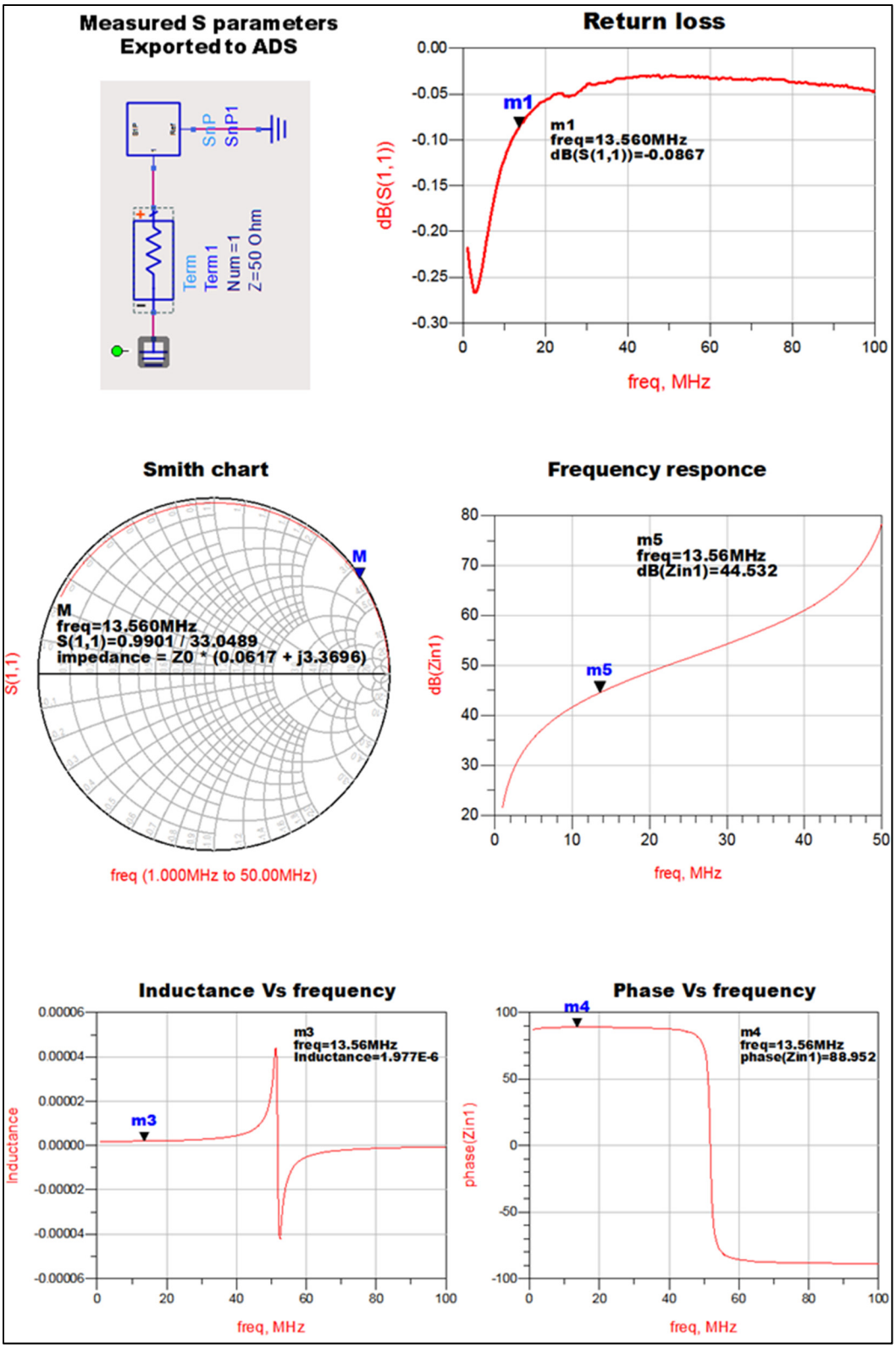

Figure 5.10 Air core antenna performances before tuning

$$\frac{V}{I} = \frac{(R1 + jL1W)}{(1 - W^2 L1C1) + jWR1} \tag{5.7}$$

Figure 5.10 shows that the inductance of the antenna is equal to 1.977 uH, the self-resonance frequency is expressed as follows and is equal to 51.94 MHz

$$\text{Fsr (self} - \text{resonance frequency)} = \frac{1}{2\pi\sqrt{C1L1}} \tag{5.8}$$

To tune the antenna to the desired resonance frequency (13.56 MHz), we added a capacitor C2= 69.62pF parallel to the antenna. We calculated this value according to the following formula:

$$13.56MHz = \frac{1}{2\pi\sqrt{(C1 + C2)L1}} \tag{5.9}$$

Resonance is characterized by the input voltage and current being in phase. The driving point impedance is entirely real when this condition exists and the antenna is equivalent to an open circuit at the resonance frequency. Figure 5.11 confirms that after tuning the antenna is resonating at 13.56 MHz. The results in figure 5.11 also show that the bandwidth, which can be expressed as follows, is very narrow.

Resonance is characterized by the input voltage and current being in phase. The driving point impedance is entirely real when this condition exists and the antenna is equivalent to an open circuit at the resonance frequency. Figure 5.12 confirms that after tuning the antenna is resonating at 13.56 MHz. The bandwidth can be expressed as follows:

$$BW(Hz) = \frac{R1}{2\pi\, L1} \tag{5.10}$$

To increase the bandwidth, we added a resistor R =5 Ω. As illustrated in figure 5.12; we can notice, that the bandwidth has been increased.

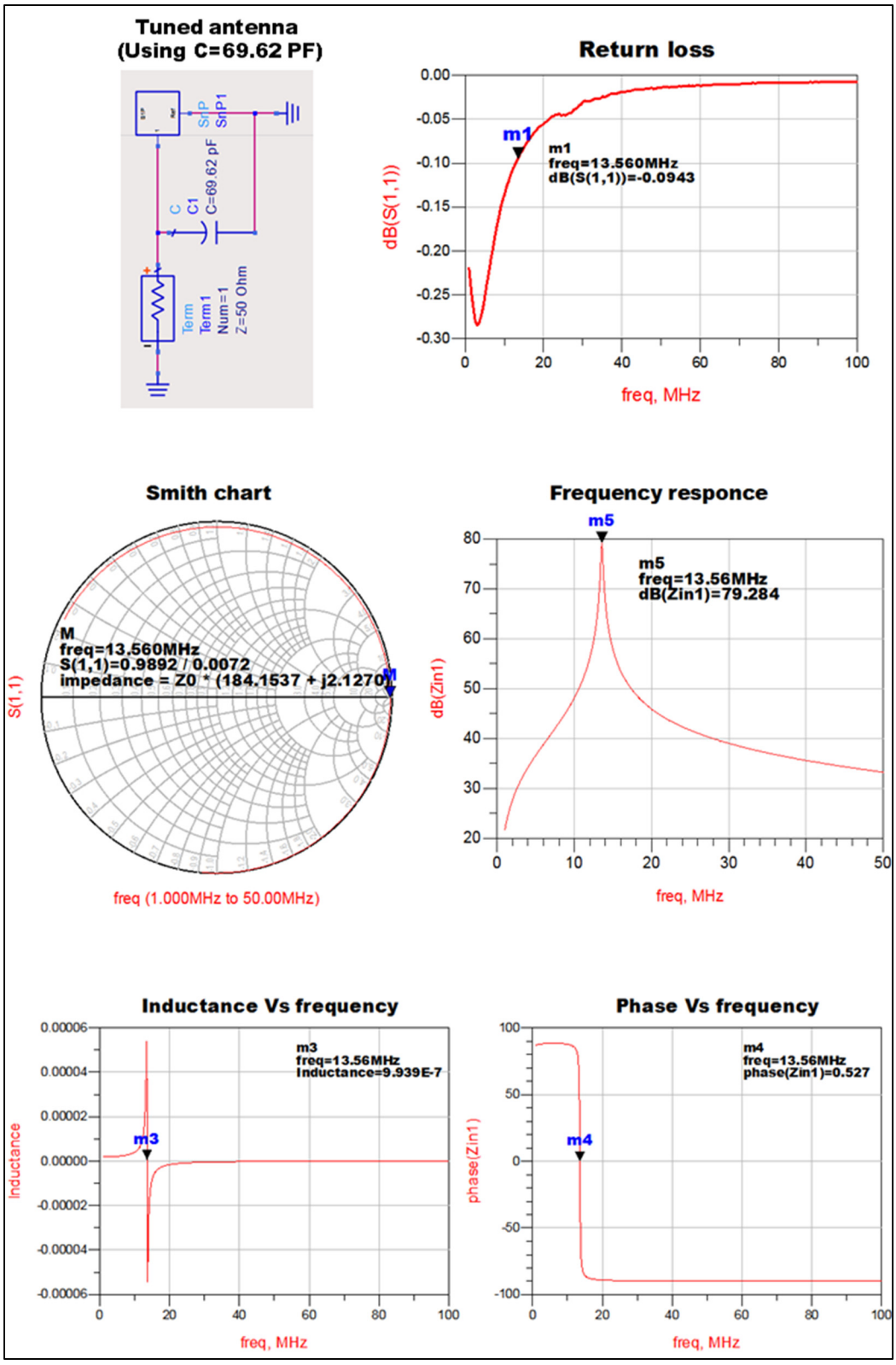

Figure 5.11Air core antenna performances after tuning

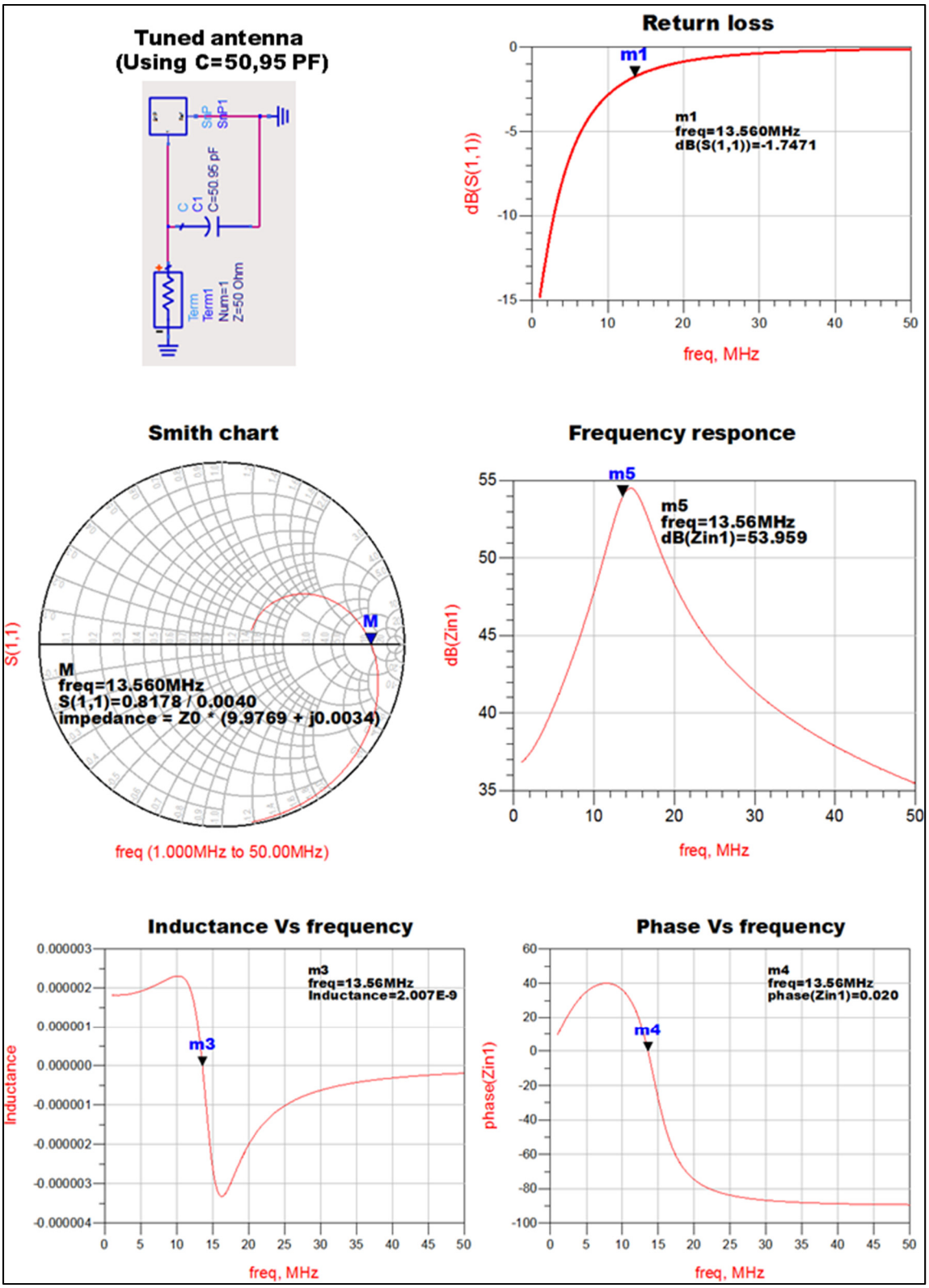

Figure 5.12 Bandwidth tuning

5.4.2 Flexible spiral antenna

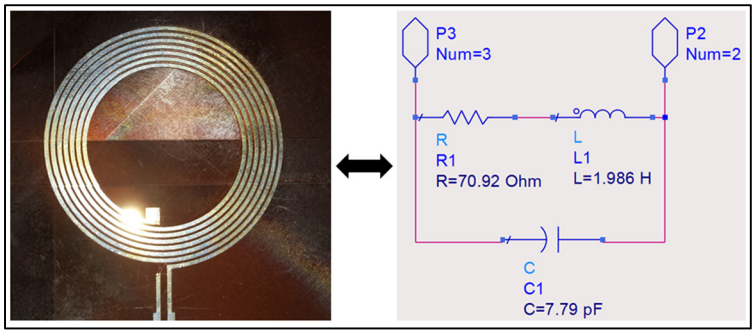

Figure 5.13 Flexible spiral antenna equivalent circuit

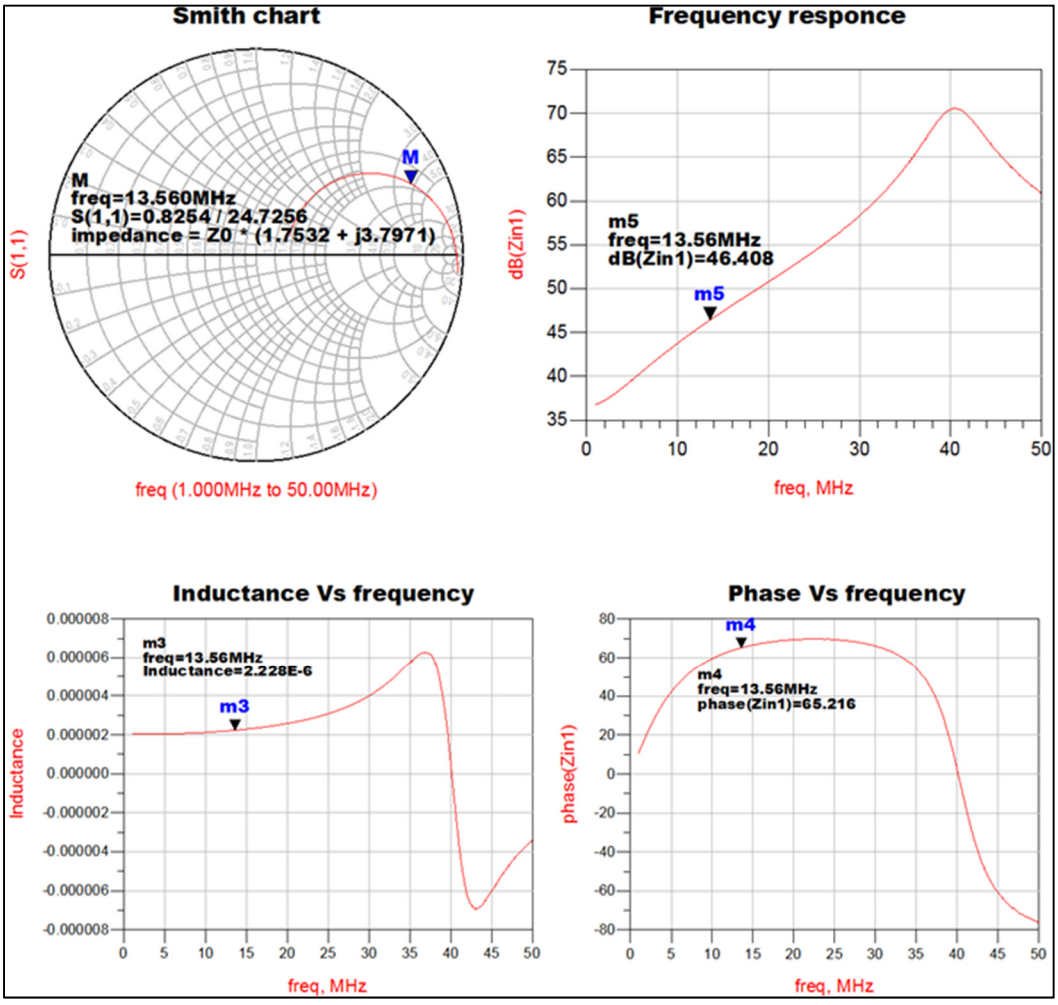

Figure 5.14 Flexible spiral antenna performances before tuning

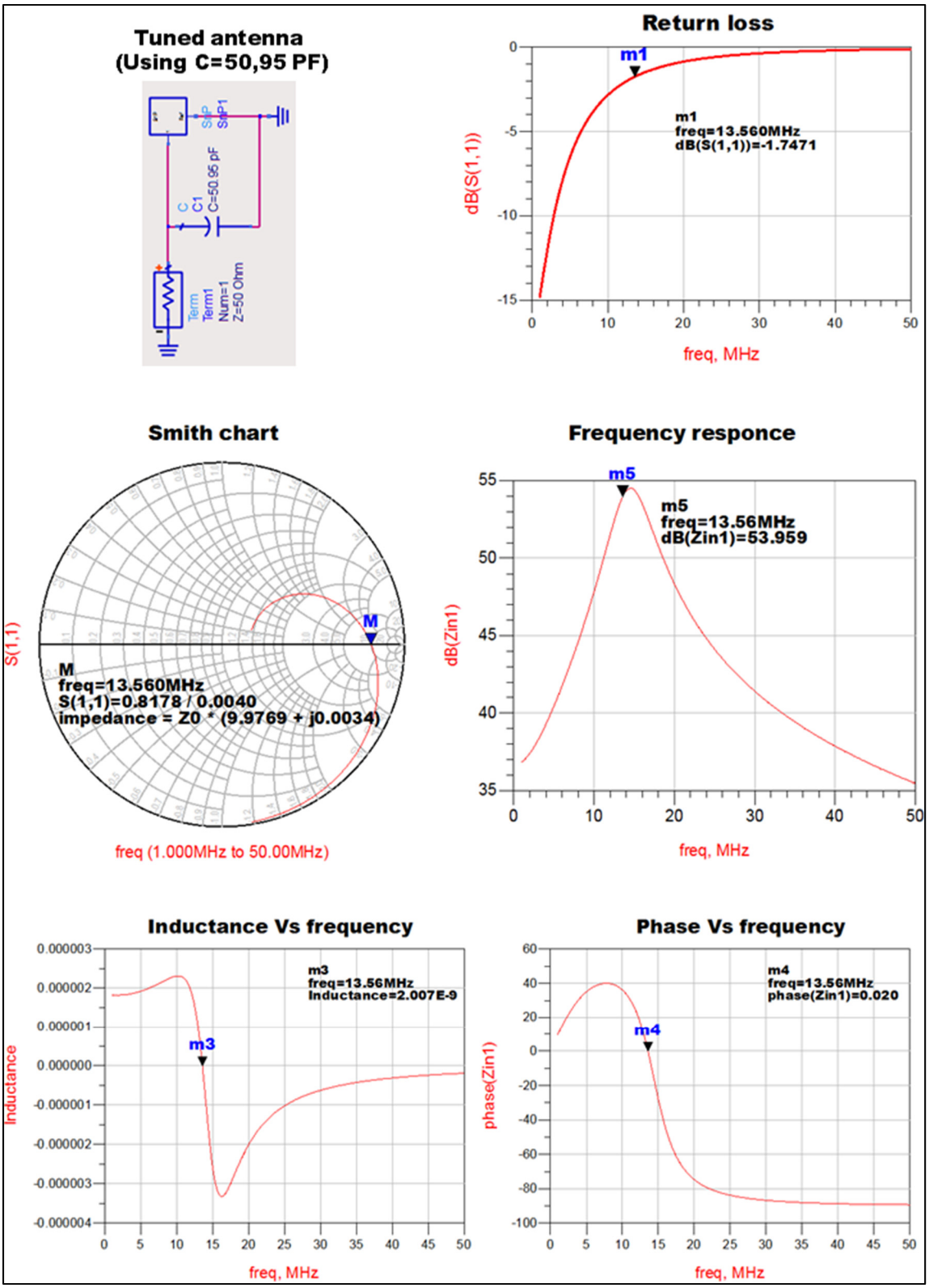

Figure 5.15 Flexible spiral antenna performances after tuning

For flexible electronics, we designed a flexible antenna (figure 5.13) using microfabrication techniques (7 turns, trace width = 0.4mm, spacing between traces = 0.3 mm, sputtered silver thickness = 9 um, out diameter = 28.5 mm).

Figure 5.14 shows that the antenna is resonating at 40 MHz (self-resonance frequency). To tune the antenna, we added a capacitor = 50.95pF. Figure 5.15 confirms that the tuning was efficient: the antenna is now resonating at 13.56MHz. In this case, we do not need to add a resistor to increase the bandwidth because the spurted layer of silver is thin (900 nm) which resulted in an increased value of the antenna's resistance (70.92Ω).

5.4.3 LTCC antenna

In this part, we designed and developed an LTCC-based one-layer receiver antenna the number of turns was 10, the metal routing width was 200 µm and the spacing was 250 µm. Figure 5.16 illustrates the equivalent circuit.

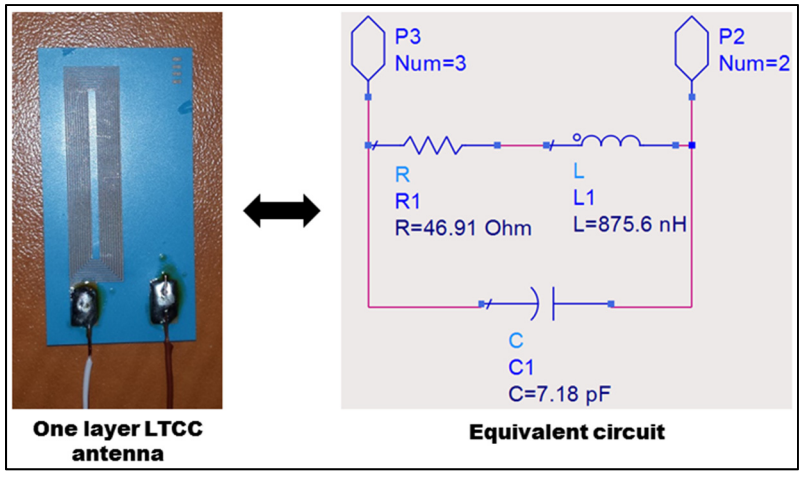

Figure 5.16 One layer LTCC spiral antenna equivalent circuit

Figure 5.17 shows that the LTCC based one-layer antenna is detuned. To tune the antenna, we added a capacitor in parallel with the antenna (C = 113,84 uH). Figure 5.18 confirms that the tuning was efficient: the antenna is now resonating at 13.56MHz (Phase=0, imaginary part=0).

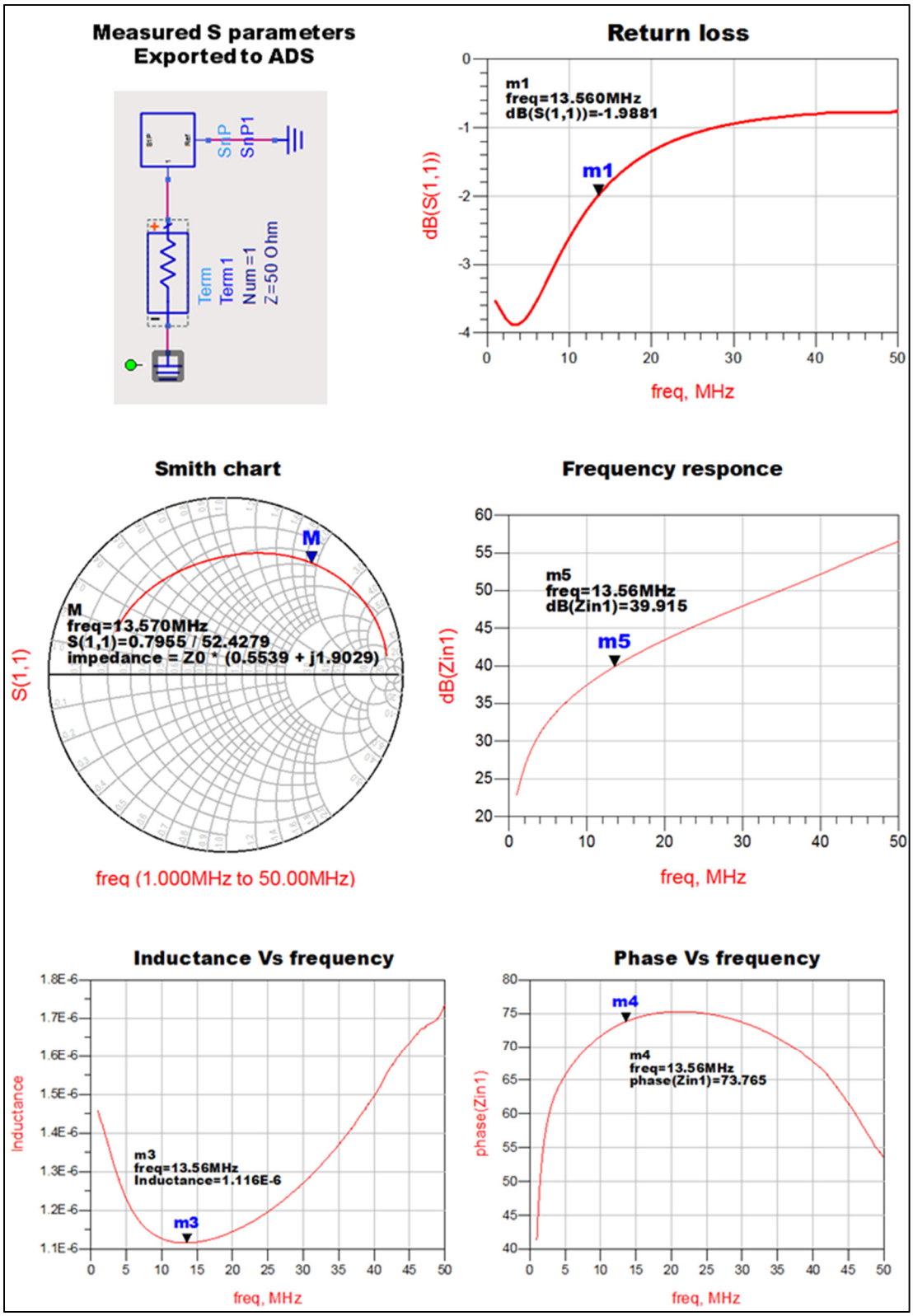

Figure 5.17 One layer LTCC spiral antenna performances before tuning

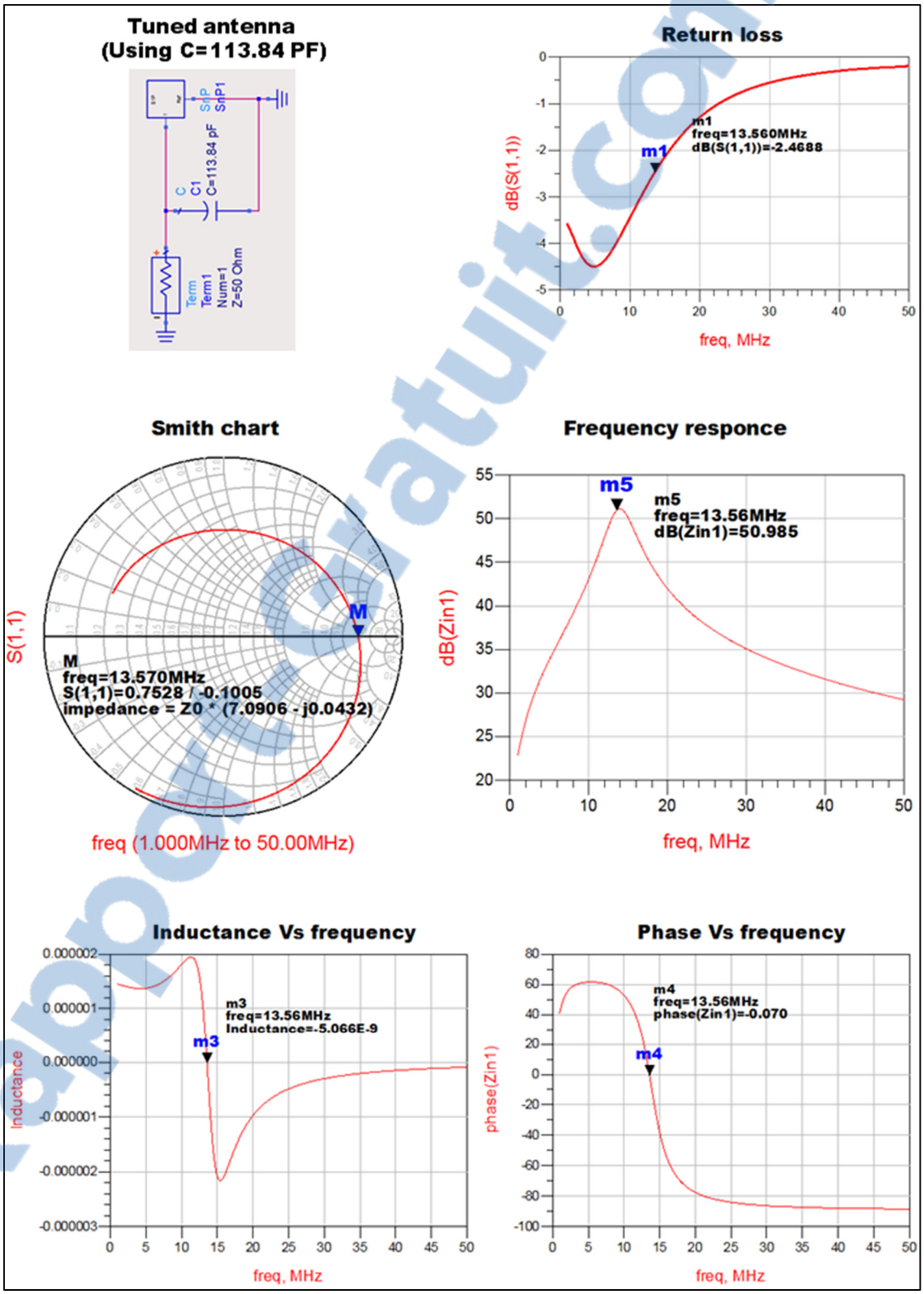

Figure 5.18 One layer LTCC spiral antenna performances after tuning

We also investigated multi-layer coil. Which was fabricated using 4-layers DuPont's 951AT substrate. The receiver coils were designed to have the same number of turns in each layer. Spiral inductors in different layers were connected by vias. For each layer, the number of turns was 10; the metal routing width was 200 µm, and the spacing was 250 µm. The non-fired ceramic tape was 112 µm thick, and the metal routing thickness was 8 µm. Silver metalization was used for all layers. The diameter of punched via-holes was 150 µm. The relative permittivity of the dielectric was εr=7.8. The silver paste is assumed to have a conductivity of σ=5.9×107 S/m.

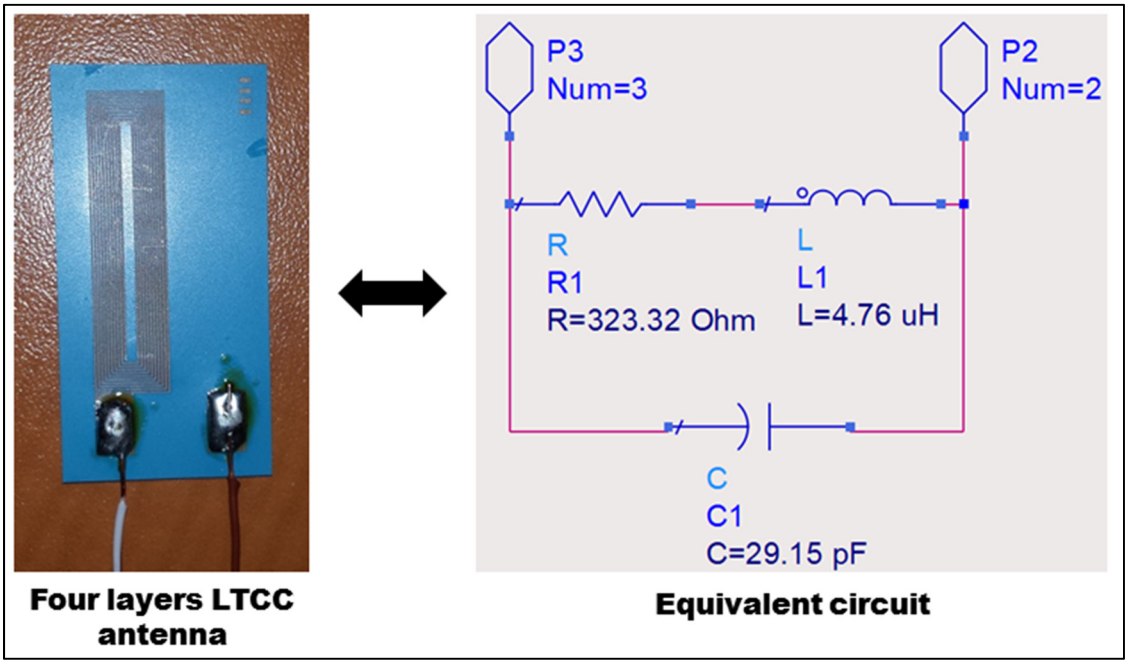

Figure 5.19 Four layers LTCC spiral antenna equivalent circuit

Figure 5.19 shows that by increasing the number of layers, we increased the value of the inductance which became 4.76 uH at 1MHz. However, doing so, we also increased the parasitic capacitance and the serial resistance, results illustrated in figure 5.20 show that, because of this parasitic capacitance, the antenna is not acting as an inductor at 13.56MHz, in fact, it acts as a capacitor.; this is because we are operating after the self-resonance frequency. This is why FCC is suggesting having an antenna with Self-resonance frequency ≥ 25 MHz.

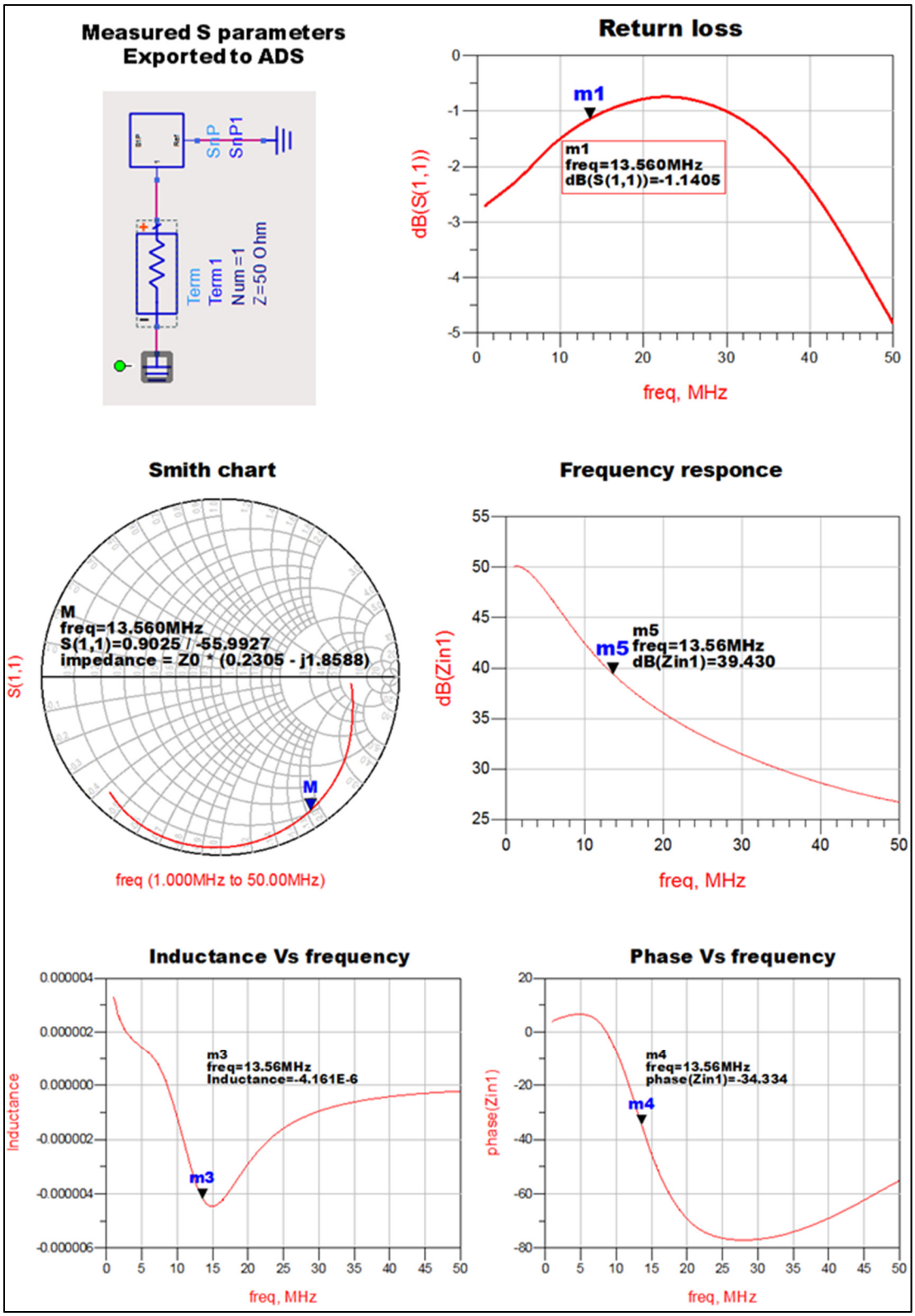

Figure 5.20 Four layers LTCC spiral antenna performances

5.5 Results and conclusion

After matching the transmitter antenna and tuning the receiver antenna to the resonance frequency (13.56MHz) we used a network analyzer to measure the wireless power transfer efficiency:(Kim et Kim, 2014) we connected the transmitter to port 1 and the receiver to port 2, then we progressively increased the distance between the two antennas.

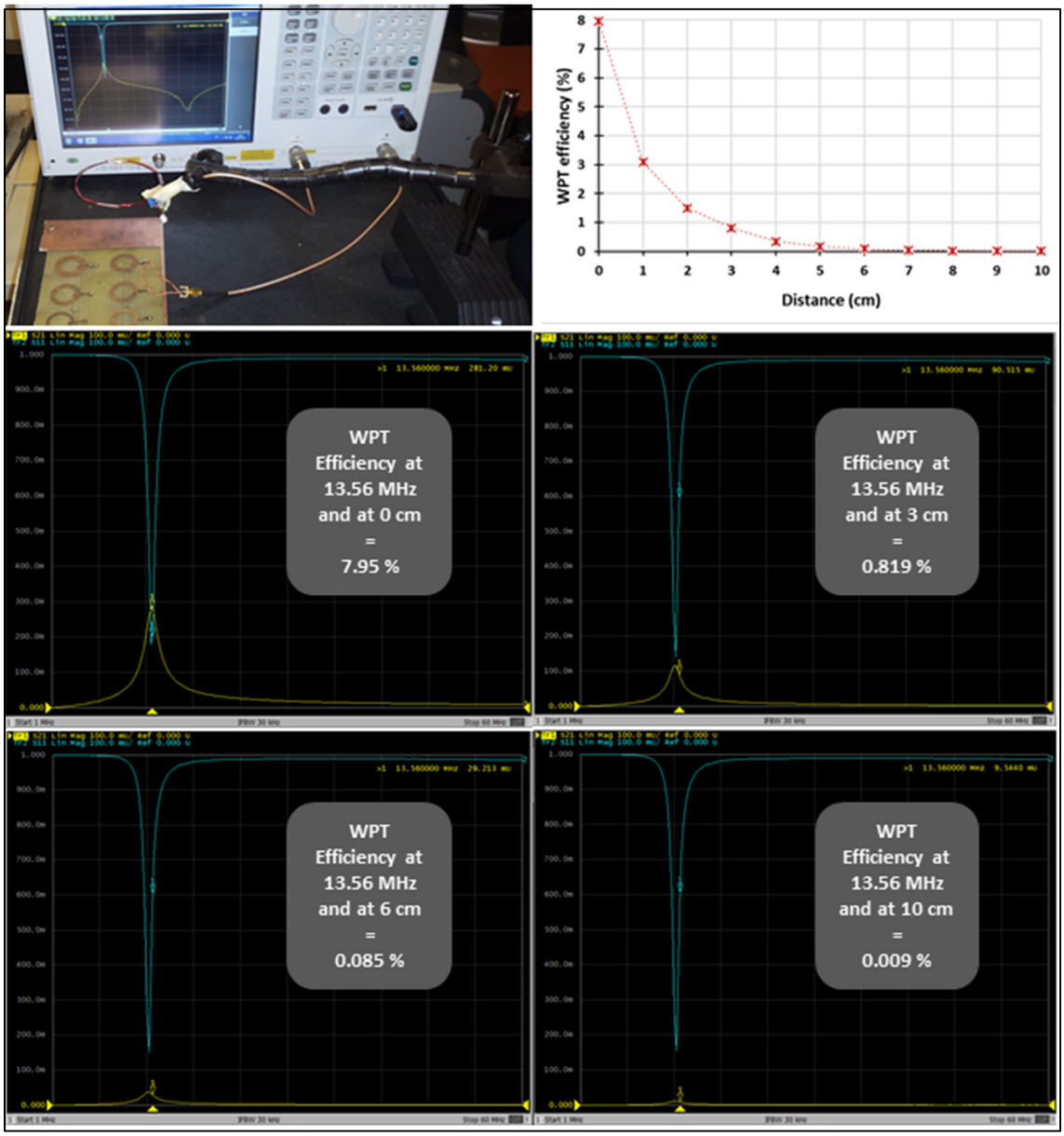

Figure 5.21 Wireless power transfer efficiency

In this experiment, we did not study the effect of different orientations we just examined the effect of the distance. As we can see, the efficiency (Equation 5.11) is exponentially decreasing when we increase the distance (figure 5.21).

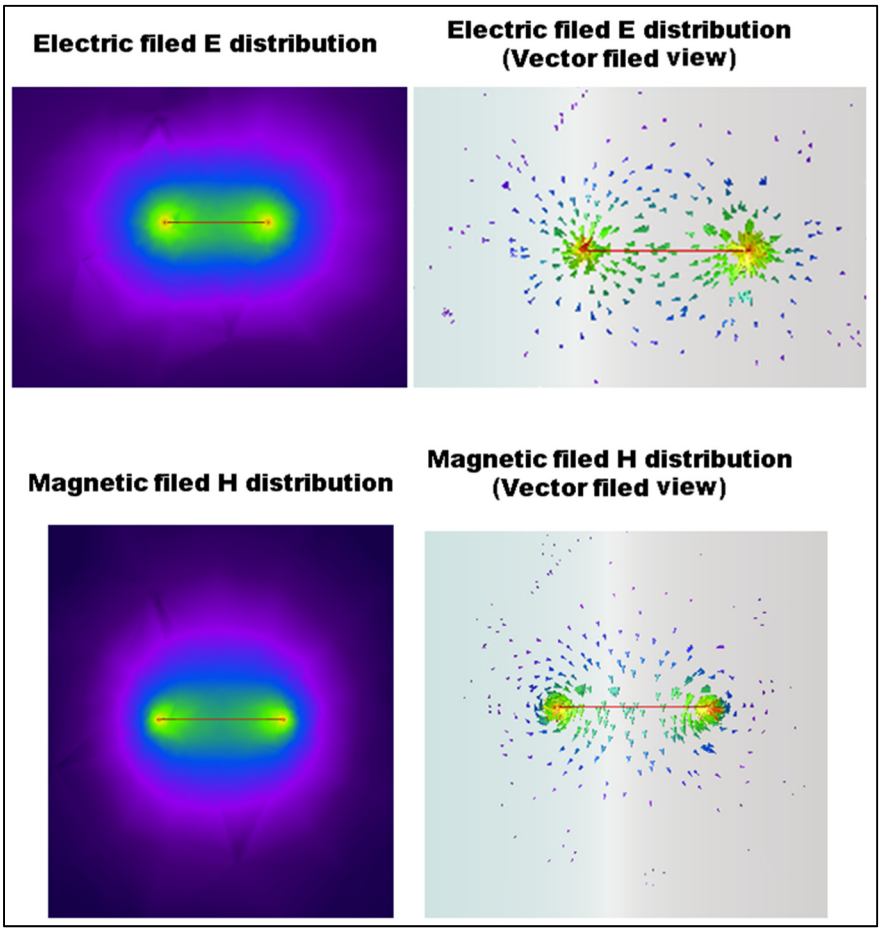

Figure 5.22 Electric and magnetic field distribution

Wireless power transfer efficiency is expressed as follows (Yu et Li, 2013):

$$WPT\ efficiency\ (\%) = |S21|^2 \times 100 \tag{5.11}$$

The curve in blue shows S11 (linear magnitude). As we can see, the reflected power is significantly reduced around frequency = 13.56 MHz. The yellow curve shows S21 (linear magnitude), which is the wireless power transmitted from the transmitter to the receiver, the

pic of power is around a frequency = 13.56 MHz. The maximum efficiency 7.95% was observed at the minimum distance between the two antennas.

Having an efficiency of 7.95% does not mean that 92.05% of power was all dissipated by heating, but it means that a portion of that 92,05 % was lost in the form of heat, and the other part simply didn’t reach the receiver. In fact, the transmitter antenna is not very directive as illustrated in figure 5.22. We can notice that the electromagnetic field is surrounding the antenna in all directions, in addition to that, we used a transmitter bigger than the receiver which means that the receiver cached only a portion of the electromagnetic field.

CONCLUSION

The measure and the control of the pH are fundamental in numerous applications, such as food processing, manufacturing, industrial processing, environmental and clinical monitoring. Some devices or methods are already available to perform the pH measurement; they have many advantages and they still have a promising future. However, they also have some disadvantages (the bulkiness the lack of integration, excessive prices, etc.) which are limiting their applications in some specific field.

In this work we tried to find an alternative to offer a better miniaturization, lower consumption, lower costs, etc. According to literature, we found that IrO_x is an excellent material for pH sensing, so we investigated different deposition techniques (sol-gel and electrodeposition) we concluded that the miniaturization does not have an impact on the sensitivity we also found that electrodeposition offers a better sensitivity and a better surface quality compared to sol-gel.

To miniaturize the pH sensor, we had chosen between MEMS and LTCC. We figured out that MEMS is not well adapted for the fabrication of the pH sensor (at least with the sol-gel and electrodeposition of IrO_x). In fact, it is incompatible with electrodeposition (thin sputtered metal peel off during electrodeposition activity). Also, there are some problems with sol-gel deposition (presence of heat stresses during heat treatment, also the use of solvents eliminates the deposited gel). Instead of using solvents we developed a process based on laser etching, and it solved the problem with sol-gel deposition, but it is still not compatible with electrodeposition (thin sputtered metal peel off) the good point is that thin metal is flexible; then, it is a perfect fabrication technique for flexible devices.

LTCC proved to be the most suitable fabrication technique, in fact, it allows a better integration and miniaturization; it is compatible with both, sol-gel and electrodeposition of IrO_x, and it allows batch production which reduces costs. Then we developed the prototype of a miniaturized LTCC based pH sensing device, integrating the sensor and interface electronics

Table 6.1 Comparison of different pH sensing devices

Sensor	Integration	Sensitivity	Response time	Price	Simplicity	Impedance	Flexibility	Target applications
Paper strip	★★★★★ (0/5)	★★★★★ (1/5)	★★★★★ (3/5)	★★★★★ (5/5)	★★★★★ (5/5)	–	★★★★★ (5/5)	Applications requiring low precision and low cost
Glass	★★★★★ (1/5)	★★★★★ (3/5)	★★★★★ (2/5)	★★★★★ (2/5)	★★★★★ (2/5)	★★★★★ (1/5)	★★★★★ (0/5)	General
ISFET	★★★★★ (4/5)	★★★★★ (3/5)	★★★★★ (3/5)	★★★★★ (1/5)	★★★★★ (2/5)	★★★★★ (2/5)	★★★★★ (2/5)	General
MEMS	★★★★★ (5/5)	–	–	★★★★★ (4/5)	★★★★★ (3/5)	–	★★★★★ (4/5)	–
Laser Micro-machined	★★★★★ (3/5)	★★★★★ (3/5)	★★★★★ (5/5)	★★★★★ (4/5)	★★★★★ (4/5)	★★★★★ (5/5)	★★★★★ (4/5)	Medical monitoring
LTCC	★★★★★ (4/5)	★★★★★ (5/5)	★★★★★ (5/5)	★★★★★ (4/5)	★★★★★ (3/5)	★★★★★ (5/5)	★★★★★ (0/5)	Food and environmental monitoring

on the same ceramic substrate; it is suitable for environmental and food quality monitoring applications. However, LTCC has few limitations. For instance, it is not flexible, it is breakable, and it is not biocompatible. For those reasons, LTCC is not suitable for few applications where flexibility, biocompatibility, and robustness are required. Then, other substrates (we showed some examples such as Kapton, Glass, etc.) could be used as an alternative.

Selection criteria depend on the requirement of the target application, the table above gives a rating (from 0 to 5 stars) for each criteria in order to have an approximative comparison between different pH sensing devices.

After designing the sensing device, we developed a wireless user interface; we used modular approach (Sensing device and communication part are separated). Future work may integrate them in the same substrate. Due to biocompatibility, infections and size concerns, the need for wireless and battery-less is evident, especially for medical devices. A new expectation raises for those devices, in fact, power becomes an essential issue. To solve this problem, we developed and tuned an inductive link (transmitter and receiver antenna) to transfer power to battery-less applications wirelessly.

LIST OF BIBLIOGRAPHICAL REFERENCES

(AIMS), Australian Institute of Marine Science. 2016. « Climate change and the tropical marine environment ». Official web page. <http://www.aims.gov.au/docs/research/climate-change/position-paper.html>. Visited on August 2016.

(ASOC), Antarctic and Southern Ocean Coalition. 2010. « Ocean Acidification ». <http://www.asoc.org/advocacy/climate-change-and-the-antarctic/ocean-acidification>. Visited on August 2016.

(IMOS), Integrated Marine Observing System. 2016. « Deep Water Moorings ». < http://imos.org.au/deepwatermoorings.html >. Visited on August 2016.

A, P.G. 1948. *ph-responsive glass electrode*. < https://www.google.ca/patents/US2444845 >. Visited on September 2015

America, Federal Regulations of the United States of. 2003. *The Code of Federal Regulations of the United States of America*. Office of the Federal Register National Archives and Records Administration. <https://play.google.com/books/reader?id=sps8AAAAIAAJ&printsec=frontcover&output=reader&hl=fr&pg=GBS.PP1 >. Visited on May 2016

Bhadra, S., D. S. Y. Tan, D. J. Thomson, M. S. Freund et G. E. Bridges. 2013. « A Wireless Passive Sensor for Temperature Compensated Remote pH Monitoring ». *IEEE Sensors Journal,* vol. 13, nº 6, p. 2428-2436.

Chemistry, American Association for Clinical. 2014. « Lab Tests Online Acidosis and Alkalosis ». Web Portal. < https://labtestsonline.org/understanding/conditions/acidosis/ >. Visited on August 2016.

Farooqui, M. F., et A. Shamim. 2016. « Low cost inkjet printed smart bandage for wireless monitoring of chronic wounds ». In *2016 IEEE MTT-S International Microwave Symposium (IMS)*. (22-27 May 2016), p. 1-4.

Franklin, R. K., S. Joo, S. Negi, F. Solzbacher et R. B. Brown. 2009. « A comparison of fabrication methods for Iridium Oxide reference electrodes ». In *Sensors, 2009 IEEE*. (25-28 Oct. 2009), p. 1086-1089.

Fu, F., J. Lin et X. Xu. 2011. « Effect of pH on optical properties during blood coagulation progress by optical coherence tomography ». In *2011 4th International Conference on Biomedical Engineering and Informatics (BMEI)*. (15-17 Oct. 2011) Vol. 1, p. 268-271.

Hu, Jin, Mamdouh Abdelsalam, Philip Bartlett, Robin Cole, Yoshihiro Sugawara, Jeremy Baumberg, Sumeet Mahajan et Guy Denuault. 2009. « Electrodeposition of highly ordered macroporous iridium oxide through self-assembled colloidal templates ». *Journal of Materials Chemistry,* vol. 19, nº 23, p. 3855-3858.

Huang, W. D., S. Deb, Y. S. Seo, S. Rao, M. Chiao et J. C. Chiao. 2012. « A Passive Radio-Frequency pH-Sensing Tag for Wireless Food-Quality Monitoring ». *IEEE Sensors Journal,* vol. 12, nº 3, p. 487-495.

Huang, Wen-Ding. 2010. « A pH SENSOR BASED ON A FLEXIBLE SUBSTRATE ». ProQuest Dissertations Publishing, University of Texas at Arlington. In ProQuest. <http://search.proquest.com/pqdtglobal/docview/926210491/A41FB00146894249PQ/1?accountid=27231 >. Visited on December 2014.

Huang, Wen-Ding, Hung Cao, Sanchali Deb, Mu Chiao et J. C. Chiao. 2011. « A flexible pH sensor based on the iridium oxide sensing film ». *Sensors and Actuators A: Physical,* vol. 169, nº 1, p. 1-11.

Irish, J., D. Vandemark, S. Shellito, J. Salisbury, A. Plagge, K. Hanley et M. Emond. 2010. « CO<inf>2</inf> gas exchange and ocean acidification studies in the coastal Gulf of Maine ». In *OCEANS 2010 MTS/IEEE SEATTLE*. (20-23 Sept. 2010), p. 1-10.

Jensen, William B. 2004. « The Symbol for pH ». *Journal of Chemical Education,* vol. 81, nº 1, p. 21.

Jimenez-Jorquera, Cecilia, Jahir Orozco et Antoni Baldi. 2010. « ISFET Based Microsensors for Environmental Monitoring ». *Sensors,* vol. 10, nº 1, p. 61.

Ke Dehong, Shou-fishing. 2014. *Highly sensitive pH test paper and preparation method thereof*. < https://www.google.ca/patents/CN102519959B?cl=en >. Visited on May 2016

Keskin, N., et H. Liu. 2015. « Complementary Class-E amplifier for wireless power transfer ». In *2015 IEEE 65th Electronic Components and Technology Conference (ECTC)*. (26-29 May 2015), p. 2235-2240.

Kim, J. J., et J. Kim. 2014. « Modeling method of coil module for wireless power transfer system by two-port S-parameter measurement in frequency domain ». In *Wireless Power Transfer Conference (WPTC), 2014 IEEE*. (8-9 May 2014), p. 251-254.

Klaus, J., R. Paris et R. Sommer. 2016. « Systematic MEMS ASIC design flow using the example of an acceleration sensor ». In *2016 13th International Conference on Synthesis, Modeling, Analysis and Simulation Methods and Applications to Circuit Design (SMACD)*. (27-30 June 2016), p. 1-4.

Li, Q., et Y. C. Liang. 2015. « An Inductive Power Transfer System With a High-Q Resonant Tank for Mobile Device Charging ». *IEEE Transactions on Power Electronics,* vol. 30, nº 11, p. 6203-6212.

Liu, D., H. Hu et S. Georgakopoulos. 2016. « Misalignment Sensitivity of Strongly Coupled Wireless Power Transfer Systems ». *IEEE Transactions on Power Electronics,* vol. PP, nº 99, p. 1-1.

Maciel, P. S. P., S. B. da Silva, G. F. B. de Medeiros et T. V. Rodrigues. 2013. « Innovative pH control for water: Reusing rainwater ». In *Global Humanitarian Technology Conference (GHTC), 2013 IEEE*. (20-23 Oct. 2013), p. 288-293.

Mand, M., x017E, uka, E. Begi, x, Z. Begi, x, D. Bo, x, kovi et x. 2015. « Software for acid-base status disorders management ». In *Information and Communication Technology, Electronics and Microelectronics (MIPRO), 2015 38th International Convention on*. (25-29 May 2015), p. 360-364.

Miyake, Masafumi, Li D. Chen, Gianluca Pozzi et Philippe Bühlmann. 2012. « Ion-Selective Electrodes with Unusual Response Functions: Simultaneous Formation of Ionophore–Primary Ion Complexes with Different Stoichiometries ». *Analytical Chemistry,* vol. 84, nº 2, p. 1104-1111.

Mohan, S. S., M. del Mar Hershenson, S. P. Boyd et T. H. Lee. 1999. « Simple accurate expressions for planar spiral inductances ». *IEEE Journal of Solid-State Circuits,* vol. 34, nº 10, p. 1419-1424.

Muaz, A. K. M., U. Hashim, N. Azizah, M. K. M. Arshad, K. L. Foo, A. R. Ruslinda, R. M. Ayub, S. C. B. Gopinath et C. H. Voon. 2015. « Integrated of IDEs with TiO2 nanoparticles thin films for pH sensor ». In *Micro and Nanoelectronics (RSM), 2015 IEEE Regional Symposium on*. (19-21 Aug. 2015), p. 1-4.

Pietrikova, A. 2001. « Potentiality of LTCC for sensor applications ». In *Electronics Technology: Concurrent Engineering in Electronic Packaging, 2001. 24th International Spring Seminar on*. (2001), p. 112-116.

Pozar, David M. 2012. *Microwave Engineering, 4th Edition*, 4th. Wiley, 732 p.

Puchberger-Enengl, D., C. Krutzler et M. J. Vellekoop. 2011. « Organically modified silicate film pH sensor for continuous wound monitoring ». In *Sensors, 2011 IEEE*. (28-31 Oct. 2011), p. 679-682.

Shah, A., et O. P. Chauhan. 2015. « IT16. Applications of bio-sensors in agri-food industry and mitigation of bio-threat paradigm ». In *Physics and Technology of Sensors (ISPTS), 2015 2nd International Symposium on*. (7-10 March 2015), p. XXXII-XXXII.

Shorrock, S. M., S. Kun, R. A. Peura et R. M. Dunn. 2000. « Determination of a relationship between bacteria levels and tissue pH in wounds: animal studies ». In *Bioengineering Conference, 2000. Proceedings of the IEEE 26th Annual Northeast*. (2000), p. 117-118.

Sumari, S. M., F. Muhamad-Darus, N. Kantasamy et S. a. Urban Sinyaw. 2010. « Rainwater characterization at Global Atmospheric Watch in Danum Valley, Sabah ». In *Science and Social Research (CSSR), 2010 International Conference on*. (5-7 Dec. 2010), p. 479-484.

Tesla, N. 1914. *Apparatus for transmitting electrical energy*.
< https://www.google.ca/patents/US1119732 >. Visited on June 2016.

Warudkar, G., et S. Dorle. 2016. « Review on sensing the fertility characteristics of agriculture soils ». In *2016 International Conference on Information Communication and Embedded Systems (ICICES)*. (25-26 Feb. 2016), p. 1-6.

Yu, S., et L. Li. 2013. « Experimental study of effects of coaxial cables in magnetic resonant wireless power transfer system ». In *Wireless Symposium (IWS), 2013 IEEE International*. (14-18 April 2013), p. 1-4.